Conceptual Design of Blended Wing Body Airliners

within a semi-automated design framework

M.T.H. Brown

Flight Performance & Propulsion

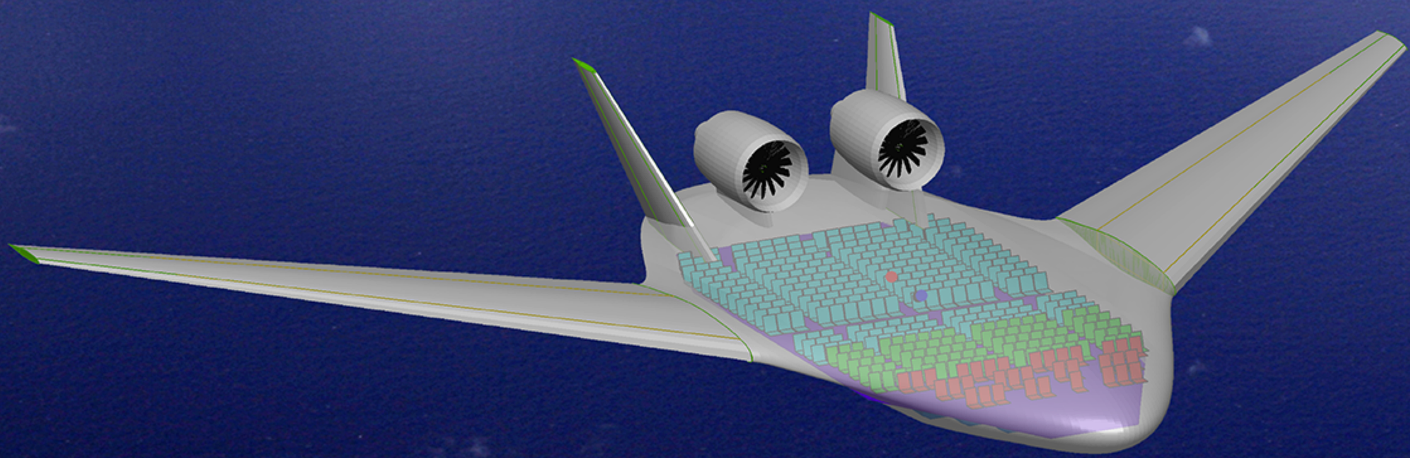

TU Delft Delft University of Technology

Challenge the future

Conceptual Design of Blended Wing Body Airliners

within a semi-automated design framework

by

M.T.H. Brown

in partial fulfillment of the requirements for the degree of

Master of Science
in Aerospace Engineering

at the Delft University of Technology,
to be defended publicly on Tuesday May 9, 2017 at 09:00 AM.

Student number:	4015818	
Project duration:	August 1, 2016 – May 9, 2017	
Thesis Number:	131#17#MT#FPP	
Supervisors:	Dr. ir. R. Vos	
Thesis committee:	Prof. dr. ir. A. Gangoli Rao,	TU Delft
	Dr. ir. R. Vos,	TU Delft
	Dr. H. G. Visser,	TU Delft

An electronic version of this thesis is available at http://repository.tudelft.nl/.
Equivalent words: 30703

Delft University of Technology

Abstract

Blended wing body aircraft represent a paradigm shift in jet transport aircraft design. Stepping away from the conventional tube-and-wing philosophy, they promise benefits over existing or future conventional aircraft. The most significant challenge with the concept is the increased coupling between aircraft design disciplines that has necessitated the development and implementation of multidisciplinary design optimisation routines. A novel conceptual aircraft design program named the Initiator has been developed that is able to design conventional and unconventional passenger transport aircraft, enabling comparisons to be made which are based on the same top level requirements and analysis fidelity. It however lacks the ability to design or analyse the blended wing body. The aim of this thesis is to make comparative studies between the blended-wing-body aircraft and its conventional tube-and-wing counterpart based upon the same design requirements. To this end the work investigates the methods that are required to implement the blended wing body aircraft in a semi-automated design framework such as the Initiator.

By developing a novel geometric parametrisation of the blended wing body, the design possibilities have been increased while maintaining straightforward shaping manipulation and robustness. All relevant topics of conceptual aircraft layout are considered, making the resulting aircraft feasible in terms of the integration of its components. Furthermore, methods have been implemented or developed which are capable of analysing the mass, aerodynamic performance and longitudinal stability of the aircraft to a fidelity which is suitable for conceptual design.

The mass estimation methods that have been implemented are verified and validated to be within 10% of reference blended wing bodies with a smaller error of 5% being common. There is however significant scatter in reference results, making conclusive statements about accuracy difficult. Drag estimations perform less accurately with drag being overpredicted by approximately 20%. The cause of this over prediction was largely due to empirical corrections for miscellaneous and unaccounted drag sources as is done for conventional aircraft. Wave drag is considerably higher than reference cases (7 versus 1 counts). Considering the applicability of the implemented method to blended wing bodies and the limited specific transonic design that is performed, it is chosen to accept this result as a conservative estimate until higher order validations of the wave drag can be performed. Induced drag was also higher for the test cases but results are inconclusive whether this is an error or a true result of the design choices. Zero-lift drag has however been accurately estimated by the novel implementation of empirical methods.

Test case blended wing body and tube and wing aircraft were formed in the 150, 250 and 400 passenger classes. The comparisons of the resulting aircraft show that the blended wing body is feasible at the fidelity level achieved. They have reduced mass, improved aerodynamic efficiency and higher fuel economy. Trends show that the improvements over tube and wing aircraft increase with aircraft size. The qualitative results contained herein should still be treated as provisional since the implementation of the concept is not complete and remaining topics could still have significant effects on the results.

Acknowledgements

It is the final hour on the final day and as this long road draws to a close I would like to take the opportunity to pay tribute to the people who have aided me in my journey. Firstly I would like to thank my supervisor Roelof Vos for his enthusiastic support and guidance through the execution of this thesis assignment and other aircraft design projects I have undertaken. He inspired me to keep asking the hard questions and believed in my abilities to answer them. I will continue doing this as in my future endeavours. Secondly I would like to thank my friends and fellow students for all of the help that they have given me. Many hours were spent discussing problems at the whiteboard and without the team effort the Initiator would not be what it is today. There were also those outside of university that supported me in my free time, recharging and rejuvenating my thoughts and providing a listening ear when I needed to vent my frustrations. Last, but certainly not least, I would like to thank my family for their unwavering belief in me and my ability to achieve my dreams. Their love and caring got me through the roughest times and without them none of this would be possible.

M.T.H. Brown
Delft, May 2017

Contents

List of Figures

List of Tables

Nomenclature

Latin Symbols

A	Aspect ratio	-
b	Wing span	m
c	Chord	m
C_D	Coefficient of drag	-
C_L	Coefficient of lift	-
C_M	Coefficient of pitching moment with alpha	-
C_{f_i}	Flat plate skin friction coefficient	-
C_{D_0}	Coefficient of zero-lift drag	m
C_{D_i}	Coefficient of induced drag	-
C_{D_w}	Coefficient of wave drag	-
C_{M_α}	Derivative of pitching moment coefficient with alpha	-
d	Diameter	m
h	Height	m
l	Length	m
L'	Thickness location correction factor	-
R_{ls}	Lifting surface correction	-
R_{wf}	Wing-body interference factor	-
S	Area	m^2
S_v	Vertical tail volume coefficient	-
t/c	Airfoil thickness to chord ratio	-
u	Cabin sectional length ratio	-
v	Cabin sectional width ratio	-
w	Width	m
w_{cp}	Cockpit width	m

Greek Symbols

λ	Taper ratio	-

1

INTRODUCTION

Blended wing body aircraft (BWB) are one of the unconventional aircraft design philosophies that are currently being intensely investigated by academia and the aerospace industry [1, 2]. They are a promising aircraft design that have many important advantages over the conventional tube and wing (TAW) aircraft such as higher aerodynamic efficiency leading to lower fuel burn and emissions, lower noise emission and overall lower operational costs to airlines and operators [1]. These factors are becoming increasingly important in modern society and trends in aircraft design and operation have reflected this [3, 4].

Conceptual design of BWB aircraft is still in its fledgling stage even though it is not a new idea. Modern efforts into their design resurged in 1988 and currently there are active design and research projects such as the NASA ERA [5] and Lockheed HWB [6]. Many technical challenges have been found with the concept which have hampered progress such as the fuselage structure and flight stability [1]. Other factors are also at play such as the inertia of manufacturers to commit to the radical design change and the recent marginal success of large airliners such as the Airbus A380 and Boeing 747-8 due to changing markets and economic conditions. Many BWB designs at the time were aimed at larger aircraft (>400 PAX) and as such their appeal, in terms of today's trends, is somewhat tarnished. However, future markets could once again require a larger aircraft if techniques such as feeder-cruiser concepts come to fruition or naturally through the widely accepted fact that the air travel market continues to grow year on year. This aside, it can also be possible that smaller BWB concepts can be feasible for missions served by the Boeing 787/Airbus A350 family or even the Boeing 737/Airbus A320 family.

This hints at the need for the possibility to design, analyse and compare both conventional TAW and BWB aircraft of various missions and configurations using similar methods, allowing for an increased understanding of the feasibility of the BWB concept, as a whole, over a wide design space. This is no easy task. The nature of conceptual aircraft design calls for rapidly implementable methods with acceptable accuracy, on which requirement satisfaction, layout, dimensioning, performance and mass budgets can be based. With improved synergy between established design methods and computer based methods this task is becoming easier and yields good results [7]. Computer based design methods have been used extensively in the past but openly available programs tend to be limited in their ability to model unconventional designs, especially the BWB [8]. Furthermore, new techniques of multidisciplinary design optimisation (MDO) and knowledge based engineering (KBE) are improving the process and (semi) artificial intelligence and machine based learning are showing feasibility in the (near) future [9].

The Flight Performance and Propulsion department at TU Delft has identified these needs and responded by creating the Initiator. This conceptual aircraft design program is able to design and analyse passenger jet airliners based on top level requirements (TLR) and limited input parameters [10]. It makes use of semi-empirical and semi-analytical design methods in an iterative convergence loop to select an overall consistent and feasible design. Conventional as well as unconventional aircraft are implemented but it lacks proper functionality for blended-wing-body aircraft. This presents an opportunity for improvement of the Initiator by implementing the BWB into its design and analyses routines.

The structure of the report is as follows: firstly a short background into relevant literature is given followed by the scope and goals of the research and the research questions that will be answered. Chapter 2 details the parametrisation implemented for the BWB and the decisions on which it is based. Following this, the theoretical basis and implementation of the mass, drag and stability analysis procedures is outlined in Chapter 3.

Verification and validation of the methods implemented is performed in Chapter 4. Results from the Initiator for three test case TAW and BWB aircraft are discussed in Chapter 5 where the comparison between the design and performance of the two concepts is brought to the fore. Conclusions about the work are drawn in Chapter 6 and lastly some recommendations are made as to future work and progress with the Initiator in Chapter 7.

1.1. BACKGROUND

In this section a short review of conceptual design of blended wing body aircraft is given, followed by a brief background into the Initiator. A comprehensive summary of the progress made with the BWB design and its current status can be found in reference [1]. The main finding of this study is that a multidisciplinary design synthesis and optimisation approach is required for designing a BWB which is feasible and able to take full advantage of the design's proposed benefits. This is due to the highly integrated and coupled nature of the BWB which gives design choices a greater impact on other disciplines.

There are currently no blended wing body aircraft in service or production and the available literature is thus confined to research and development projects. These projects have been able to make significant progress regarding the challenges of BWB design and the concept has matured throughout. Scaled wind tunnel and flight demonstration models have been made in some cases in order to ascertain the accuracy of assumptions, models and flight performance predictions. Research has been carried out mainly by European and American institutions with both industry such as Boeing, Lockheed Martin and Airbus as well as various laboratories and universities such as NASA, DLR, ONERA, MIT, Cambridge, Cranfield and Hamburg among numerous others. A graphical overview of recent BWB design project history can be seen in Figure 1.1.

Generally BWBs are used for passenger airliners but cargo transports have also received attention. More data on selected aircraft can be found in Table 1.1. Available data is however very limited and forms one of the challenges of the BWB as verification of methods by comparing results to reference data, as is commonly done during conceptual design, is inconclusive and unreliable. That being said, researchers have greatly matured BWB design over the years and clear trends can be seen in Figure 1.1, also between research institutions. Planform geometries have become smoother with improved parametrisation and blending of aerodynamic fairings. There has also been a shift towards a lower number of engines and placement of them above the aft centre body. Early designs tended to only use winglets with a control surface to facilitate directional stability and control. Recent designs however mostly include vertical fins. Some designs have used canted vertical fins. The traditional shape of the BWB with a shorter wider fuselage with approximately mid fuselage mounted wings has persisted with only the AHEAD program relying on a much longer fuselage. This design is also the only one to feature canards. Lockheed Martin has chosen to use a traditional T-tail design. Notable is the low aspect ratio of these aircraft which is an inherent property of the BWB due to the inclusion of the large fuselage as a main lifting surface [1].

Table 1.1: Overview of selected BWB aircraft design parameters

Parameter	Pax	MTOM	OEM	Payload	FM	$\frac{PL}{MTOM}$	$\frac{OEM}{MTOM}$
Unit	-	[t]	[t]	[t]	[t]	[-]	[-]
VELA 3 [11]	750	700.00	327.00	137.00	236.00	0.20	0.47
NACRE [11]	750	630.00	309.00	127.00	194.00	0.20	0.49
OREIO [12]	-	215.82	112.85	45.36	57.61	0.21	0.52
N2A-EXTE [13]	-	214.00	101.82	46.72	65.49	0.22	0.48
ACFA [14]	450	401.00	225.00	50.00	126.00	0.13	0.49
Regional Jet [15]	98	43.89	24.82	10.60	8.47	0.24	0.57
Parameter	Range	Altitude	M	L/D	W/S	T/W	A
Unit	[km]	[ft]	-	-	N/m^2	-	-
VELA 3				22.1			
NACRE				23.4	3090		5.02
OREIO	6500	35012	0.80	23.3	2845	0.26	5.65
N2A-EXTE	11112	38739	0.81	21.42	2269	0.33	4.56
ACFA	13334	43100	0.85				
Regional Jet	926	40000	0.80	15.6	2129		3.70

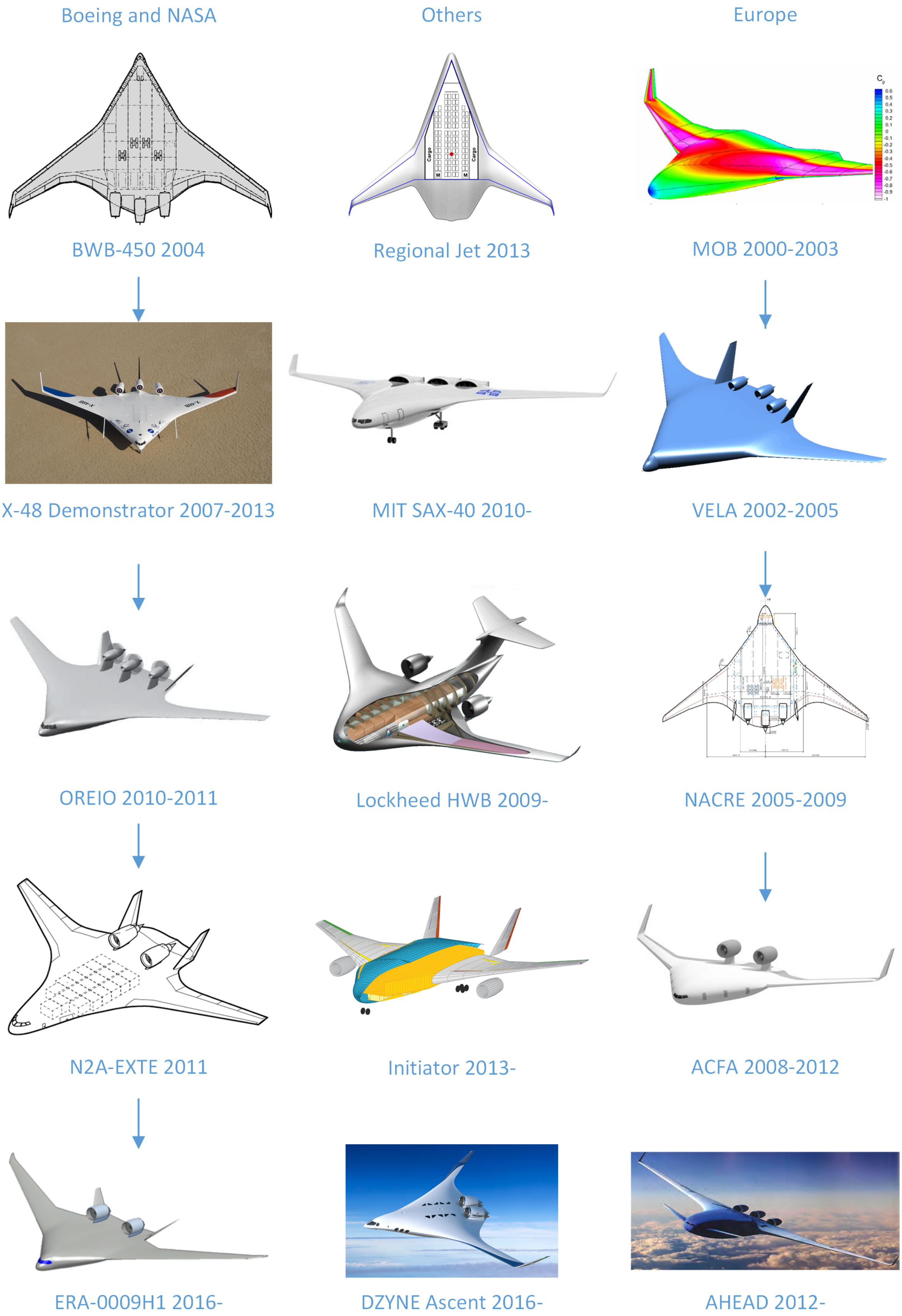

Figure 1.1: Modern design project history of the blended wing body

In terms of their missions, the BWB began as a very large passenger airliner similar to the Airbus A380. This reflected the expectations of the air travel market at the time [16]. However current market requirements have changed as airlines are preferring smaller long range aircraft that are extremely efficient and can operate from smaller airports [3]. Cargo transport is also interesting for a BWB mission since cabin height limits are more flexible allowing for a different sized aircraft, passenger comfort issues such as cabin partitioning and windows are eliminated and emergency exit location and evacuation routing issues are resolved. Furthermore the air cargo market is forecast to grow at a faster rate than the passenger market [3]. Coupled to this is the desire of cargo operators to use smaller, cheaper and less busy secondary airports for cargo hubs which often have strict night time noise limitations due to proximity of surrounding populations [3]. BWB aircraft, with their lower noise signature and cargo volume flexibility, can solve these issues [13]. Generally the wing loading for a BWB aircraft is lower than that for TAW ($\approx$ 2000-3000 vs. $\approx$ 5000-7000 N/m^2) [1]. This is due to two factors, firstly the BWB has lower $C_{L\,\max}$ values than TAW requiring a lower wing loading for acceptable low speed performance [17]. Secondly the low aspect ratio of the BWB causes induced drag to increase rapidly, resulting in $M(L/D)_{\max}$ occurring at a very low cruise C_L [1]. In order to fly at this low C_L the wing loading is lowered. Raising the cruise altitude helps match the C_L and $M(L/D)$ improving aerodynamic efficiency but has a negative impact on engine thrust specific fuel consumption [18]. However at increased altitude there is increased pressure differential on the fuselage to maintain required cabin altitudes, impacting heavily on the already challenged fuselage concepts, leading to increased structural mass [19, 20]. Cruise speed is another important choice and BWB tend to maintain conventional TAW cruise speeds due to $M(L/D)$, flight durations and aircraft availability [1]. Even higher cruise speeds have also been investigated and the BWB shows promise to be able to handle higher speed with minimal transonic drag rise due to the design flexibility that can be exploited [21, 22]. $M = 0.93$ can be achieved with only a 10% decrease in $M(L/D)$ versus $M = 0.85$ but any faster and a sharp drag rise is unavoidable.

Structural solutions for the fuselage have been a subject of intense investigation because the non-cylindrical pressure vessel present in the BWB is less structurally efficient and requires novel design [23]. Various concepts have been proposed and deemed feasible, grouped mainly by possessing a single or double skin. Single skin concepts are those such as the integrated skin-shell concept of [16] and the oval fuselage of [19] and use the same structural skin for pressure and aerodynamic loads. Double skin concepts such as the multi-bubble of [24] or the y-braced vaulted multi-bubble of [23] use an inner skin designed to carry pressure loads and outer skin to carry aerodynamic loads. The oval fuselage [19] has already been implemented in the Initiator because it demonstrates potential feasibility and advantages over other designs such as lower part and join counts giving manufacturing and cost savings, improved cabin layout flexibility and greater synergy with structural elements such as the wing carry-through structure [19] and [25]. It does however pose drawbacks with aerodynamic shaping as it is heavily linked to the structural shape and increased unused pressurised volume. Mass estimation of the BWB is a challenge due to the unconventional fuselage and its effect on the rest of the structure, but methods to do so have been developed and verified. Most notably are those of reference [26] for the whole airframe and references [19, 25, 27] for the oval fuselage specifically.

Stability and control are also vital topics for the BWB, especially longitudinally since most BWB designs lack a horizontal stabiliser or canard. Stability thus needs to be a result of the planform shape and aerodynamics of the aircraft as a whole. Planform modifications include the sweep angle of the wings to move the aerodynamic centre (AC) and can be effectively applied as done in [15]. However, reference [28] has found that combining sweep and twist can lead to higher induced drag due to a loss of effective span. In order to combat this [28] proposed the method of front loading the fuselage airfoils, giving them a positive C_m, which is used to counter the negative C_m of conventional transonic airfoils on the outer wings. This method showed lower drag production and improved performance over a range of lift coefficients. Short moment arms to control surfaces make for low control effectiveness and large control hinge moments [16]. Typically a number of independent control surfaces are present which makes for a complicated control allocation problem which requires careful design in order to achieve the lowest trim drag [29]. These factors negatively impact the flight control system and can cause increased weight [1].

As mentioned before the Initiator is a conceptual aircraft design tool that executes the design synthesis process given in Figure 1.2. During this process various convergence loops are executed in order to achieve consistency between design disciplines. The first loop begins with analysis of the aircraft's TLR and an initial Class I mass estimation [30]. The geometry is then laid out and sized [10] followed by higher fidelity Class II mass estimations [31] and the semi-empirical and analytical estimation of the aerodynamic performance of the aircraft [10, 32]. This is followed by an analysis of the engine performance in terms of specific fuel consumption (SFC), in the design and off-design condition [10]. This completes the first loop and the results of the modules are fed back into the beginning of the design process and the process begins the next iteration. This continues until convergence, in terms of the aircraft maximum take-off mass (MTOM), is achieved. Following this is the next design loop that analyses the longitudinal [33] and directional stability [34] and makes design changes to assure the aircraft meets its requirements in this regard. Lastly for this loop is the analysis of the missions for which the aircraft is designed, namely all input, harmonic and ferry missions, in terms of performance, fuel burn and emissions [20]. The results of the stability, control and mission analysis routines is again fed back to the beginning of the process and the next iteration begins. Design choices regarding the previous analyses are thus taken into account and a new convergence point is found during the first loop. These two loops subsequently iterate with each other until the overall convergence point is found. The last two modules are the higher fidelity physics-based Class II.5 mass estimations. *EMWET* is an in-house developed code which determines the wing structural mass [35]. The code has been extensively verified and validated by reference [35] to an average wing mass error of 2.10% and is recognised in the faculty. This is followed by the fuselage structural mass estimation. This physics-based semi-analytical method has again been developed in house, firstly by references [19, 25] for isotropic materials and recently by reference [27] for composite materials. Again the updated mass results are fed back and iterated. Once convergence is achieved in the last loop the process is complete and the aircraft has achieved a consistency in terms of geometry, mass, drag and overall input and output parameters and which is feasible in all main aspects of aircraft conceptual design. The data is stored in the form of output reports and a data file in XML structure and the program exits. Comparisons between concepts can be made based on these results or the next stage of aircraft design can be initiated, using the Initiator results as input and hence the namesake: *Initiator*.

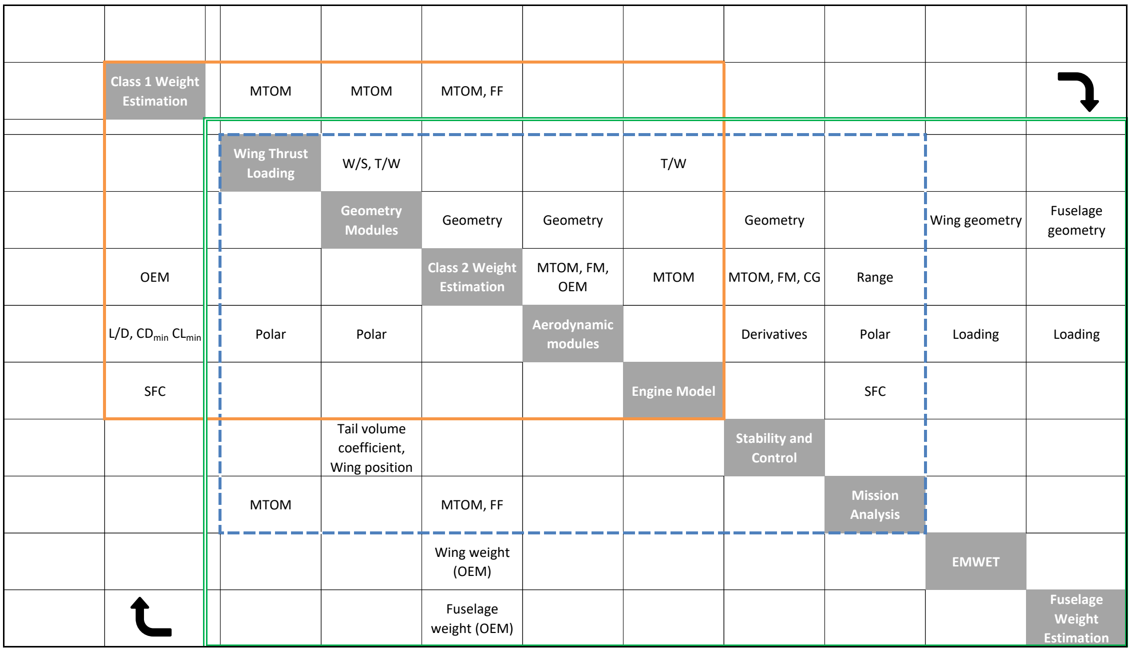

Figure 1.2: N2 chart of the Initiator showing the implemented design and analysis methods.

1.2. RESEARCH SCOPE AND GOALS

The scope of this research is limited to a conceptual design level with methods of according fidelity. It is focused on the BWB passenger transport aircraft and the comparison to its conventional TAW counterpart. Methods are also bound to those which are implementable in the Initiator within the time frame available, meaning for example that external analysis tools that are already developed but require complex interfacing routines with the Initiator are not feasible. It is the goal of this work to ultimately improve on the existing BWB knowledge base by providing a method of rapidly designing and analysing a wide array of BWB aircraft on which conceptual comparisons can be based. In so far it will also achieve the goals of implementing a suitable geometry model of the BWB, performing requirement satisfaction, mass, drag, stability and control analyses and mission performance estimation completing the main sections within the analysis loop of the Initiator shown in Figure 1.2.

1.3. RESEARCH QUESTIONS

The main research question posed for this thesis is as follows:

- How do a range of blended wing body aircraft compare to tube and wing aircraft for equivalent top level requirements while achieving the same design goals and using similar design methods?

This can be further expanded with the following sub-questions:

- What methods are appropriate such that an accurate, sub-group inclusive and feasible geometric model of the blended wing body aircraft can be designed to a conceptual level within an automatic design environment?
- What are the most important and limiting topics of blended wing body design, sizing and analysis considering its performance and feasibility to a level which is suitable for conceptual comparison to tube and wing aircraft?
- What constitutes a fair comparison between aircraft designs at a conceptual level?

2

Geometry Methodology

A proper analysis of an aircraft design can not continue without a model of the aircraft geometry of some form. An adequate model is one of sufficient detail from which required geometrical properties used in subsequent analyses can be extracted. For the Initiator, and conceptual design, this includes the 3-view layout, aircraft component parameters (such as wing sweep angle), provision of payload carrying components (such as the cabin layout), aerodynamic surface properties, structural elements and feasibility analysis such as take-off scrape angle or fuel tank volume. Such models are already implemented in the Initiator but lack the functionality to satisfactorily design a BWB. The model for the BWB implemented herein makes use of the current geometric elements where possible. New elements added are discussed in the proceeding sections and the total BWB geometric model is presented thereafter. The process followed in the build up of the geometry is shown in Figure 2.1. A convergence is run, as explained in more detail in Section 2.2, in order to achieve consistency between fuselage and outer wing geometry. The process could be improved in terms of execution time by looping back to fuselage planform shaping, instead of cabin planform shaping, because the cabin is not influenced by the wing as discussed later. The Initiator's chosen module structure does not allow for such an improvement but it is recommended if this scheme is used elsewhere.

Before progressing, the philosophy behind the geometrical methods is explained. In order to simplify methods and implementation the geometry is first defined on the 2D XY-plane (planform shape). The Z components of the geometry are then determined from separate routines and concatenated to the XY data, forming the complete 3D geometry. This decouples the shaping methods and allows for alterations to be made to each shaping routine individually. The benefit of this is that it makes conceptual shaping easier since the influence of input parameters is more straightforward and are design logic orientated. The methods implemented also do not require complicated computer aided design (CAD) kernels and as such can also be programmed in many open source coding environments.

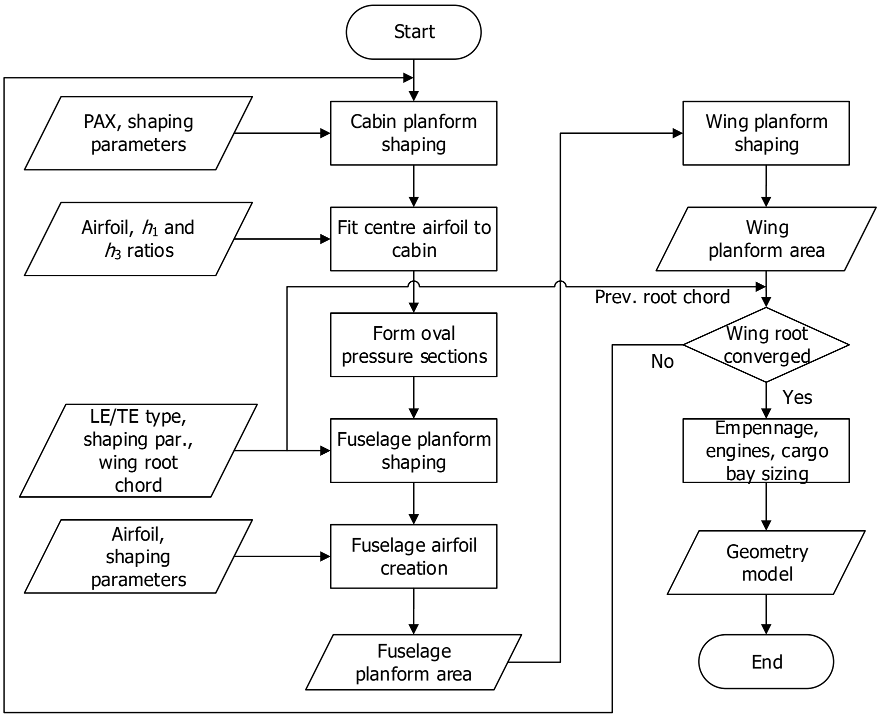

Figure 2.1: Process followed during geometry estimation of the BWB in the Initiator

2.1. CABIN GEOMETRY

The geometry sizing process begins with the cabin of the aircraft since this is the component that needs to carry the payload around which the aircraft is formed. In literature most BWB cabins have a *home-plate* shape with a forward straight tapered section with a rectangular section behind it [36]. This is in some way similar to conventional aircraft which can have an additional tapered section at the rear. It was decided to combine these two points into the straightforward cabin planform parametrisation given in Figure 2.2. The parametrisation allows for an aft taper where the airfoil thickness is reducing towards the trailing edge (TE). The aft taper helps fit the outer corner of the cabin inside the the thinnest part of the fuselage near the TE at this corner. Furthermore, the parametrisation allows more cabin shapes to be created compared to the *home-plate* definition increasing the design options at this conceptual stage. The length of the centre and aft section are linked to the length of the first section l_0 through the length ratios u_1 and u_2 respectively. The widths of these sections are also linked to l by the width-to-length ratios v_1 and v_2 respectively. This parametrisation might seem unconventional, but it maintains the shape of each section independent of the other sections and overall cabin size, allowing for easier and more intuitive manipulation of the cabin shape and unitary scaling between different sized BWB cabins. It also has a lower variable count than other parametrisations tried which would benefit future optimisation routines. These length and width ratios along with the cockpit width w_{cp} are the 5 input variables that fully determine cabin shape. The size of the cabin is determined from the required number of passengers (pax) and a empirical passenger-per-area ratio giving the required floor area S_{floor}. Length l_0 is determined by solving Eqn. 2.1 from which the lengths and widths of the sections are evaluated with their length and width ratios.

$$S_{floor} = [0.5v_1 + u_1 v_1 + 0.5u_2(v_1 + v_2)]\, {l_0}^2 + 0.5 w_{cp} l_0 \tag{2.1}$$

Seating layout is applied to the sized cabin planform, an example of which is shown in Figure 2.3. This is done by placing predefined seats in rows as wide as the cabin locally allows while holding to §CS 25.817 which states that no more than 3 seats abreast may be placed on each side of an aisle. The routine has not been greatly modified from that used for conventional aircraft due to time constraints and the acceptable results that are achieved with the conventional methods for this stage of implementation. Emergency ex-

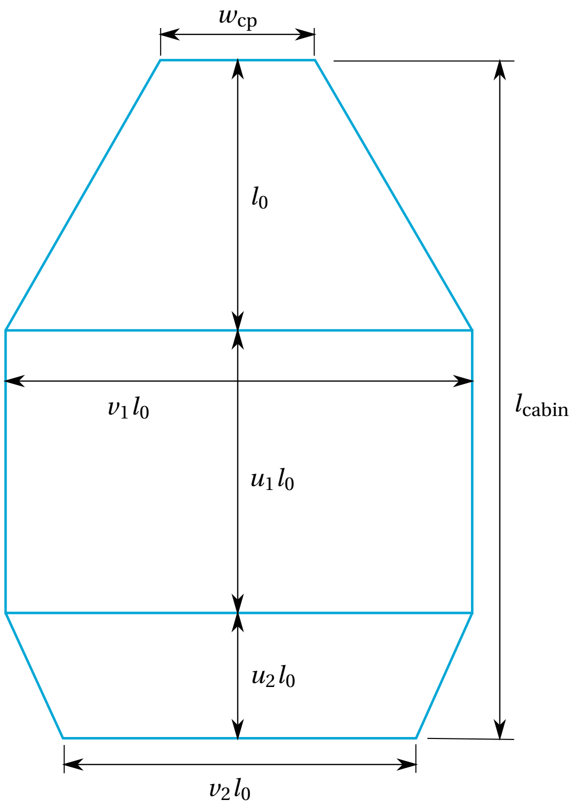

Figure 2.2: Parametrisation of the cabin floor, note l_{cabin} is not a variable but a result of the parametrisation.

its are determined based on the number of pax and placed with the maximum spacing in accordance with §CS25.807 thereby providing the number of exits on the sides of the fuselage as shown. Feasibility of the exits at the same fuselage station (FS) as the wing can be brought into question as it is expected to be difficult to place exits here from a structural point of view. Galleys and lavatories are placed at these exits (if required) and stretched across the span of the cabin due to using the conventional TAW aircraft methods. Such a long narrow galley might however be impractical for actual use. Diagonal aisles, as commonly seen in BWB cabin designs [16], are not implemented and aisle alignment in general needs to be improved. However, these are not always necessary [37] and depend on the emergency exit location. The seat placement routine can be significantly improved in future by addressing these issues and implementing aspects unique to the BWB. These are studied and implemented in [38], but include diagonal aisles, emergency exits in the aft pressure bulkhead and centrally located galleys and lavatories (not spanning the full cabin width). Additionally, the current routine has originally been programmed to fill the last row of a seating class if it is only partially filled by the required pax in the class. In a BWB this can lead to considerably more seats being placed than required due to the increased number of pax in a row. These are added to the passenger count and mass, reducing the allowable cargo mass when designing for constant payload mass, as is the case with the Initiator. This could be improved in future. The impact of these updates should only result in a minor change with respect to cabin area required but will improve the cabin's feasibility.

All BWB aircraft use an airfoil shape of some kind over the centre body. The fuselage definition used in the Initiator requires the airfoil shape at the centre section as input. Therefore the previously sized cabin needs to fit within this center airfoil. This is done by scaling the chord of the airfoil and optimising the fit of the cabin box defined by the required overall cabin length l_{cabin} and cabin structural height h_{struc}. The waterline datum definition within the Initiator is the cabin floor and as such needs to be placed at $Z = 0$. The airfoil is then moved up and down for best fit. Rotating the airfoil can also lead to a better fit, sometimes reducing wetted area considerably. The routine also levels the floor of the cabin, allowing for easier analysis of the geometry. This does however set the incidence angle of the fuselage airfoil with respect to the cabin. The cabin deck angle needs to be a reasonable value in cruise ($\leq 3°$) and needs to be checked once the cruise angle of attack (AoA) is known. The results of this process are shown in Figure 2.4.

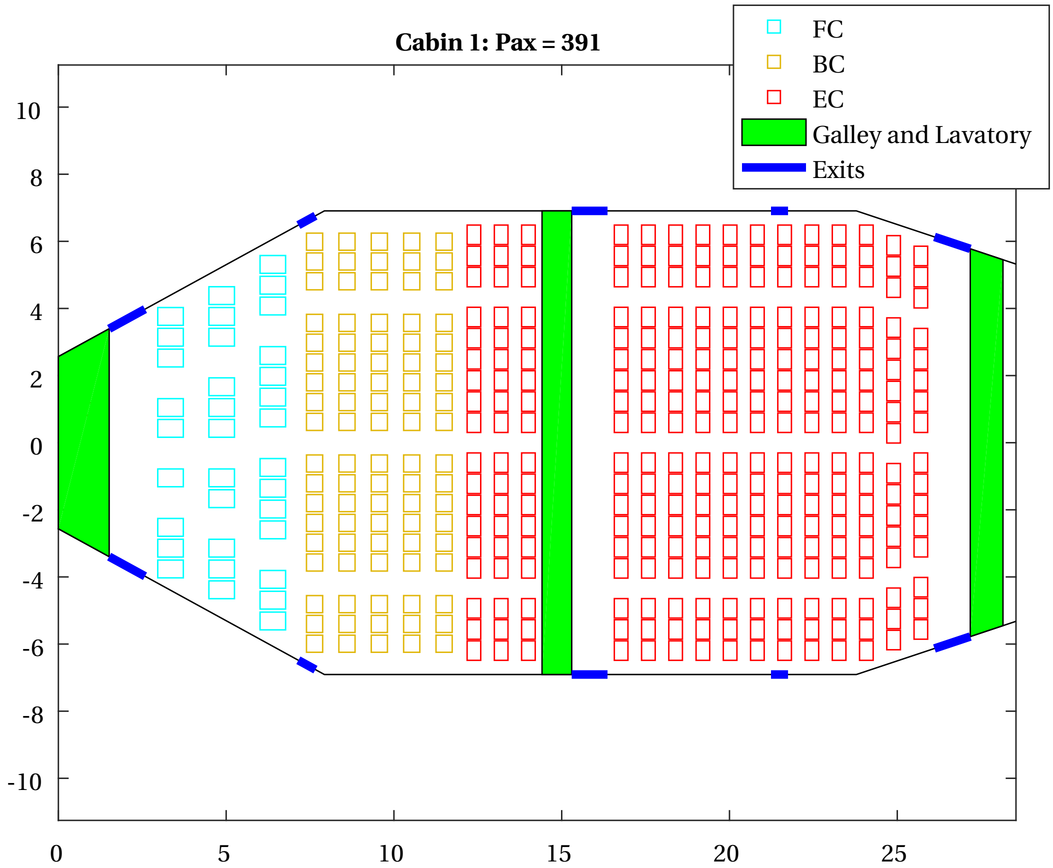

Figure 2.3: Seat placement and cabin layout of a typical BWB in the Initiator

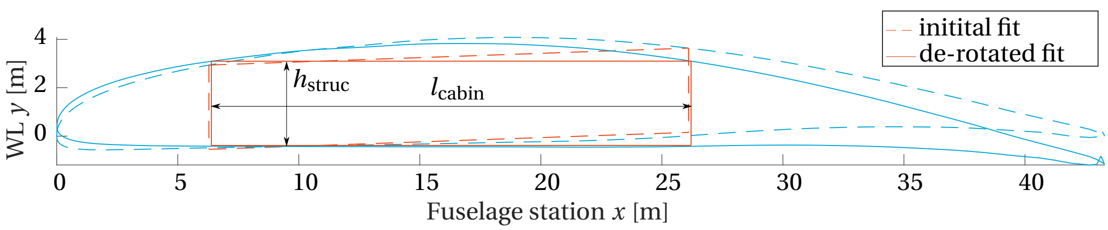

Figure 2.4: Fitting of the cabin outline within the centre airfoil showing de-rotation of the cabin

Once a suitable centre airfoil is fitted and the floor planform is defined, the cabin pressure structure can be formed. This is done using the oval fuselage definition developed by references [19, 25] and is shown with the main design parameters in Figure 2.5. The three discrete but tangent arcs result from the local heights h_1 and h_3 and the local cabin floor width w_{cabin}. The structural height is the total height of the section and is used to fit the airfoil at the most fore and aft section as, shown in Figure 2.4. Importantly, h_1 and h_3 can not be zero, as this would cause the radius of the top or bottom arcs to be infinite, leading to a flat panel which is inefficient at carrying the out-of-plane bending loads due to pressurisation. As the radius of the arc tends towards infinity, the required thickness of the structural panel increases, and so too does the weight, as demonstrated in reference [26]. The oval section is determined at each of the four discrete cabin corner points, forming the total pressure shell as shown in Figure 2.6.

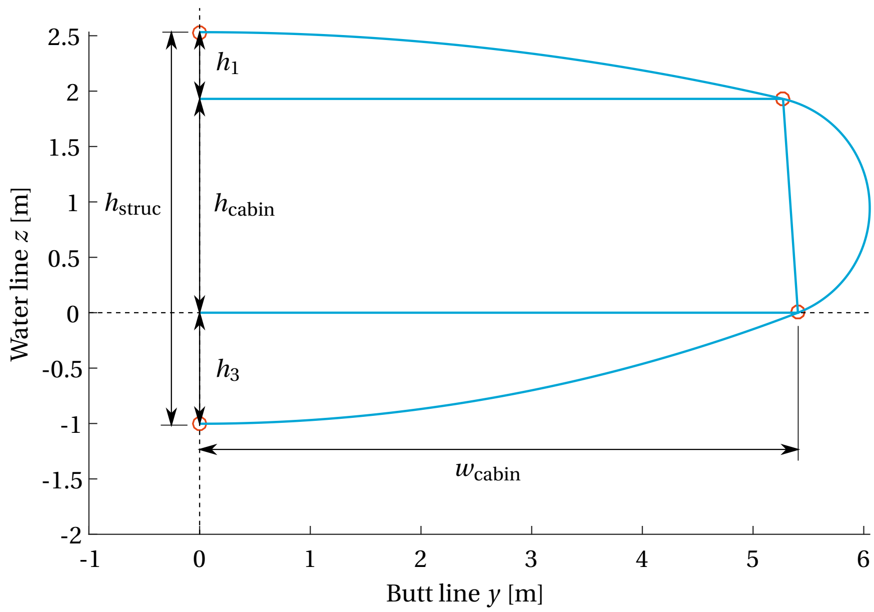

Figure 2.5: Definition of the oval fuselage half cross section on the YZ-plane

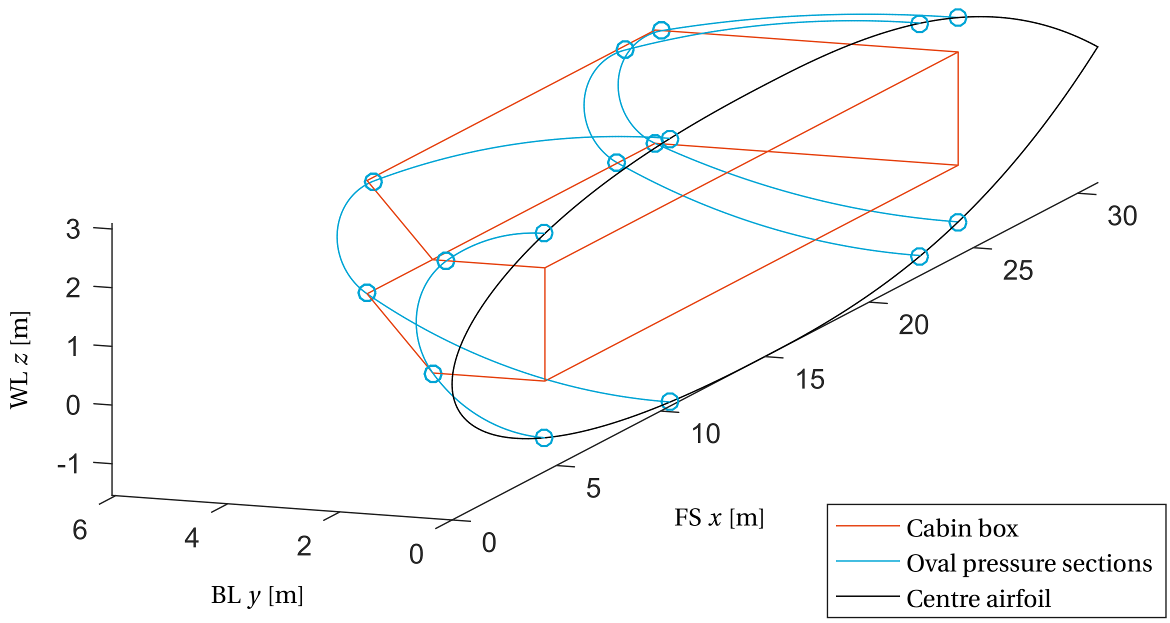

Figure 2.6: Half oval fuselage sections fitted to the centre airfoil and cabin corner points giving the 3D pressure shell geometry

2.2. FUSELAGE PLANFORM SHAPING

Now that the shape and definition of the cabin and main pressure shell is complete, the aerodynamic planform shape of the aircraft, including the nose and tail sections, can be formed around this cabin. There is no common shape which has been applied to the fuselage planform in literature and no clear consensus as to the best shaping routine could be found. Hence, it has been chosen to develop a new, highly flexible and straightforward parametrisation method. The method is performed in two main steps: the first is to choose the overall shape of the leading edge (LE) and TE and the second is to refine the planform shape with the specific shaping parameters. Since LE and TE shapes of BWB aircraft vary in literature, from straight lines to reflexed curves, three global options have been implemented and are shown in Figures 2.7a, 2.7b and 2.7c. Different types of LE and TE can be mixed, for example a *structural* LE with a *straight* TE, which allows for more design freedom. These options allow a vast array of different BWB planform shapes to be created and analysed using the same methods, which is typically not possible with other design tools.

The rationale behind the *structural* LE or TE type, shown in Figure 2.7a, is that the structure of the pressure shell forms the LE or TE between the dashed black lines without the need for an aerodynamic fairing. This should reduce the part count, structural mass and manufacturing costs. It also has a lower planform and wetted area, leading to a more compact design and reduced friction drag. It can however have an overall aerodynamic penalty because the airfoil shape is fully dependent on the pressure shell shape. This can be suitable for the LE, where a blunt nose can still perform satisfactorily, but a blunt round end at the TE can lead to separation and significant drag. The extent and impact of this can however not yet be confirmed and thus the option for a *structural* TE is kept, allowing for future investigations. The planform is completed with the shaping of the nose, tail and wing fairing sections. Of these sections only the nose is pressurised for the cockpit.

The second option is the *loose* LE or TE, shown in Figure 2.7b, where the path of the LE or TE is independent of the pressure shell. This option requires some form of fairing to link the LE or TE to the pressure shell, forming a double skin. This increases the part count, structural mass and wetted area. More curved panels are used, potentially leading to a negative impact on manufacturability. The main advantage is that an aerodynamically shaped cap is added to the nose and tail of the fuselage airfoils, forming a more conventional airfoil. These shapes can subsequently be altered to improve the aerodynamics of the fuselage, as will be further described in Section 2.3. It is expected that this method is most beneficial for the TE as it helps prevent the separation and drag mentioned with the *structural* type. It also allows for a variation in the chord distribution which can help achieve a more efficient lift distribution, further reducing drag. It also decouples the cabin shape from the fuselage shape, while the resulting geometry still remains consistent, allowing them to be optimised separately. Conflicts can however occur as the LE or TE must remain outside of the cabin. A LE or TE passing through the cabin would not be feasible and should be resolved by varying the shaping of either the *loose* LE or TE or the cabin planform shape.

Lastly a *straight* TE can be used, shown in Figure 2.7c. This is similar to the *loose* option, but straight lines are used. This is to take the previously mentioned point of manufacturing into account and is also considered with regards to the instalment of control surfaces. It is expected that elevators will be required on the TE of the fuselage for longitudinal control and trim of the aircraft. These could be simpler to implement and manufacture for a straight TE than for a curved one. The longitudinal position of the control surfaces is important as a more aft location leads to increased moment arms and better longitudinal pitch control [11]. The *straight* TE could also show better performance in this regard than the *loose* one but is dependent on the actual shape resulting from the method, as found in reference [11]. Finally, this option also maintains the airfoil shaping advantages of the *loose* type.

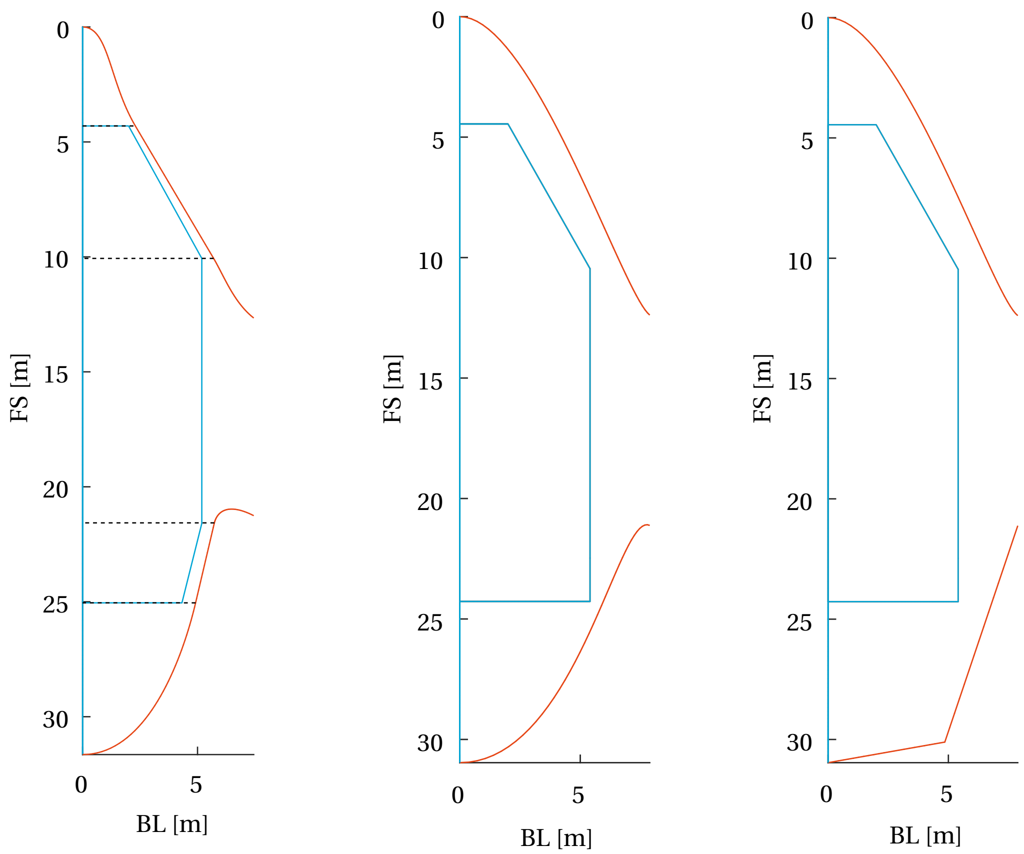

(a) *Structural* LE or TE

(b) *Loose* LE or TE

(c) *Straight* TE

Figure 2.7: Depictions of the three implemented LE and TE shaping options which define the overall fuselage planform shape

Once the overall shape of the LE and TE is chosen, the second method of fuselage planform shaping is performed by modifying the shaping parameters based on the LE and TE type. The parametrisation of each type will be described separately.

The *structural* type has the parametrisation shown in Figure 2.8. The nose section is formed from a Bezier curve which begins blunt at the fuselage nose (centre airfoil LE) and ends tangent to the proceeding straight structural line. This line is defined by the outer widths of the pressure shell at the first and second oval sec-

Table 2.1: Design parameter summary of the fuselage LE or TE type

Parameter	#	Influence	Range (typical not firm)
Structural LE or TE			
NoseBluntness	1	bluntness of nose shape	$[0 \rightarrow 1] = [0 \rightarrow w_{\text{cp}}]$: distance along tangent line in Y
LEFairingShape(1)	2	rate of tangent approach	$[0 \rightarrow 1] = [w_{\text{cp}} \rightarrow 0]$: distance along tangent line in Y
LEFairingShape(2)	3	rate of tangent departure	$[0 \rightarrow 1] = [X_{\text{CntPt}} \rightarrow X_{\text{w apex}}]$: distance along tangent line in X
LEFairingShape(3)	4	rate of tangent approach	$[0 \rightarrow 1] = [Y_{\text{w apex}} \rightarrow Y_{\text{CntPt}}]$: distance along tangent line in Y
TailBluntness	5	bluntness of tail shape	$[0 \rightarrow 1] = [0 \rightarrow v_1]$: distance along tangent line in Y
TEFairingShape(1)	6	rate of tangent approach	$[0 \rightarrow 1] = [X_{\text{CntPt}} \rightarrow l_{\text{f}}]$: distance along tangent line in X
TEFairingShape(2)	7	rate of tangent departure	$[0 \rightarrow 1] = [X_{\text{CntPt}} \rightarrow l_{\text{f}}]$: distance along tangent line in X
TEFairingShape(3)	8	rate of tangent approach	$[0 \rightarrow 1] = [Y_{\text{wing TE}} \rightarrow d_{\text{f}}]$: distance along tangent line in Y
Loose LE or TE			
NoseBluntness	1	bluntness of nose shape	$[0 \rightarrow 1] = [0 \rightarrow w_{\text{cp}}]$: distance along tangent line in Y
LEFairingShape(1)	2	rate of tangent approach	$[0 \rightarrow 1] = [Y_{\text{w apex}} \rightarrow d_{\text{f}}]$: distance along tangent line in Y
TailBluntness	3	bluntness of tail shape	$[0 \rightarrow 1] = [0 \rightarrow d_{\text{f}}]$: distance along tangent line in Y
TEFairingShape(1)	4	rate of tangent approach	$[0 \rightarrow 1] = [Y_{\text{w TE}} \rightarrow d_{\text{f}}]$: distance along tangent line in Y
Straight TE			
TEFairingShape(1)	1	TE kink location	$[0 \rightarrow 1] = [0 \rightarrow v_2 l]$: distance along Y
TEFairingShape(2)	β	angle of TE	degrees from perpendicular

tions. Joining this line to the outer wing apex is another Bezier curve which begins tangent to the pressure shell and ends tangent to the outer wing LE. The TE line is constructed in a similar fashion. Shaping of these Bezier curves is controlled with the variable control points located on the various tangency lines. The minimum of control points have been used which lead to smooth transitions and enough design flexibility. Table 2.1 gives an overview of these control points, their influence on the shape and their scaling. The scaling of the variables is done such that input values between zero and one can be used, independent of the size of the BWB, which increases the ease of use.

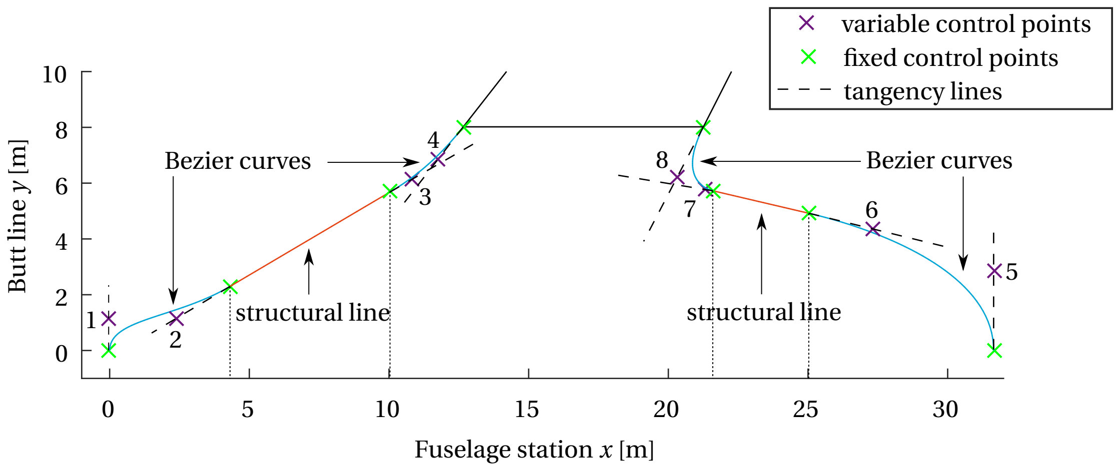

Figure 2.8: Parametrisation of the *structural* LE and *structural* TE type

Parametrisation of the *loose* type is done in a straightforward manner and is based on the work of reference [39]. A single Bezier curve is constructed from the nose of the fuselage to the outer wing apex. It begins blunt at the nose (centre airfoil LE) and ends tangent to the outer wing LE. It is controlled by 4 control points as shown in Figure 2.9. The TE is similar to the LE and the shaping parameters are summarised in Table 2.1. This type has a lower number of parameters than the *structural* type which increases ease of use and potentially reduces optimisation difficulty. Finally, the parametrisation of the *straight* TE is given in Figure 2.10. The TE is formed from two straight lines which end sharply at the centre airfoil TE and outer wing TE. The location of the kink is set by the Y coordinate of the variable control point and the angle of the TE. The parameters are also given in Table 2.1.

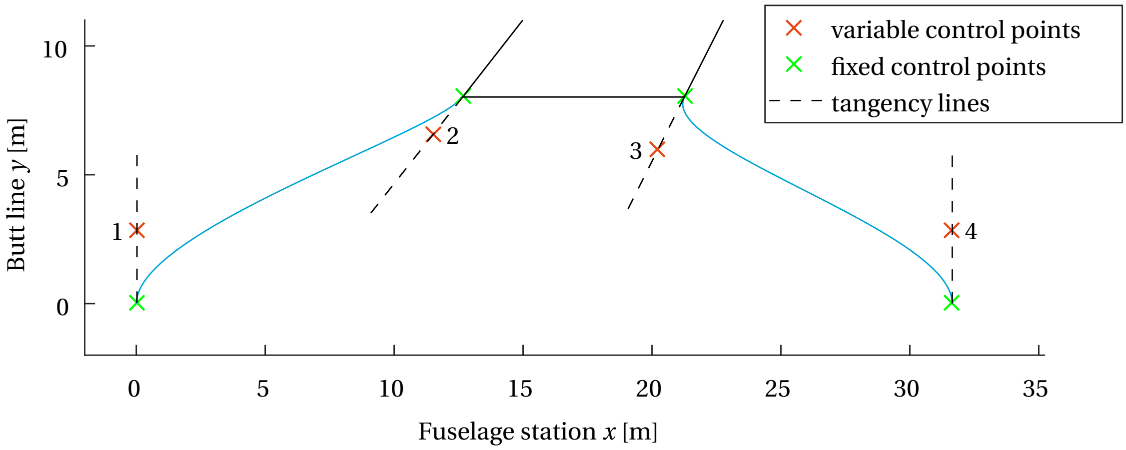

Figure 2.9: Parametrisation of the *loose* LE and *loose* TE type

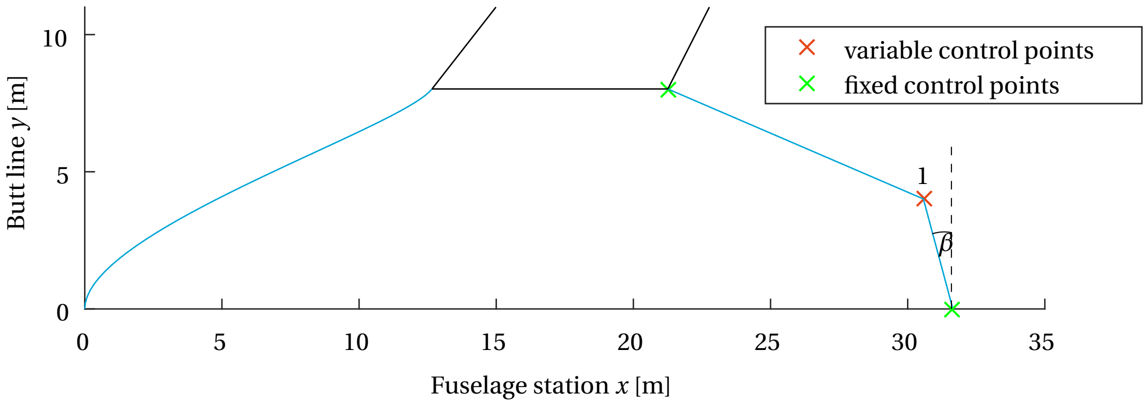

Figure 2.10: Parametrisation of the *straight* TE type

The last topic concerning the sizing of the planform is the link to the fuselage airfoil shapes which are placed along the spanwise direction. More explanation of the actual airfoil fitting is provided in the next section but the link with planform shaping comes in the Z location of the LE and TE. The planform shape (LE and TE curves) has only been defined on the XY-plane. Due to actual airfoil shape and twist, the LE and TE do not necessarily fall on this plane, i.e. $Z = 0$. Since the airfoil shape is governing, the previously defined LE and TE curves need to coincide with the airfoil LE and TE in the Z-coordinate. This is done by creating straight lines, in the YZ-plane, joining each actual airfoil LE and TE respectively and concatenating these Z-coordinates to the XY-coordinates previously found, creating the final LE and TE line in three-dimensional space.

It can be seen in Figures 2.8 - 2.10 that the geometry of the outer wing is required as input for the planform shaping of the fuselage. This forms the link between the sizing for the fuselage and of the outer wing, shown in Figure 2.1, and is one of the main couplings within BWB design. The underlying theoretical reason for this coupling is the inclusion of the fuselage planform area in the total lifting surface area required to achieve the design wing loading [1, 12, 40]. Since the wing geometry is not yet known on the first iteration, an initial guess for the basic wing design parameters is made. This is done for an outer wing of 40 % of the reference wing area as this was found to be a good starting point which minimised the computation time needed to reach convergence. The actual outer wing geometry is used, instead of these guess values, once it is known from subsequent iterations. Thus, once the method converges, both the fuselage and outer wing geometry will agree. The most important wing parameter, which influences the fuselage shape, is the outer wing root chord because it determines the end point of the TE. It is for this reason that the wing root chord is chosen as the convergence parameter for the loop in Figure 2.1. Iterations continue until the difference between the root chords is less than 1 mm (approximately 7 iterations or 15 seconds). The planform area of the fuselage, as defined by the area between the LE and TE curve on the XY-plane, is required and is calculated with suitably discretised spanwise trapezoids. This planform area is used as the fuselage reference area and is also used as the contribution of the fuselage to the required wing area from the chosen wing loading.

2.3. FUSELAGE AIRFOIL GENERATION

In this section the creation of the aforementioned fuselage airfoils is explained. These airfoils give the fuselage its final three-dimensional shape, following the philosophy explained at the beginning of this chapter. As stated before the oval fuselage concept is single skinned, hence the pressure shell forms the bulk of the airfoil shape. This can be more clearly seen in Figure 2.11. A cap is added to the nose or tail of the airfoil if a *loose* or *straight* LE or TE is chosen. If not, the pressure shell forms the whole airfoil. Therefore the pressure shell needs to be sectioned in the XZ-plane (free stream direction) at suitable spanwise positions. The number and spanwise position of these sections are input parameters. Increasing the number of sections does not necessarily improve performance or accuracy as these airfoil sections are also the ones input to aerodynamic analyses described in 3.4. It was found that too sparse or too dense an airfoil distribution can negatively impact panelling and accuracy in the aerodynamic solver. Four linearly distributed (spanwise) airfoil sections were found to give smooth transitions in geometry with acceptable accuracy and computational time.

If required, the caps shown in Figure 2.11 are formed from Bezier curves based upon the successful method developed in reference [41]. Upper and lower surfaces are designed separately, each with their own Bezier curve controlled by four control points. The cap is made to end tangent to the pressure shell with the intersection point being determined from the first point at which the resulting Bezier curve is convex. Convexity is chosen as the determining factor as this proved to be the most robust method tested in terms of finding the intersection between pressure shell and airfoil cap. Resulting airfoil shapes are smooth and consistent but convexity does limit the airfoil shapes that can be formed. Concave airfoils, such as those found in reference [41], are not possible. If in future it is decided that these airfoils are needed, or lead to significant performance improvements, the intersection between the cap and pressure shell should be determined with a different method. An example of such a method, which was tested but gave poorer results, is to find the point at which a straight line originating at the LE or TE tangentially intersects the pressure shell. The middle two control points of each Bezier curve are variable based on input shaping parameters. They represent the nose bluntness and curvature of the cap at the LE and the boat tail angle and curvature at the TE. This gives a simple and efficient way of manipulating the cap shape with only eight parameters for a full airfoil or four for partial airfoil if a *structural* LE or TE is used. These caps are then appended to the pressure shell sections at the intersection points and form the final airfoil.

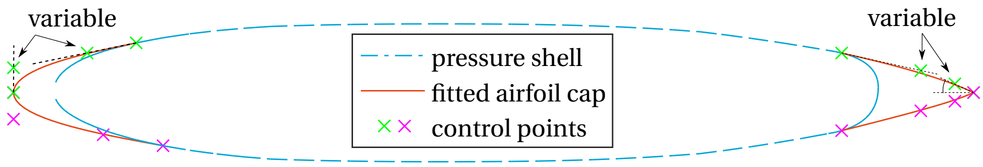

Figure 2.11: Formation of the fuselage airfoil from the combination of the sectioned pressure shell and a fore and aft cap

Sectioning and creation of these fuselage airfoils occurs at user defined input locations. This divides the fuselage into its aerodynamic sections and creates the airfoil stack which will later be used during aerodynamic analysis of the fuselage. For visualisation purposes within the Initiator, the aerodynamic surface which forms the fuselage is linearly lofted between these airfoil sections. Linear interpolation has been chosen since this is the method used by the aerodynamic analyses in AVL and other empirical relations explained in Chapter 3. This linear interpolation brings a noteworthy inconsistency with the current BWB implementation. The oval fuselage concept is intended to use the pressure shell as the aerodynamic outer shell for mass considerations [19]. The oval arcs of this definition do not allow for a linear variation across the span, as seen in

Figure 2.5. Hence the aerodynamic surface does not perfectly match the pressure surface. This is an unavoidable consequence with the current aerodynamic analysis methods and its impact can not be quantified. The impact of this is lessened by the sectioning of the fuselage to create the airfoils. At these sections the aerodynamic and oval pressure surface match and it is only between them that discrepancies build up. This is further limited by increasing the number of airfoil sections. Again this number is limited regarding the panelling for aerodynamic analysis stated previously. Four airfoil sections again result in acceptable errors as seen in Section 4.1.

2.4. OUTER WING SIZING

Using the completed fuselage geometry, the outer wing can be sized, as shown in Figure 2.1. The outer wing is a straight trapezoidal wing, as is the case for all BWB aircraft in literature [1]. Literature is unclear as to the definition of the total reference area but the authors of [40] and [12], among a few others, use the total gross planform area of the fuselage and outer wings. This is also chosen for the current work and stated in Eqn. 2.2, where S_f is the previously defined fuselage reference area (Section 2.2) and S_w is the planform area (XY-plane) of one of the trapezoidal outer wings. The reference wing area, S_ref, is determined from the design wing loading discussed Section 3.2. The required area for the outer wings is therefore the difference between S_ref and S_f. Firm definitions of the aspect ratio are also unclear in literature and various types are used, such as the trapezoidal, gross and wetted aspect ratios [12]. It is more common to see the gross aspect ratio being used and this is also adopted as the aspect ratio A unless otherwise stated. Eqn. 2.3 shows the definition of the aspect ratio where b is the total reference wing span from wing tip to wing tip. This aspect ratio is an input parameter for the Initiator and the reference span can be evaluated from Eqn. 2.3.

$$S_\mathrm{ref} = S_\mathrm{f} + 2S_\mathrm{w} \tag{2.2}$$

$$A = \frac{b^2}{S_\mathrm{ref}} \tag{2.3}$$

The longitudinal and lateral positioning of the wing root apex is set by input fractions of the fuselage length and width respectively. The span of the outer wing is defined from the apex to the wing tip and represents a conventional half span. These conventions are laid out in Figure 2.12. The sweep angle of the LE is initially determined from wave drag limitations using simple sweep theory and refined by the Korn equation [42] which has been implemented and tested in the Initiator by Vargas [32]. This sweep angle is revised later on in the design process during the stability analysis (Section 3.5). In subsequent design iterations the sweep angles from this stability analysis are used as inputs and compared to the sweep required for the Korn equation, with the larger of the two being limiting. Wing taper ratio λ_w is determined from statistical fit in Torenbeek [43] for the obtained wing sweep. Using this taper ratio and the wing reference area, the root chord c_r can be determined from Eqn. 2.4. The tip chord c_t follows from the definition of the taper ratio. Input airfoils are placed at the root and tip sections. Airfoils chosen for the outer wing are the same as for conventional TAW aircraft and are supercritical sections based on the Boeing 737 kink and outboard airfoils [44]. Different airfoils have been tested to check that methods are functioning but no thorough investigations were done as to the best airfoil choice. The chosen airfoils should however still be feasible considering the results of reference [28] where it was found that conventional supercritical airfoils can be used and actually benefit the design. The root chord resulting from Eqn. 2.4 is compared to the one used during fuselage planform estimation, outlined in Section 2.2. The root airfoil of the wing is also used as the airfoil at the termination of the fuselage such that these surfaces are consistent at their intersection.

$$c_r = \frac{2S_\mathrm{w}}{b_\mathrm{w}\,(1+\lambda_\mathrm{w})} \tag{2.4}$$

The Korn equation requires the C_L of the wing as an input for the method as the wave drag created is dependent on the amount of lift the wing must generate [42]. On a conventional aircraft this is done by equating the lift required to the MTOM and reference wing planform area. For a BWB however this would result in a very low C_L, due to the inclusion of the fuselage planform area in the reference area, which would lead to an underprediction of the drag divergence Mach number and accompanying wing LE sweep angle. The C_L of the outer wing needs to be determined in order to properly implement the method. This has been done by using the design lift distribution over the complete fuselage-wing combination. It has been chosen to make the design lift distribution an input parameter for the BWB. This was done to take the results of

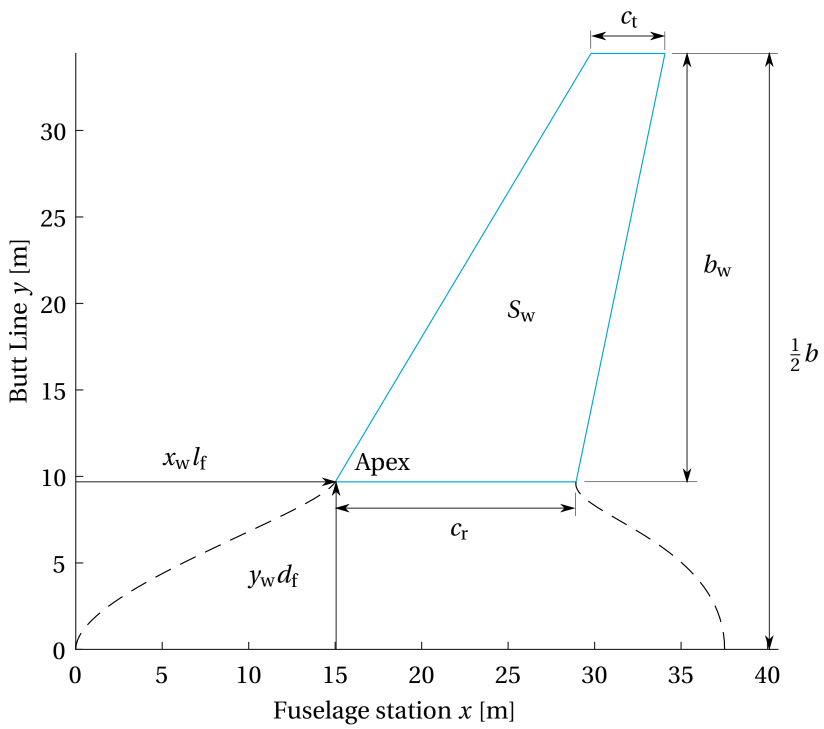

Figure 2.12: Definition of the outer wing geometry

the accompanying literature survey into account concerning the link between lift distribution and wave drag over a BWB and the difficulty of analysing wave drag at conceptual level. It was envisaged that aerodynamic convergence or optimisers would later adjust the geometry and airfoils of the fuselage and wing in order to meet this design lift distribution. This would allow for analysis of the impact of the lift distribution on aerodynamic efficiency, wing mass, stability and overall aircraft performance. Due to time constraints this was not feasible to implement but the input lift distributions are still determined for the aircraft at hand.

Qin [45] found that a distribution which was elliptical over the fuselage and changing to a triangular loading over the outer wing was optimal in terms of the combination of induced and wave drag and it also lowers wing root bending moment and wing mass. For these positive reasons this distribution is implemented in the Initiator. Secondly, the standard fully elliptical distribution is implemented following the recommendations of reference [40]. Lastly, for completeness, a fully triangular distribution is also added. These lift distributions are solved for the current aircraft cruise mass and requirements, giving the magnitude of lift over the span of the fuselage and wing. The portion carried by the outer wing is determined from the area under its distribution and hence the value of C_L for the outer wing is found. This is the C_L under which the outer wing as a whole operates, similar to a conventional aircraft wing, and hence the lift which will determine the wave drag produced. These are the conditions required by the Korn equation [42]. Accordingly this C_L is used to determine the required sweep of the outer wing for acceptable drag. The actual wave drag produced by the configuration is determined later as described in Section 3.4.2.

2.5. AIRCRAFT LAYOUT

After convergence of the fuselage and wing is achieved the rest of the aircraft geometry is estimated. This includes the vertical stabilisers, engines, landing gear and cargo bay. The sizing and layout of these components is largely similar to conventional TAW aircraft and is detailed in the subsequent sections.

2.5.1. VERTICAL STABILISERS

The choice of vertical stabilising surfaces is to be defined by the designer with the option to use vertical tails, winglets or a combination of both. This is done to allow for design freedom as both methods are seen in literature [2, 37, 46]. Winglets are sized based on their input shaping parameters as for conventional aircraft in the Initiator. There is currently no direct estimation of their required size for stability and control purposes as no suitable sizing method could be found in literature. It is therefore up to the user to choose suitable winglets where the work of [46] can be consulted as a starting point. Vertical tail sizing is done as for conventional aircraft by using tail volume coefficients, conform to references [2, 47]. Interestingly, Larkin [2] has found that using this method, a BWB can be sized with satisfactory directional stability with a volume coefficient significantly smaller than conventional aircraft. The test case required a volume coefficient of 0.02417 which is 40.5 % lower than an Airbus A380. The study also found that due to size limitations twin vertical tails should be used. Inclining these tails improves the aircraft's yaw response to sideslip and rudder inputs but it increases the drag slightly over straight tails. The author however recommends inclining the tails which is common in literature and followed in this study.

The total area required for the vertical tails S_v is determined from Eqn. 2.5 where k_v is the vertical tail volume coefficient, b is the reference wing span and S_{ref} is the planform reference area. l_v is the tail moment arm, defined as the distance between the aircraft CG and the quarter chord of the mean aerodynamic chord of the vertical tail. This area is equally distributed to the two vertical tails, which are defined by their input aspect and taper ratios. The sweep angle is set 5% larger than the outer wing sweep to prevent flow separation at design dive Mach numbers as for conventional aircraft [2, 44]. The angle of inclination is also a user input and set in accordance with reference [2]. The tails are positioned at the rear of the fuselage and separated by a distance such that the engines can be located between them.

$$S_v = \frac{k_v b S_{ref}}{l_v} \tag{2.5}$$

2.5.2. PROPULSION

Conventional turbofan engines have been chosen for the current BWB investigations as the objective is to compare the BWB to conventional TAW aircraft. Turbofans also represent lower developmental risk [48] on top of the already riskful design of the BWB and show potential to keep improving on fuel efficiency and maintaining future viability [6]. Other engine systems such as open rotors [12] and boundary layer ingestion [49] suit the BWB configuration well but the complexity in analysing these propulsion types at conceptual level [50] negates their use in the Initiator for this study due to time limits. Engines are sized based on the engine length and diameter that results from statistical fits through reference engine data for the required thrust per engine [51]. It is chosen to locate the engines over the rear of the fuselage. This helps balance the aircraft, shield noise and limits foreign object damage [1, 6]. It also lends itself well to structural integration as the strengthened rear bulkhead is located roughly underneath the pylons and gives the opportunity for structural synergy. The outer wings will however lose bending relief and increases in mass are expected. Engines are placed at the XYZ-coordinates determined from input fractions of the fuselage length, diameter and height respectively. The input fractions are not automatically updated by the Initiator throughout the design process, requiring an initial manual check of the engine location for conflicts with other structures, for example with the vertical tail. Installation drag penalties due to interference are taken into account based on the results of reference [17] which found that a drag penalty of 1.4% is achievable. A 2% unaccounted drag penalty is already added to the zero-lift drag of the aircraft, as discussed in Section 3.4, and it is assumed that this includes the increase in drag due to installation of the engine.

2.5.3. LANDING GEAR

Landing gear layout and design is done following the procedures given in [52] as for conventional aircraft. This is suitable for the BWB as the landing gear needs to perform to the same ground handling and airport specifications as TAW aircraft. The landing gear is placed and sized by the following constraints from [52]: aft tip-over, lateral tip-over, rotation tail strike, nacelle ground clearance, wheel-to-fuselage clearance and the minimum and maximum nose gear load. Both the nose and main gear are placed on the fuselage for a BWB as it is commonly wide and long enough to accommodate the gear at suitable locations [11–13]. It is proposed that the main gear retracts underneath the cabin in the thick underbelly. There is sufficient thickness around the centre of the fuselage for the width of the main gear. It must still be manually checked that the gear fits within the fuselage shell as an automatic check for this constraint has not yet been implemented.

2.5.4. CARGO BAY

The cargo bay is located underneath the passenger cabin in the pressurised oval shell. The oval fuselage lends itself well to the placement of cargo in the BWB concept. The large uninterrupted space allows for efficient placement of cargo containers. In order to do this, all standard unit load devices (ULD), are iterated for their fits within this space. Firstly, the available cargo floor area is checked, based on each ULD's height with suitable margins, by intersecting the pressure shell with an XY-plane at the appropriate height. ULDs of the current type and dimension are placed in rows according to the local width of the intersected floor. Total available cargo mass is checked versus the required cargo mass, indicating if the current ULD is feasible. If no ULDs are feasible bulk cargo is placed. If the use of bulk cargo is not permissible, the user is required to modify the fuselage shaping such that thickness is increased and sufficient ULDs can be placed. This can be achieved by increasing the h_3 parameter of the cabin (Figure 2.5), by using a thicker centre airfoil or by modifying the cabin planform shape such that a longer cabin is sized. A longer cabin will increase the centre airfoil chord length, making the airfoil thicker and so too increasing the height underneath the cabin.

3

Design and Analysis Procedures

Design and analysis procedures implemented in the Initiator are those shown in the N2 chart of Figure 1.2. The BWB needs to be properly integrated into these methods. The topics and implementation that are most relevant to the research questions posed are covered in this report. Mass of the aircraft needs to be estimated in order to begin sizing the aircraft or make performance comparisons. Drag estimation also needs to be performed in order to analyse the required fuel burn to within acceptable levels of fidelity. The input initial guess for lift to drag ratio is not a sufficient base to form meaningful comparisons between TAW and BWB aircraft. Longitudinal stability and control of the BWB is also analysed as it is one of the main challenges of the design and can have significant impacts on mass and drag of the aircraft which in turn affect the comparisons between designs [1, 14]. Simulation of the missions for which the aircraft is designed is also beneficial in order to establish a more accurate estimation of the fuel required to fly each mission. This procedure is already implemented and verified by Wortmann [20] and is suitable for the BWB as it is not configuration specific. These design and analysis procedures allow for a comprehensive analysis of the key performance indicators of the BWB in order to form preliminary conclusions as to its comparison to TAW aircraft. The implementation of the analysis methods of the mass, drag and stability and control disciplines will be outlined in this chapter.

3.1. Class I Mass Estimation

Mass estimations within the Initiator are done in steps of increasing fidelity (as seen in Figure 1.2) in the form of the common Class I and Class II philosophy. Class I entails estimation of the operational empty mass (OEM) and the required fuel mass which, together with the payload mass (PM) from TLRs, gives the maximum take-off mass (MTOM). OEM is estimated using a linear least-squares fit through reference BWB data for payload mass vs. OEM. This fit is given in Figure 3.1 with the reference data used from Table 1.1. Available reference data is scarce and the results also contain a considerable scatter and as such the confidence bounds in the fit are wide. Fidelity of this level is not suitable for a final result but it is appropriate for the initial guess of the OEM which is updated in the higher fidelity Class II method. Fuel fractions (FF), and subsequently fuel mass (FM), are also calculated using the lost range parameter formulation as discussed in [30]. This method showed better accuracy than the Brequet equation and is also used for TAW aircraft. There are no conflicts in using it for the current BWB as it is not aircraft configuration specific but it is engine type dependent. Since it has been chosen to use turbofan engines, this is not an issue. Reserve fuel is also determined for the input diversion range and loiter time. The MTOM is then determined from Eqn. 3.1. This Class I MTOM is used in combination with the design wing and thrust loading from Section 3.2 to form the geometry previously mentioned.

$$\mathrm{MTOM} = \frac{\mathrm{PM} + \mathrm{OEM}}{(1 - \mathrm{FF_{tot}})} \tag{3.1}$$

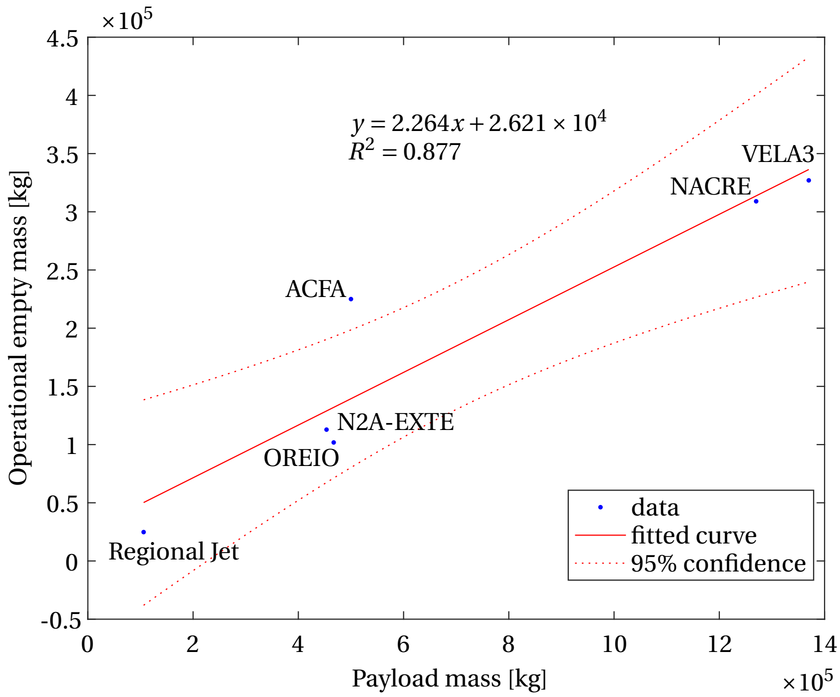

Figure 3.1: Statistical linear fit through payload mass and OEM reference data used in Class I mass estimation (data from Table 1.1)

3.2. REQUIREMENT ANALYSIS AND DESIGN SPACE

A design point needs to be chosen for the aircraft in terms of wing loading and thrust loading. This is done by analysing the input TLRs and airworthiness requirements as is done for conventional aircraft. The method makes use of the relations found in Roskam [52] and the implementation has been discussed in reference [30]. The requirements which are met are as follows:

- Take-off and landing distance
- Minimum climb gradient according to §FAR25.111c, §FAR25.119 and §FAR25.121a-d
- Thrust required in cruise
- Buffet in cruise at a load factor of 1.3
- Maximum wingspan based on airport requirements
- Fuel volume requirements (if needed)

These requirements delimit the feasible ranges of wing and thrust loading in the same manner as for the TAW. All aircraft, irrespective of their configuration, need to achieve the same minimum performance limits set out by regulations. The actual performance of the aircraft during take-off, climb and landing is checked with the methods described in reference [20]. The results of these analyses are not fed back to the determination of the design point and as such have no influence on the design as yet.

3.3. CLASS II MASS ESTIMATION

Once the geometry is known, the Class II estimation is performed. Class II determines the aircraft component masses based on the aircraft's dimensions, geometry parameters, TLRs and airworthiness requirements. There are a limited number of methods available in open literature which are applicable to BWB, owing to their unique and complicated structures. Airframe structural mass estimation is performed first. As successfully used in [7], the method of Howe [26] has been chosen for implementation due to its ability to model and take geometrical differences into account, its relative accuracy for being a semi-analytical method and

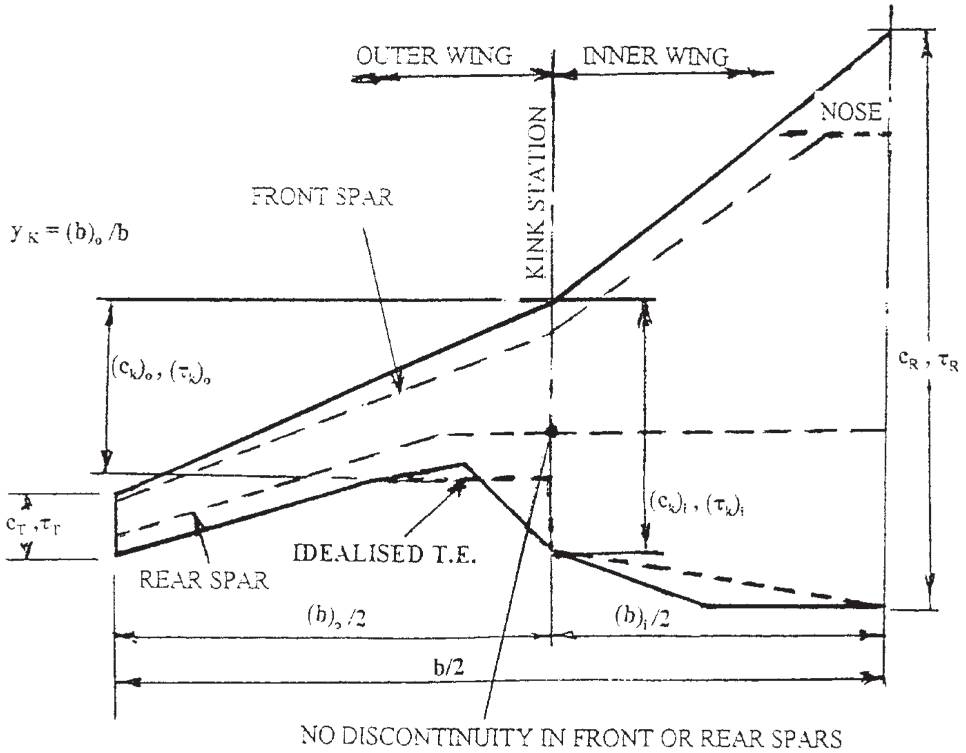

Figure 3.2: Idealisation of BWB geometry used for structural mass calculations in [26]

its very short execution times. Furthermore, the method has appropriate corrections for the use of composite materials which are expected to form an important design choice for the BWB [26], [53], [54]. Using this method, the mass of outer wing, fuselage and winglets (if used) are determined. In order to do this the structural idealisation of the geometry used in Howe [26], and shown in Figure 3.2, needs to be applied to the BWB geometry formed by the Initiator. The Initiator version of this idealisation is depicted in Figure 3.3 and shows that it is in agreement with that of Howe. Howe's structural mass calculations do not include estimations of the vertical tail mass if one is used. Since the vertical tail is similar to conventional aircraft, the same method from Torenbeek [43] is used.

The mass of the rest of the aircraft components such as landing gear and fixed equipment are determined from Torenbeek's Class II method and are already implemented in the Initiator [31, 43] for conventional TAW aircraft. This method has been shown to be more accurate than other methods of similar fidelity [31]. Modifications made to these methods to suit the BWB are limited. This is for two reasons. Most of the relations are based upon empirical data which do directly involve the layout of the aircraft. The origin of some of the relations could however have taken geometrical considerations into account, which would influence their applicability to BWB aircraft. This leads to the second reason as it is the goal of this work to compare TAW and BWB aircraft using similar methods, thereby negating the use of new methods customised for BWBs. This will also provide insights into the performance of these methods for the BWB and show which methods may need to be improved. Implementation of the new structural estimations was unavoidable in this respect since the relations made for conventional aircraft would definitely lead to unacceptable errors.

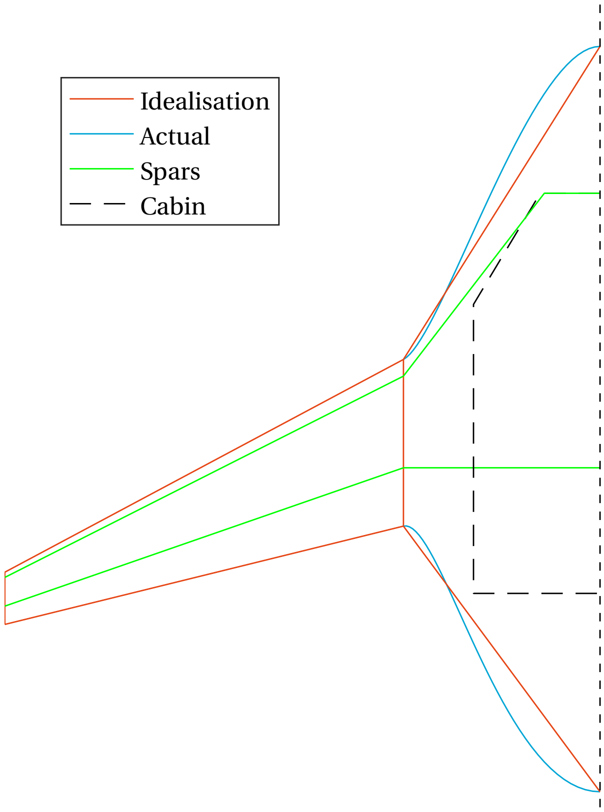

Figure 3.3: Implementation of the idealisation of [26] to the BWB in the Initiator

3.4. DRAG ESTIMATION

No conceptual aircraft design method can function properly without a method of analysing the drag the aircraft creates in order to determine aerodynamic performance and efficiency. Initial estimations used to determine fuel burn are based upon input guesses for the *L*/*D* ratio. This fidelity would not suffice when trying to make meaningful conclusions about the BWB aircraft and the *L*/*D* ratio needs to be more accurately calculated. Furthermore, the drag over a range of C_L values should be determined to evaluate drag in different flight conditions, forming the drag polar. Drag has various sources which sum to the total drag used to make the final drag polar. This is given in Eqn. 3.2 where C_D is the total drag, C_{D_0} is the zero-lift drag, C_{D_w} is the wave drag and C_{D_i} is the induced drag. Estimation of these drag components is approached separately in the Initiator and expanded on in the next sections.

$$C_D = C_{D_0} + C_{D_\mathrm{w}} + C_{D_\mathrm{i}} \tag{3.2}$$

3.4.1. ZERO-LIFT DRAG

Zero-lift drag (C_{D_0})is defined by Roskam [52] as the summation of skin-friction drag and pressure drag but excludes wave drag because it is determined separately. Wetted area has a large influence on C_{D_0} and results in literature disagree as to the wetted area of a BWB relative to a TAW [1, 21], making C_{D_0} a highly influential element in the drag summation. As also explained in Section 1.1, the only appropriate methods for this stage of design are the semi-analytical methods which have been developed for conventional aircraft. Both the methods of Torenbeek [43] and Roskam have been previously implemented in the Initiator and shown to have acceptable accuracy. It was however chosen to move forward with that of Roskam since it has increased sensitivity to geometric layout, which is important in the case of a BWB, over the other method or those in literature such as in [7]. Implementation remains similar to conventional aircraft in terms of the outer wing, vertical stabilisers and pylons which are very similar to TAW aircraft. However the fuselage poses a challenge. It has been chosen to regard the fuselage as a wing lifting surface and using the accompanying equations to determine its C_{D_0}. This is done since the classical fuselage method entails the use of the fineness ratio of a tubular fuselage to fit data [52]. The BWB however does not follow the same trends regarding fuselage area distributions. Base drag is also not present in the same form since the TE of the BWB fuselage ends sharp as for a wing. Furthermore, a TAW fuselage is not responsible for significant lift generation and, as such, does not present the same pressure drag as a wing would. This parameter is again fitted with the fineness ratio for a TAW in the classical fuselage method which would not be suitable.

Accepting this, the sections of the fuselage between the defined airfoils are treated as trapezoidal wing sections, where the mean thickness, chord, sweep and sectional wetted area are used. The zero lift drag of the fuselage is then determined from Eqn. 3.3 for the N trapezoidal sections. R_{wf_i} is the interference factor for each section and is assumed to be 1 for a flying wing [52]. R_{ls_i} is the correction for a lifting surface determined from a fit for the sectional sweep angle at the maximum airfoil thickness location given in [52]. C_{f_i} is the sectional flat plate skin friction coefficient and is determined using the method given in [55]. Therefore, this method takes the variation of Reynolds number over the rapidly varying chord into account for skin friction. As such, skin friction coefficients should increase along the fuselage span with a decreasing Reynolds number. It must be noted that since it is difficult to estimate the transition point on such a 3D body, which is yet untested with the Initiator, it is chosen to fix the transition point at a Reynolds number of 1 million (as is standard for conventional fuselages). The airfoil thickness location correction factor L' is also detailed in [55] and determined for each section. Lastly, the thickness to chord ratio t/c of the mean geometric chord of each section and the wetted area of the section is used. These sectional drag values are summed and scaled with the reference planform area.

$$C_{D_{0_\mathrm{f}}} = \frac{1}{S_\mathrm{ref}} \sum_{i=1}^{N} R_{\mathrm{wf}_i} R_{\mathrm{ls}_i} C_{\mathrm{f}_i} \left[1 + L'_i (t/c)_i + 100\,(t/c)_i^4\right] S_{\mathrm{wet}_i} \tag{3.3}$$

The remainder of the component zero-lift drag is determined with similar methods found in [52]. These are added to the fuselage drag giving the total C_{D_0}. In order to take unaccounted drag effects into account, such as rivets and antennae, a miscellaneous drag increase is given in the form of an input percentage of the total C_{D0} according to the method given in [52]. These empirical corrections are based on experience and flight test data of conventional aircraft and are similar to values suggested in [44]. It is expected that BWB aircraft will incur similar penalties as they will also require similar antennae for example. and it is the goal to compare the TAW and BWB using similar methods and penalties when they are applicable.

3.4.2. WAVE DRAG

Wave drag (C_{D_w}) is determined following the Delta method laid out in [56] and implemented in the Initiator for conventional aircraft by [57]. This method has shown better performance in the Initiator than other methods for TAW which are applicable to this level of design and resource availability. Wave drag over the outer wing of the BWB is determined using the routine for a wing surface. This is done because the outer wing behaves mostly as a conventional wing on a TAW aircraft. It operates at similar C_L and is composed of similar airfoils. For the fuselage it is unknown how well this method can predict the wave drag since it has been formed for straight tapered wings and the fuselage does not conform to this. Furthermore, the fuselage is composed of thick airfoils which incurred unrealistic drag penalties using the wing method. It has also been shown in the accompanying literature study that shockwaves are greatly reduced over the fuselage due to a large pressure relief, making 3D results significantly lower than 2D results. It has been deduced that this effect was not fairly represented by the wing based method and as such also contributed to large overestimations of the fuselage wave drag. Thus it was chosen to treat the fuselage as a conventional fuselage, determining the cross-sectional area distribution including nacelles, pylons and vertical tails, and determining the maximum cross-sectional area. This is then fitted to data for conventional fuselages, resulting in the fuselage wave drag. This is added to the wing wave drag to get the total wave drag.

3.4.3. INDUCED DRAG

Induced drag (C_{D_i}) has been determined in the Initiator for conventional aircraft using AVL [1]: a vortex lattice solver which uses the linearised potential flow equations and implemented in the Initiator by [51]. AVL has shown to give acceptable results for induced drag of TAW aircraft within the Initiator, being 7.5 drag counts from flight test data for an Airbus A320-200 [10, 51]. AVL's performance on BWB aircraft in terms of induced drag has also been investigated and used by many studies, namely [7, 41, 58, 59] among others. For these two reasons it is chosen to use AVL to determine the induced drag of the BWB in the Initiator, supporting the research goals of comparing TAW and BWB using similar methods. The outer wing and fuselage are modelled in AVL using the sections and airfoils already defined. Panelling is done similar to conventional aircraft and convergence studies show consistent results at the panelling chosen.

At this stage the trim drag is not yet included. This is because control deflections to achieve trim are too large, as explained later in Section 4.2, leading to erroneous trim drag. As such, pitching moments are not trimmed out and induced drag is set to increase when this is done. This results in a known underestimation of the true lift induced drag.

3.5. STABILITY AND CONTROL

Providing stability and control of a BWB is challenging compared to conventional TAW for three main reasons [1, 16, 28, 40]; there are no dedicated longitudinal stabilising or control surfaces, short moment arms require large forces (leading to larger stabilising or control surfaces) and the proper estimation of the CG and its shift (which has a large impact on stability and control). Due to time constraints only the longitudinal stability and control is analysed as this is the more challenging one among lateral and directional stability.

3.5.1. LONGITUDINAL STABILITY

Longitudinal stability is of utmost importance. Current §CS25.171 airworthiness requirements are followed, meaning that the aircraft must posses positive static stability. In conventional aircraft this is done by a horizontal stabiliser which ensures that the neutral point always lies aft of the most aft CG point, throughout the flight envelope and in all aircraft configurations. This ensures that $C_{M_\alpha} < 0$ meaning the aircraft will naturally return to trimmed flight from a pitch upset making it statically stable. In the case of the BWB the neutral point coincides with the aerodynamic centre (AC) of the aircraft due to the absence of a horizontal tail or canard [40, 43]. Thus the AC of the wing-fuselage combination must lie aft of the most aft CG position that will be encountered in flight [28]. This can be attained in three ways: sweep distribution over the outer wing, outer wing location and airfoil choice [1, 28, 40]. The latter is a complex topic and the subject of intense thought and investigation in academia and no easily applied topic during a master thesis of this scale. However the first two options are more suitable for the current work.

Stability is ensured within the Initiator using a combination of sweep and wing location. Firstly the aerodynamic centre should be suitably determined. Methods to do this, which are applicable to the Initiator in

[1] Athena Vortex Lattice, http://web.mit.edu/drela/Public/web/avl/avl_doc.txt, Accessed 23-04-2017

terms of resources, are limited. Most are empirical methods, such as those in Tornebeek [43], applicable only to straight tapered wings at moderate sweep and taper ratios. Numerical solutions and solvers perform better but using higher order solvers is not feasible due to modelling, resource and time constraints. In order to achieve good pitching moment and aerodynamic centre estimations. the chordwise pressure distribution needs to be accurately resolved. [7] and [41] have both reached the conclusion that the best openly available software for this task at conceptual design level is AVL. AVL is therefore implemented in the Initiator to determine the location of the AC and the pitching moment of the aircraft. This is however diverging from conventional TAW analysis as this uses the DATCOM method with semi-empirical corrections for fuselage and nacelles which was shown to be more accurate [60, 61]. Unfortunately DATCOM is not applicable to a severely kinked varying LE as on the BWB [62]. Reference [59] has successfully implemented AVL for the purpose of stability estimation on a BWB with AVL results comparing to within 5% of RANS CFD validations for pitching moment. Nacelles have a significantly large effect on the aerodynamic centre and can not be neglected [43]. Reference [59] did implement nacelles in the AVL model. It was chosen not to do this since it is a further departure from TAW analyses, since this uses empirical corrections for the nacelle, which could result in a significant difference between the TAW and the BWB and defeat the goal of this work. Therefore corrections for the nacelles to the AC are made external to AVL following methods from reference [43] (as for TAW), resulting in the total aircraft AC. It is then checked that it lies aft of the most aft CG point, ensuring the aircraft is statically longitudinally stable. Due to the difficulties experienced with the provision of longitudinal control as, discussed in the next subsection, it was chosen to use a static margin of zero in order to further ease control requirements. A positive margin should be applied following future improvement of the control routines.

3.5.2. LONGITUDINAL CONTROLLABILITY

Control of a BWB is a challenging topic due to the short moment arms of control surfaces and the array of options available in terms of control allocation. Elevators are commonly placed on the aft section of the fuselage and often work in conjunction with elevons on the outer wing [1]. Thrust vectoring is also implemented in literature because it has lower impact on the cruise AoA [41]. Belly flaps have also been proposed to help provide pitch moment relief in landing and take-off configuration. However, all of these methods need to be suitably modelled and analysed before their impact on control can be verified. This is no straightforward task during conceptual design. Due to time limits during this thesis, it has been chosen to implement a single elevator at the aft of the fuselage as done in reference [40]. This is thus the sole longitudinal control surface currently implemented for the BWB.

In order to analyse the effectiveness of the elevator it is modelled in AVL as a standard plain flap control. The hinge line is straight and perpendicular to the centre line in order to allow for a simpler elevator hinge mechanism, reducing integration issues. This requires a varying hinge location at the defined sections in AVL in accordance with the straight hinge. Trim is enabled in AVL, balancing out the pitching moment with elevator deflection, achieving $C_M = 0$ about the aircraft CG. The most forward CG location is critical for control purposes as the magnitude of C_M increases with the distance between the CG and AC. As described in later sections, elevator deflections are infeasibly large in order to trim the aircraft and as it is therefore deemed that the method cannot be trusted and is disabled. This means that BWB aircraft currently designed by the Initiator are infeasible regarding longitudinal control and should be expected to still receive penalties in L/D and MTOM due to trim drag and control allocation.

3.5.3. DESIGN FOR LONGITUDINAL STABILITY AND CONTROL

In order to asses and then make design choices concerning the stability and control, a small, local, gradient based optimisation was formed. The objective of this optimiser is to achieve static longitudinal stability while minimising the impact on the MTOM of the aircraft as given in Eqn. 3.4. The design vector k consists of the sweep and twist of the outer wing section. The MTOM of the aircraft is a function of this design vector through the influence of sweep and twist on outer wing mass and induced drag. The outer wing mass is determined from the Class II method implemented in Section 3.3, based upon input sweep and twist. The induced drag for the current sweep and twist is determined from AVL and used in Eqn. 3.7 to determine the new L/D ratio during cruise. This is then used in Eqn. 3.6 to determine the new fuel mass, using the lost range formulation discussed in Section 3.1. The new wing and fuel masses, M_{w_k} and M_{F_k} respectively, are combined with Eqn. 3.5 to form the MTOM objective that is to be minimised. Stability is ensured with the non-linear constraint that evaluates whether the AC is aft of the CG. Twist has very little regard in this effect but it is maintained in the constraint function since this function is likely to be used for controllability assurance in future and twist can be used for this purpose. The CG location is held constant at the most aft location of the shift. CG will vary with sweep but this would require a lengthy re-calculation using the CG shift routines which would impact performance. This was not feasible as this optimisation runs within the Class II loop of the Initiator (Figure 1.2) and the difference in CG will converge out with the main Initiator convergence as the true CG will be calculated in the proceeding iteration. The same holds for a re-evaluation of the wave drag (and thus *L/D*) with the varying sweep angle.

The twist or sweep of the fuselage can not easily be varied as it is based upon the chosen cabin shaping and would call for a complete re-design of fuselage In turn, this is not feasible concerning computation time inside the convergence loop. The geometry estimation routines implemented do allow the airfoil shapes of the fuselage to be altered without this re-design as it was envisaged that this would be used in this optimisation and is an option for future development. This will also come into use when longitudinal controllability is taken into account in this optimisation as the airfoil shapes have a larger impact on the pitching moment produced than the AC. Therefore the shaping of the fuselage does not yet play a role in assuring longitudinal stability of the aircraft.

$$\begin{aligned} \underset{k}{\text{minimize}} \quad & M_{\text{TO}}(k) \\ \text{subject to} \quad & x_{\text{CG}}(k) - x_{\text{AC}}(k) \leq 0 \end{aligned} \tag{3.4}$$

where:

$$\text{MTOM} = [\text{OEM}_{\text{ init}} - (M_{w \text{ init}} - M_{w_k})] + \text{FM}_k + \text{PM} \tag{3.5}$$

$$\text{FM}_k = f(L/D_k) \tag{3.6}$$

and:

$$L/D_k = \frac{C_{D\text{ init}} - (C_{D_i\text{ init}} - C_{D_i\ k})}{C_L} \tag{3.7}$$

4

VERIFICATION AND VALIDATION OF METHODS

In this chapter the methods that have been implemented for the BWB will be verified against their original sources to check that they are performing as intended where this is possible. The same methods will then be validated against reference data by checking that the values are similar to ascertain whether they are suitable to the task at hand. Lastly the applicability of the research will be shortly discussed in terms of the range of BWB aircraft that can be designed and what results can be expected.

The approach to verification and validation of the models is to firstly attempt to qualitatively check that the functioning of each routine is logical and follows expected trends from literature. The results are then qualitatively compared to the values that the original authors attained where this is possible. Validation is done in a similar way, except that results are compared to other BWB design projects that may have used different methods to estimate the same parameters. This gives an indication of the performance of the implemented methods compared to other methods. The BWB test cases used in the verification and validation are the same aircraft used to compare to TAW aircraft, given in Section 5.1.

4.1. VERIFICATION

Firstly the geometry model is verified. This can only be qualitatively done by checking that the geometry is consistent. Firstly the cabin planform is unitarily scalable as intended and the seating arrangement fits properly within its bounds. Fitting of the centre airfoil is robust and results in a tight fit of the cabin box to the bounds of the airfoil with the minimum unpacked space. The oval sections of the pressure shell are correctly formed around the cabin according to its local width and centre airfoil shape. Different airfoil shapes result in different radii of the arcs as intended and the resulting radii are sufficiently small considering structural stress. These can be further adjusted with the h_1 and h_3 settings which prove to be useful for tweaking the packing efficiency and cargo possibilities. Available area for cargo containers is accurately determined such that the chosen container fits underneath the passenger cabin floor. A cross section through the final fuselage geometry is given in Figure 4.1 which demonstrates these aspects.

Planform shaping of the rest of the fuselage, i.e. LE and TE, also performs as intended. The LE and TE of both the fuselage and outer wing match within 1 mm (XYZ) once convergence has been reached between fuselage and outer wing sizing. While verifying results it was found that a bug in the twist definition of the fuselage airfoils was causing a 6 mm discrepancy between the fuselage and outer wing LE which was causing abnormal lift distributions from AVL. This bug was corrected and the rest of the geometry checked to within the same tolerance but this shows the level of accuracy that is required and achieved. The discrepancy between the aerodynamic and oval pressure surfaces is also checked and shown graphically in Figure 4.1. Depending on the aircraft at hand it can vary from 1-5 cm, which considering the previous statement, could form an error that should at least be quantified in future work. The rest of the aircraft geometry is also determined as should be. Landing gear positioning is not always feasible but an error is generated for the users attention, after which adjustments to the geometry can be made to attempt to alleviate the problem. This is still not always successful but this is a known issue with the Initiator, for conventional aircraft as well, and is under investigation by others. This could have an impact on landing gear mass estimations as gear can

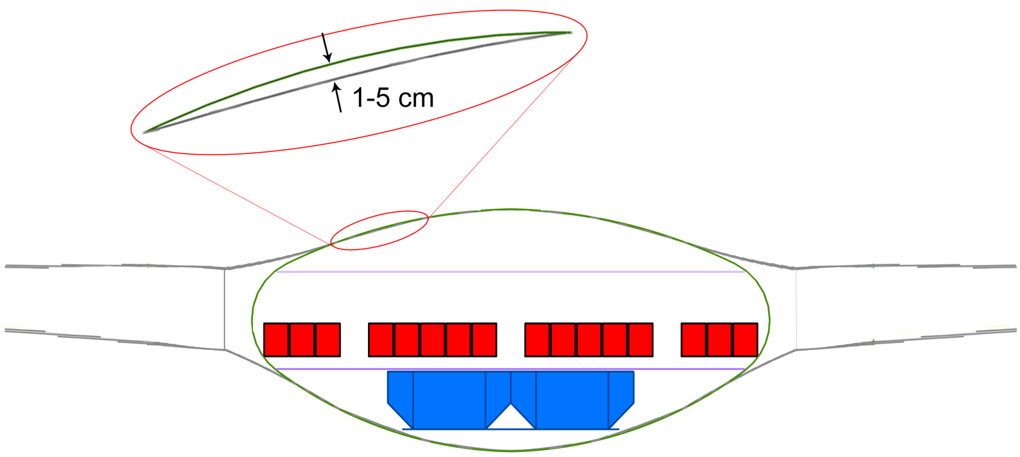

Figure 4.1: Cross section through the oval fuselage showing the fit of the cabin and cargo with a detail of the difference between the aerodynamic and pressure shell

be made too high or incorrect number of wheels.

Moving to the verification of the implemented analysis methods, the Class I mass estimation functions correctly in that the statistical fits made suitably accommodate the chosen BWB designs. Changes were not required to the fuel fraction estimations and harmonic mission determination and work as for a conventional aircraft. The implemented Class II airframe structural mass estimation from [26] is well verified. The implementation of the geometry idealisation gives similar results for most planform shapes, an example of which is shown in Figure 3.3. For the *straight* TE type the idealisation can lead to a larger discrepancy between actual and idealised geometry because the aft fuselage is broader than for other TE types. The effect of this can not be directly quantified and it is theorised that the implementation of a discontinuous TE, shown in Figure 3.2, would not improve the situation because the TE is too broad and would require a large discontinuity before a significantly better idealisation is achieved.

The actual results of the method also confirm its successful implementation, given in Table 4.1. The breakdown in the table represents the different components sized by the method [26] and the values that Howe achieved or recommends compared to those of the tree Initiator test cases. The results are for aluminium based aircraft as discussed in Section 5.1. Overall the total structural mass is well estimated being similar to that of Howe but still dependent on the actual aircraft geometry. The wing function group is slightly underpredicted where the error seems to be larger for smaller BWBs. This could be partly due to the idealisation issue mentioned before. However it must be clearly noted that Howe's method is based upon a slightly different fuselage structure than the oval fuselage in the Initiator. This is an unavoidable factor and the impact thereof can not be ascertained but it is likely also a cause for the deviations, especially in the pressure membrane. It is unknown why the door mass seems to be heavily underestimated as the actual area of emergency exits and doors, placed by the cabin sizing routine according to regulations, is used which should result in an accurate door mass. Howe does state that the accuracy of the estimations is within ±5% for $0.4 < y_k < 0.7$ and within ±10% for $0.25 < y_k < 0.9$ where y_k is the ratio of outer wing span to reference span. The Initiator, with the three test cases, results in values of 0.65,0.68 and 0.69 for y_k which are within the smaller bounds and as such an error of approximately ±5% can be expected. This is reflected in the results and verifies that the mass estimation is functioning as intended.

Verification of the drag estimation is not fully possible since the methods were largely constructed for conventional aircraft. Comparisons to the values from the sources does not give a sole indication of implementation issues as the results also contain discrepancies due to using conventional methods for BWB aircraft. However the comparison will still confirm that results follow trends and are correct in order of magnitude. Firstly the zero-lift drag is compared to the trend in Figure 4.3. Zero-lift drag is converted to the equivalent skin friction coefficient using the total aircraft wetted area [44]. Results for the BWB fit within the reasonable bounds given but surprisingly the equivalent skin friction does not tend to monotonically decrease with wetted area as would be expected. This is however also present for the TAW aircraft and does not seem to be an issue inherent to the BWB in the Initiator. It is thus not likely caused by implementation issues with the

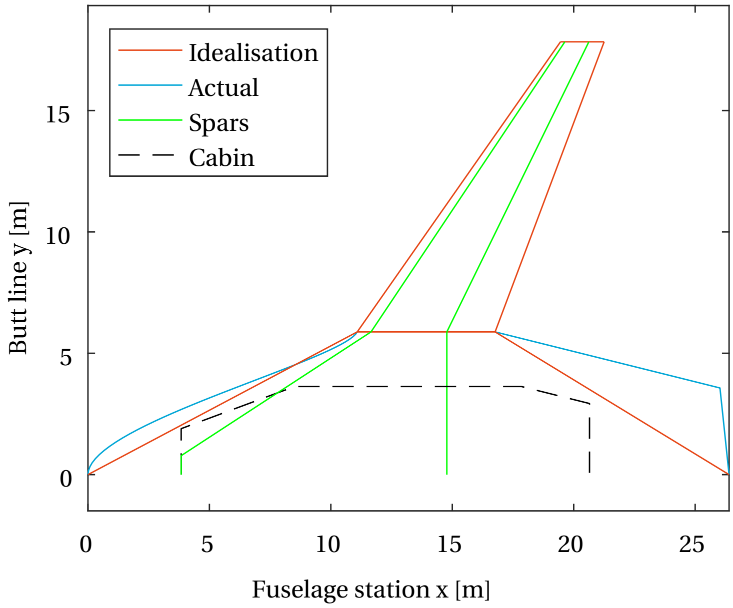

Figure 4.2: Structural idealisation of the *straight* TE type showing the larger discrepancy between actual and idealised geometry

Table 4.1: Ratio of airframe component mass to MTOM from Howe and the Initiator

Component	Suggested [26]	Cranfield BWB [26]	BWB150	BWB250	BWB400
Wing Function					
Covers	-	0.093	0.066	0.077	0.088
Ribs	-	0.055	0.041	0.038	0.039
Secondary	-	0.039	0.031	0.031	0.031
Sub total	-	0.186	0.138	0.146	0.158
Fuselage Function					
Nose	0.010	0.009	0.021	0.012	0.009
Press. Membrane	0.010	-	0.044	0.034	0.061
Bulkheads	0.007	-	0.012	0.004	0.004
Pax floor	0.017	-	0.017	0.013	0.015
Cargo floor	-	-	0.003	0.004	0.005
Doors	0.01	-	0.003	0.002	0.002
Windows	0.003	-	0.003	0.003	0.003
Sub total	-	0.055	0.104	0.071	0.099
Total airframe	-	**0.241**	**0.242**	**0.217**	**0.257**

BWB. This is further substantiated by considering Figure 4.4 where the skin friction coefficient (not equivalent) found along the span of the BWB is plotted. For the fuselage, due to the sectional implementation of the method (Section 3.4), the skin friction coefficient varies along the span. This is expected since skin friction is a function of Reynolds number [52]. As the chord decreases, so too does the Reynolds number and skin friction increases and this is reflected in the curves. For the outer wing, it is treated as a conventional wing and thus the methods were only applied to the mean geometric chord (MGC). This has been shown to be suitable for a conventional wing [44] and results in similar skin friction coefficients. Had the same been done for the fuselage, it would not have captured the varying skin friction. This would have brought significant errors as a large portion of the drag is created by the fuselage, evident from the area under the $C_f c$ distribution which has a similar principle to a lift distribution. Furthermore, the method is also able to determine the cut-off Reynolds number for surface roughness effects [44] and some sections become limited by the chosen sand grain roughness (0.0254 mm [44, 52]) as it should be. It can thus be concluded that the method is functioning as intended.

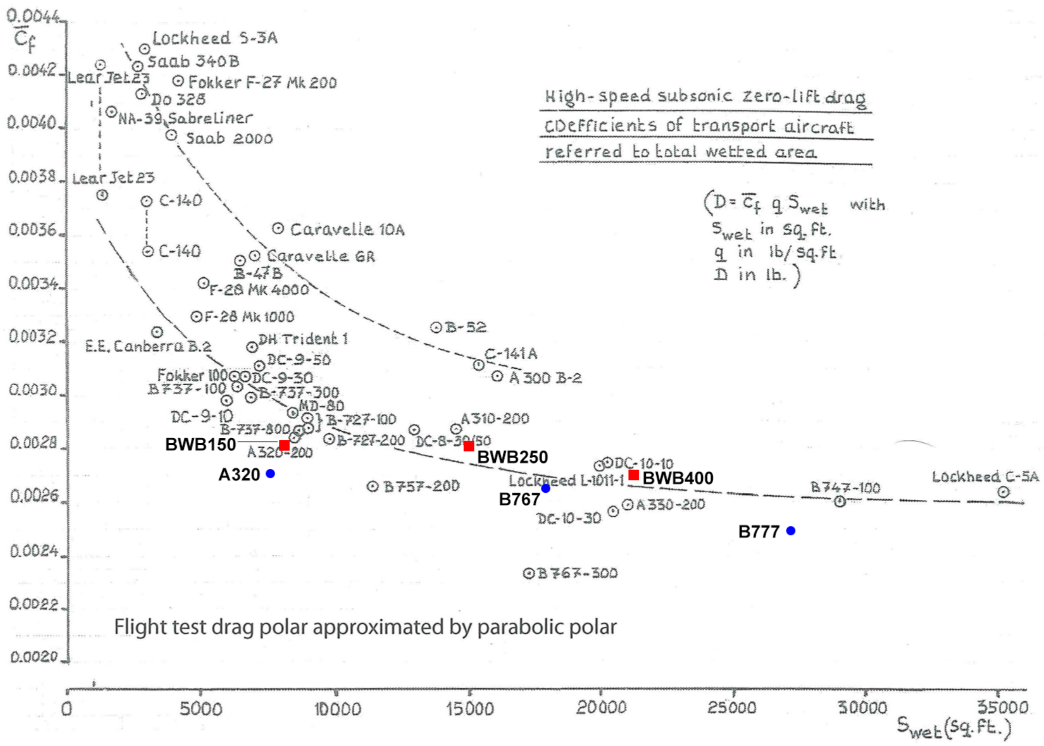

Figure 4.3: Trend in equivalent skin friction coefficient with wetted area from [44] for conventional aircraft with the results for the BWB from the Initiator

Induced drag is verified by comparing the results achieved from AVL to that predicted by the classical parabolic induced drag polar. This is shown in Figure 4.3 where the theoretical induced drag has been plotted for a range of Oswald efficiency e using the aspect ratio of the tested BWB, namely 4.8. The results from AVL fit the parabolic curves very closely with only a slight deviation at very low or negative C_L, well below cruise conditions where the induced drag has the largest effect on the Initiator results. This was the case for a range of BWB aircraft tested, of various sizes and with different planform shapes. This proves that AVL is responding as expected and the model is suitable for estimating induced drag.

The wave drag estimation is also challenging to verify since the methods were again made for conventional aircraft and as such there is no data for BWB aircraft using the method with which to compare. For the outer wing, the procedure is the same as conventional aircraft and the inputs to empirical data fits is within the estimation bounds of the respective fits. The cross-sectional area of the rest of the aircraft was also checked against a simple external CAD model and results were the same. Furthermore the distribution of the cross-sectional area is similar to that of other BWB aircraft, Figure 4.6, where both the reference and the Initiator BWB cross-sectional area approaches the Sears-Haack distribution. It can therefore be assumed that the method has been implemented correctly.

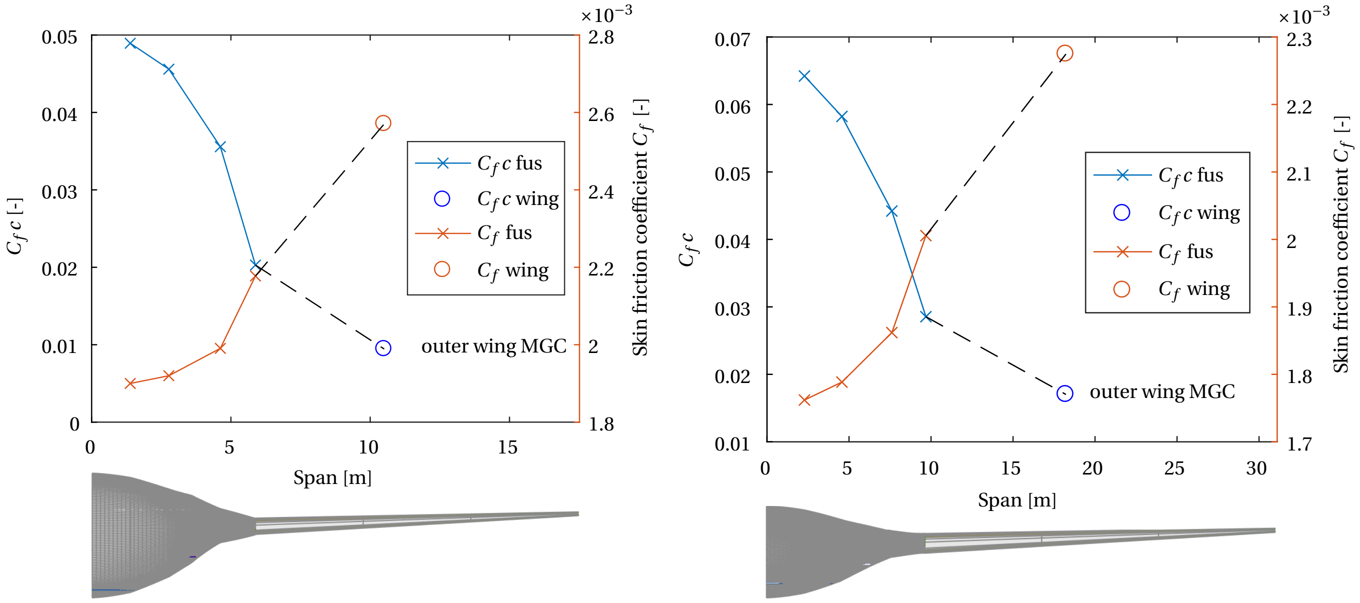

(a) BWB150 (b) BWB400

Figure 4.4: Skin friction distribution along the span of the fuselage and wing

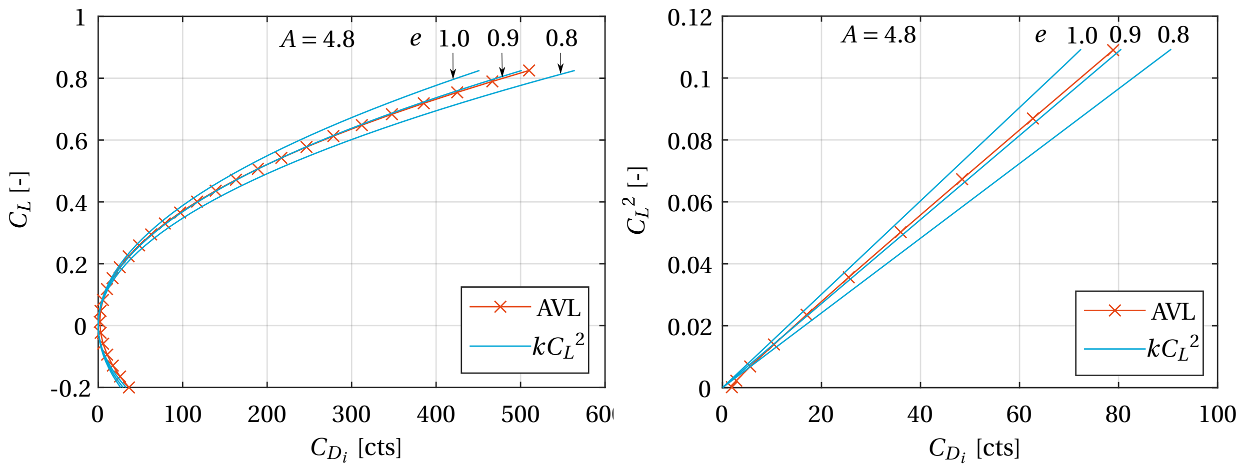

Figure 4.5: Induced drag resulting from AVL compared to the parabolic drag polar with different Oswald efficiency

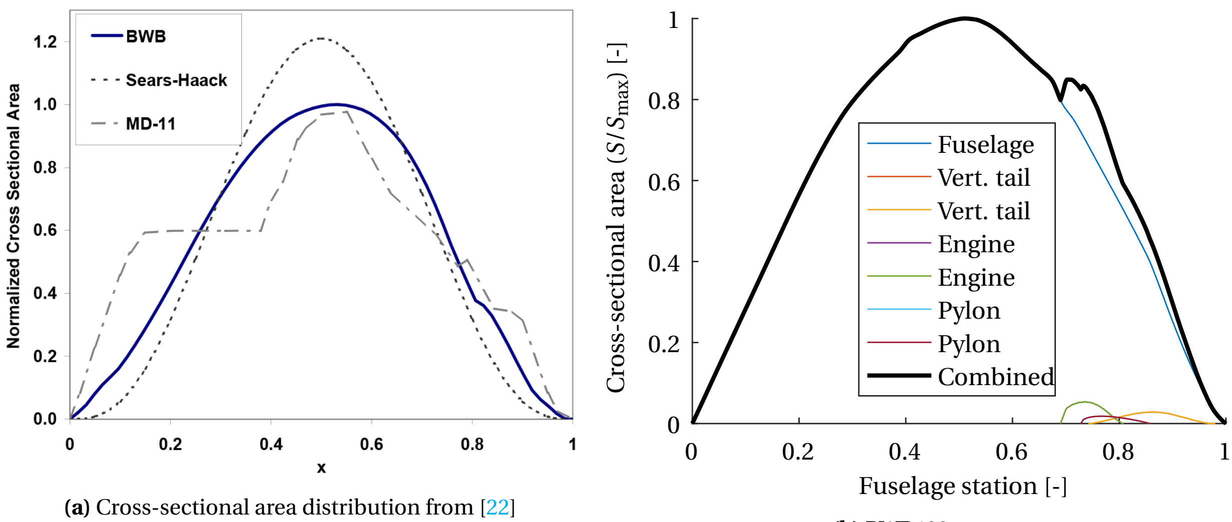

(a) Cross-sectional area distribution from [22]

(b) BWB400

Figure 4.6: Cross-sectional area distribution from the Initiator

Verification of the longitudinal stability and controllability analyses is twofold. Firstly the determination of the AC of the fuselage-wing combination is verified similarly to the induced drag as it is dependent on the same AVL model. The implementation of the BWB in AVL is shown in Figure 4.7 and can be compared to the implementation given in reference [59]. Besides for the winglets and nacelles the models are similar. Both use multiple sections to define the planform and kinks are present in both LE and TE, albeit less severe in the reference case. Panelling density seems to be higher in the reference model. Increased panel density has been tested in the Initiator but it did not result in significant changes while requiring longer execution times and strongly affecting the Initiators computation performance. As such it is assumed that the aerodynamic model is sufficiently modelled in AVL and that the location of the aerodynamic centre is accurately determined to the fidelity at which AVL is intended to perform. Secondly the corrections for the nacelle are the same as for conventional aircraft and the method was copied and implemented, giving similar results to conventional aircraft nacelles. This again held true for the range of aircraft tested and as such it can be assumed that the model is implemented correctly as it responds as expected.

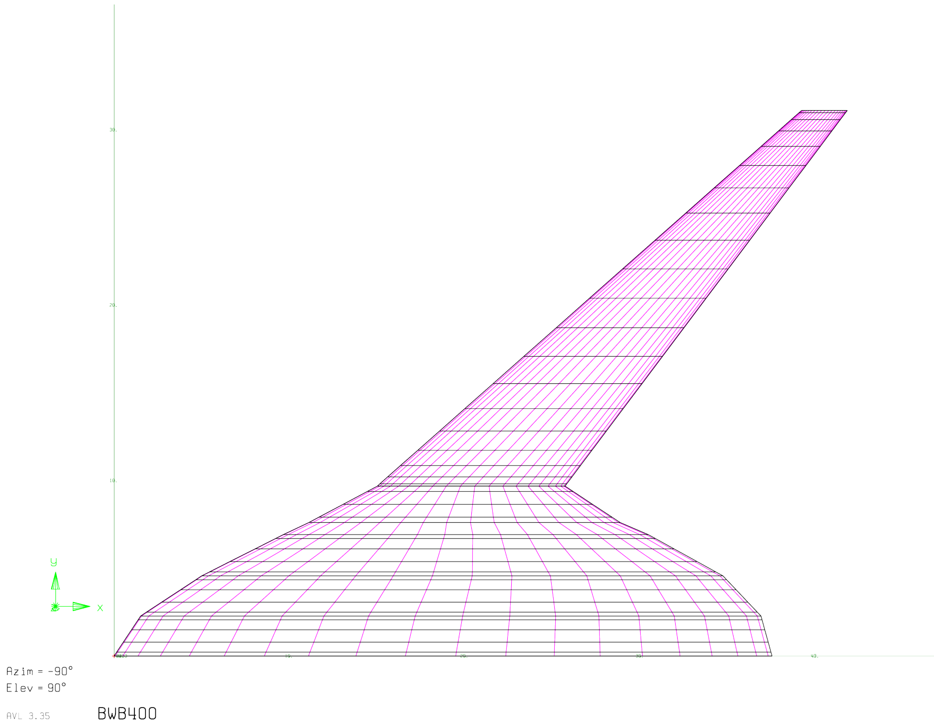

Figure 4.7: Panelling of the BWB in AVL from the Initiator

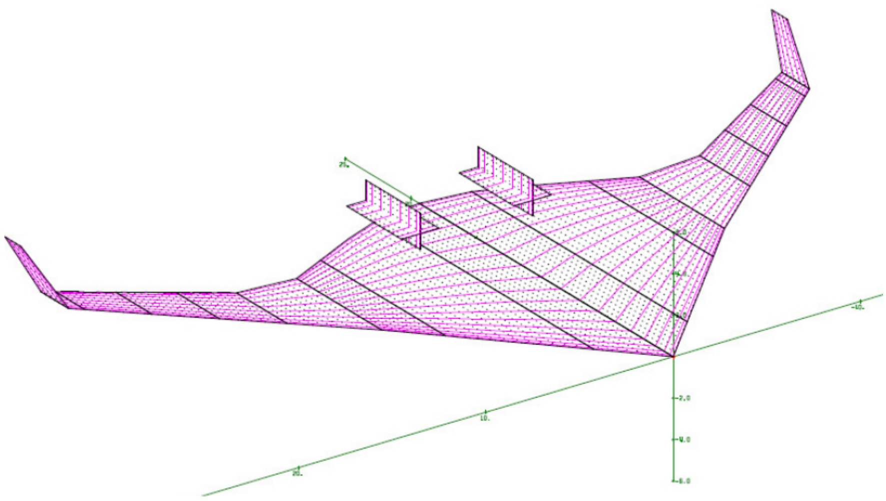

Figure 4.8: Panelling of the BWB in AVL from reference [59]

4.2. VALIDATION

The parametrisation and modelling of the geometry can not be indepthly validated as it does not result in specific values which could be compared to other BWB aircraft. However it can be said that the geometry parametrisation implemented is suitable for modelling a BWB aircraft. A wide range of configurations and aircraft sizes can be modelled which cover the majority of shapes found in literature. The main aspects of BWB design are present, such as a lifting fuselage with suitable aerodynamic shaping, a pressure cabin in which to carry the payload, adequate layout of this cabin which will carry the passengers and cargo and provision for the rest of the required aircraft subsystems. Furthermore the model is adjustable by a combination of automatic and manual design choices which are suitable to conceptual aircraft design. This allows for proper integration with the Initiator and provides all the required data, consistency and flexibility required for subsequent analyses and design.

The design point that results from the requirement analysis is compared against values achieved from other BWB studies in Figure 4.9. The result shows that the Initiator results fall well between the reference values indicating that the method is choosing a suitable design point for the BWB. A more detailed validation of the design point was not possible due to lack of time. In general the preliminary analysis of the take-off, climb and landing performance during the mission analysis does not give warnings that the requirements were not met. As there is no feedback of these results, the warnings of unmet requirements are not critical and the design process continues so it is possible that the final aircraft does not meet the requirement as analysed by this module. The test BWB aircraft do meet the requirements and this is another positive indication as to the chosen design points.

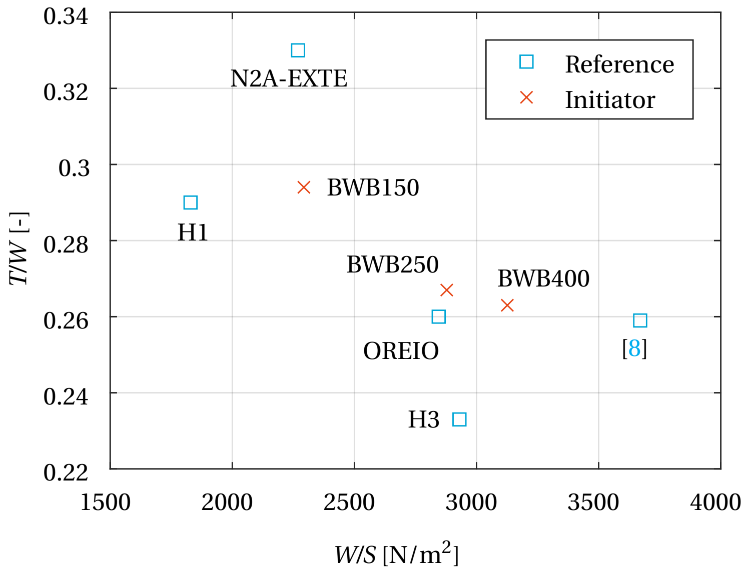

Figure 4.9: Design wing and thrust loading from reference BWB and the Initiator BWB

Validation on the mass estimations is be done by comparing the mass results of the Initiator with those found in literature. This is done in Table 4.2 where three different BWB designs from literature are chosen but available data of complete mass breakdowns is scarce. The results show that the structural mass compares well with reference values. There is a variance of approximately 5% between the Initiator results but this variance is also present in the reference values which shows that the Initiator is within the accuracy bounds that should be expected. Landing gear is slightly underestimated but landing gear design is still erroneous within the Initiator and the proper functioning of this module in future releases could influence this positively. Engine and nacelles are adequately estimated, being within the range of reference values. Fixed equipment is slightly underestimated. This is a difficult group to accurately size at this level of design due to the lack of specific layout, dimensioning and parametric methods for this sub group. This is even a hurdle for conventional TAW aircraft. The Initiator, and conceptual aircraft design methods in general, could greatly benefit from improved system estimations. However, the operational items are significantly overestimated and it is suspected that part of this mass is taken from the fixed equipment group. The specific division of components to operational and fixed equipment is not given in the reference literature so it could not be cross-checked to the Initiator's division. If the difference between operational items for reference and Initiator aircraft is added to the fixed equipment the values match much better and thus this point is not deemed an issue. This is also supported when the overall OEM fractions are compared, showing firstly quite a spread in reference values and secondly that the Initiator falls quite nicely within this range. The scatter is also clearly seen in Figure 4.10 where more reference data is used than in Table 4.2. This confirms that the Initiator falls within a feasible OEM range. Interestingly though it also shows how the Initiator achieves a higher payload efficiency than reference cases, meaning more payload can be carried for a given MTOM, in the order of 6%. This could be an underestimation of the overall MTOM by the Initiator or it shows that the new configuration design logic implemented results in a more compact aircraft, leading to mass reductions. It is believed that a combination of both effects are at play. Overall it can be said that the mass results are promising and in-line with results from literature and therefore deemed fit for this level of design fidelity. A major step forward for the Initiator should however come with the future implementation of the Class II.5 mass estimation for the oval fuselage as described in references [25, 63] giving a higher fidelity analysis of the critical fuselage mass.

Table 4.2: Ratio of MTOM of BWB mass components from reference and Initiator aircraft

	OREIO [12]	N2A-EXTE [13]	SAX-40 [41]	BWB150	BWB250	BWB400
Structure	0.254	0.241	0.315	0.241	0.225	0.264
Fuselage	0.120	0.144		0.183	0.149	0.185
Wing	0.129	0.078		0.053	0.068	0.071
Vertical tail	0.005	0.019		0.006	0.007	0.008
Landing gear	0.041	0.046	0.044	0.034	0.027	0.029
Engine & nacelle	0.105	0.069	0.111	0.084	0.072	0.070
Fixed equipment	0.133		0.154	0.125	0.110	0.101
Engine systems	0.001			0.009	0.008	0.008
Fuel system	0.019			0.002	0.001	0.001
APU	0.002			0.008	0.008	0.008
Flight cont. & hydraulics	0.025	0.029		0.012	0.009	0.008
Electrical	0.008			0.006	0.003	0.003
Pneumatics & air-con	0.017	0.001		0.002	0.001	0.001
Furnishing and eqpt.	0.012	0.064		0.067	0.064	0.059
Instruments	0.009			0.019	0.015	0.012
Load & handling	0.025					
Empty mass	0.518	0.469		0.484	0.434	0.464
Operational items	0.005	0.007		0.045	0.036	0.037
OEM	0.523	0.476	0.624	0.529	0.469	0.501
Mission fuel	0.267	0.306	0.220	0.185	0.274	0.255
Payload	0.210	0.218	0.155	0.285	0.257	0.245
MTOM [t]	216	214	151	72	170	261

Validation of the drag estimations is done by firstly comparing the lift to drag ratio, L/D, ratio achieved by the Initiator for the three BWB test cases to those achieved by reference BWB studies. Commonly the L/D ratio is multiplied by the cruise Mach number to get a better indication of the range performance of the aircraft as fuel burned is a function of drag and time spent in cruise. A comparison of available $M(L/D)_{\max}$ data is given in Figure 4.11 where the BWB results from Table 1.1 and the Initiator have been laid over those achieved by existing TAW aircraft taken from reference [4]. The Initiator results for the TAW test cases used later are also shown. It is immediately clear that the Initiator is underestimating the $M(L/D)_{\max}$ ratio by a significant amount compared to reference BWB which are mostly in the 19-20 range. This thus shows that drag is being overestimated. There is however quite a scatter in the reference results (also for TAW) and not all studies fall in the higher $M(L/D)_{\max}$ range. The source of the drag overestimation is clear if the breakdown of the drag is compared to values found in literature for other BWB designs.

Available reference data concerning the breakdown of drag for a BWB is extremely scarce. Only two trustworthy sources could be found for comparison and are shown in Table 4.3 along with the Initiator results. It is seen that the Initiator is overestimating all drag components, the worst being induced drag. This is surprising as both the SAX-40 study and Initiator use AVL solely to determine induced drag. This can be ascribed

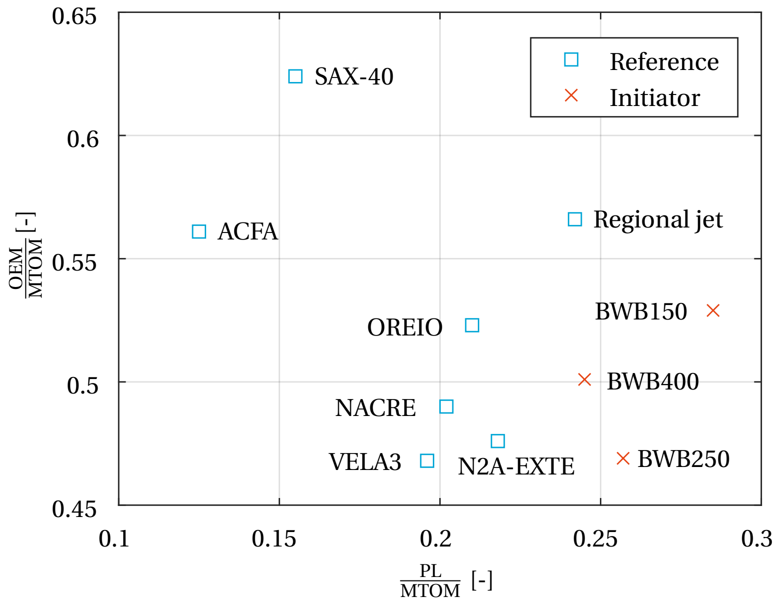

Figure 4.10: Payload fraction versus OEM fraction for reference and Initiator BWB aircraft

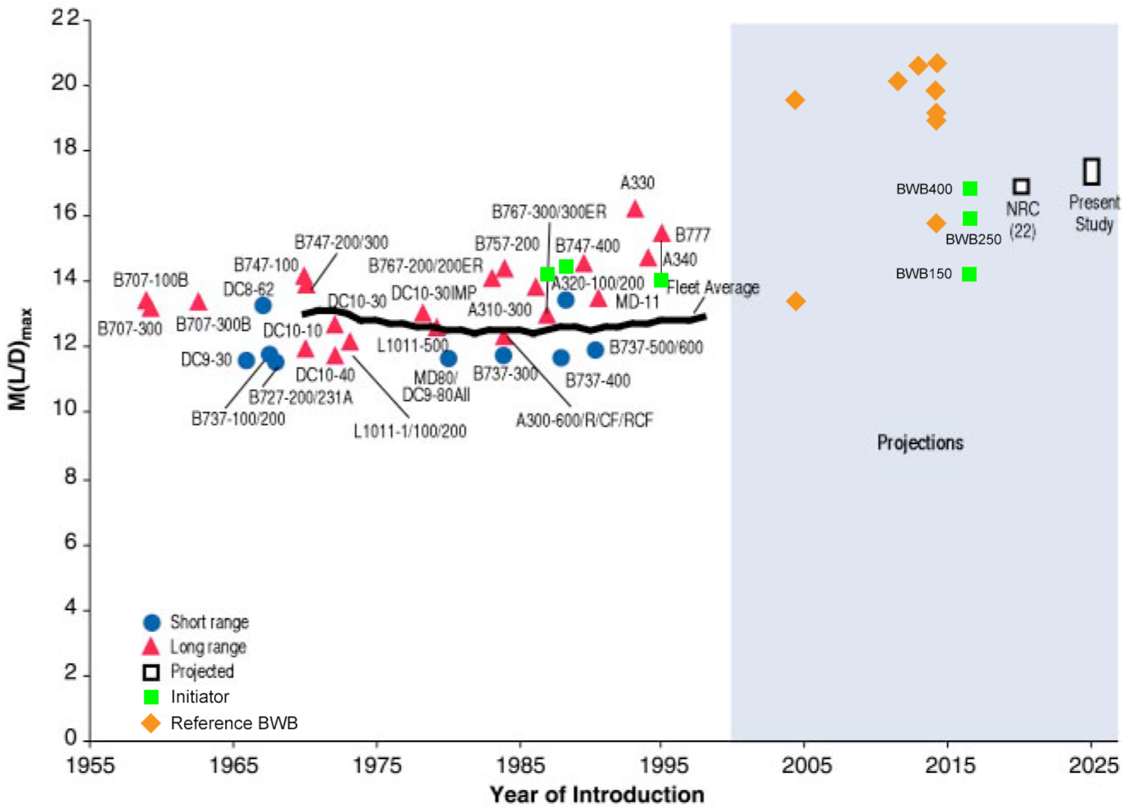

Figure 4.11: Lift to drag data from [4] combined with reference BWB values from available literature and the results of the Initiator

to three factors, either the BWB is incorrectly modelled in AVL within the Initiator, or AVL is not adequately capable of resolving the inviscid flow about the chosen geometry or the chosen designs actually produce a higher induced drag and are thus less aerodynamically efficient. After careful investigation, no apparent error in the implementation of AVL within Initiator could be found at this stage. The second point has some merit since the geometry is highly 3D with rapidly varying chord lengths and sweep angles which are which are inherently poorly captured by vortex lattice methods. However, AVL was successfully applied to the BWB in the SAX-40 study [41], among others such as references [7, 59], which forms a strong argument in favour of AVL. The last point certainly has merit in that the chosen planform, combined with the airfoils fitted through the fuselage, could result in a higher induced drag. This point is also supported by the fact that the OREIO also has a higher induced drag than the SAX-40 while higher fidelity analysis methods were used in the former, showing how induced drag can vary from design to design.

Table 4.3: Drag component breakdown comparison between reference and Initiator results
Drag values are in counts [$\times 10^{-4}$]

	SAX-40 [41]	OREIO [12]	BWB150	BWB250	BWB400
S_{ref} [m^2]	836	744	308	575	818
$C_{D_0\ \mathrm{fus}}$	31	-	44	31	35
$C_{D_0\ \mathrm{wing}}$	23	-	18	29	25
$C_{D_0\ \mathrm{nacelle}}$	4	-	4	5	6
$C_{D_0\ \mathrm{v\ tail}}$	-	-	2	3	2
C_{D_0}	58	67	67	68	68
$C_{D_{\mathrm{misc}}}$	-	-	11	11	11
$C_{D_{\mathrm{w}}}$	1	1	3	7	8
$C_{D_{\mathrm{i}}}$	24	45	57	54	47
$C_{D\ \mathrm{cruise}}$	82	113	138	141	134
$C_{L\ \mathrm{cruise}}$	0.21	0.27	0.25	0.27	0.26
M	0.80	0.80	0.78	0.80	0.84
L/D_{cruise}	25.1	23.5	18.0	19.4	19.1
$L/D_{\max}$	25.1	23.5	18.2	19.9	20.0
$M(L/D)_{\max}$	20.2	18.8	14.2	15.9	16.8

Other drag components are reasonably well predicted, C_{D_0} is quite close to reference values considering the fidelity of the method. Importantly, it seems that the miscellaneous drag that is added to the profile drag as a means to take unpredicted effects into account, such as the engine installation interference, is set too high or is even unnecessary. Profile drag counts seem to be conservative enough to allow for these effects and it is suggested that the input settings for unaccounted and miscellaneous drag be lowered in future BWB studies. This alone would increase L/D values by approximately 10% and bring them very close to the reference values mentioned before. Wave drag is strongly over predicted with both reference studies achieving extremely low wave drag of only one count. There reference results confirms the reports of good transonic performance of the BWB but could possibly be considered on the low side. It is also expected that the BWB in the Initiator will suffer a bit more in transonic conditions because the airfoils are shaped about the fuselage and lack proper transonic design. As such there could be extensive areas of sonic flow over these airfoils, terminated by rather strong shock waves. As no higher fidelity analysis is done and all reliance is placed on the Delta method, it is chosen to accept this over-prediction as a conservative estimate which should definitely be investigated by higher fidelity methods in future. Overall though it can be said that the performance of the drag modules of the Initiator are adequate for this level of design and stage of implementation of the BWB. Drag varies with configuration and layout of the aircraft and as such can be used to make qualitative and preliminary quantitative comparisons of various design ideas as is intended with the Initiator.

The longitudinal stability and controllability estimations are difficult to validate since the location of the AC and the pitching moment produced is strongly dependent on the planform geometry of the aircraft. Results can be qualitatively compared as the same trends should exist. The pitching moment polars of the three test case BWB aircraft are given in Figure 4.21. The moment response from AVL is linear with all three aircraft almost having the similar pitching moments. The stability optimisation has chosen the wing sweep such that the moment curves are stable (neutrally for the aft CG) and is thus functioning properly. The magnitude of the pitching moment could be considered high if one compares this to values in literature. Reference [59] found moment coefficients of one order of magnitude lower (less negative) while also using AVL as shown in Figure 4.16. Reference [21] on the other hand found values in the range of $C_M = [-0.074 : -0.090]$ in cruise for initial unoptimised designs using Euler and Navier-Stokes CFD solutions. These results are much closer to the values achieved by the Initiator. The vast difference between the references demonstrates the difficulty of accurately predicting pitching moment and the validation thereof. In order to remove sources of differences between the reference and Initiator results the exact geometry used in the reference should be modelled in the Initiator. Unfortunately due to time constraints this was not possible in the current work but is a starting point for future validation efforts. The accuracy of the pitching moment estimations still remains in question and so too the results of the stability and analysis.

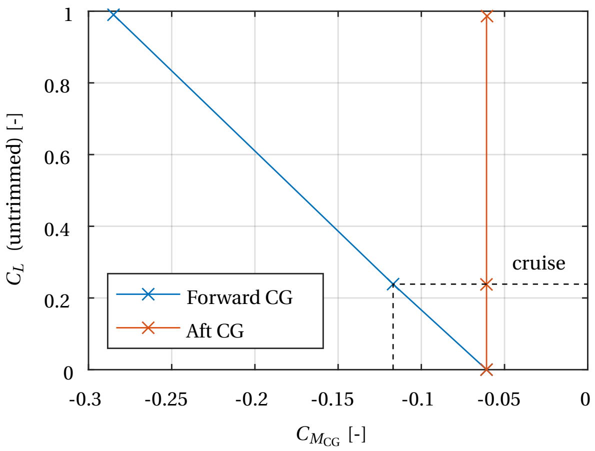

Figure 4.12: BWB150

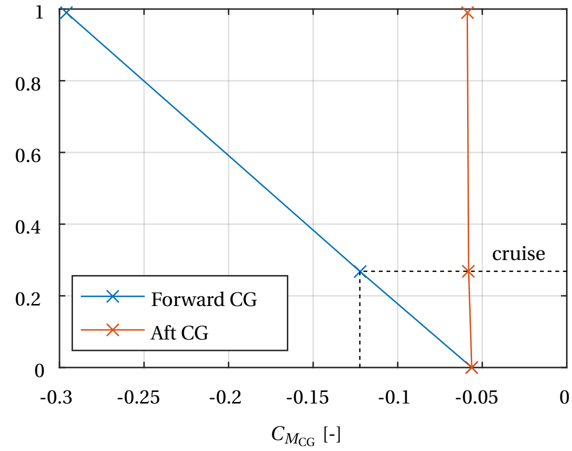

Figure 4.13: BWB250

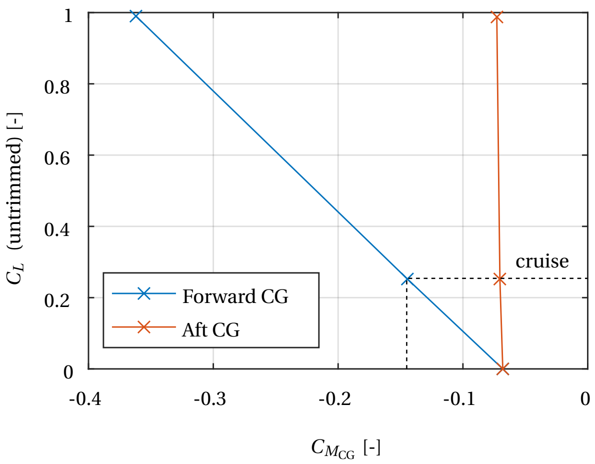

Figure 4.14: BWB400

Figure 4.15: Pitching moment polars of the BWB test aircraft

Concerning the longitudinal controllability, the elevator deflection that is required to trim the test case aircraft is shown in Figure 4.19. The definition of the BWB250 elevator is also given as an example. It is immediately clear that the large elevator deflections required at the forward CG limit are infeasible. Different elevator sizes were tested but the results made no substantial changes and remained disappointing. It is suspected that AVL is incorrectly estimating the effectiveness of the elevator. The previous comments on the pitching moment validation are also of importance here. If the pitching moment is being overestimated, larger elevator deflections will be required to be trim the aircraft. Considering that reference [59] achieved an order of magnitude lower pitching moment with AVL this point has merit. Until higher further more detailed investigations into this phenomenon are made, no concrete conclusions can be drawn as to the pitching

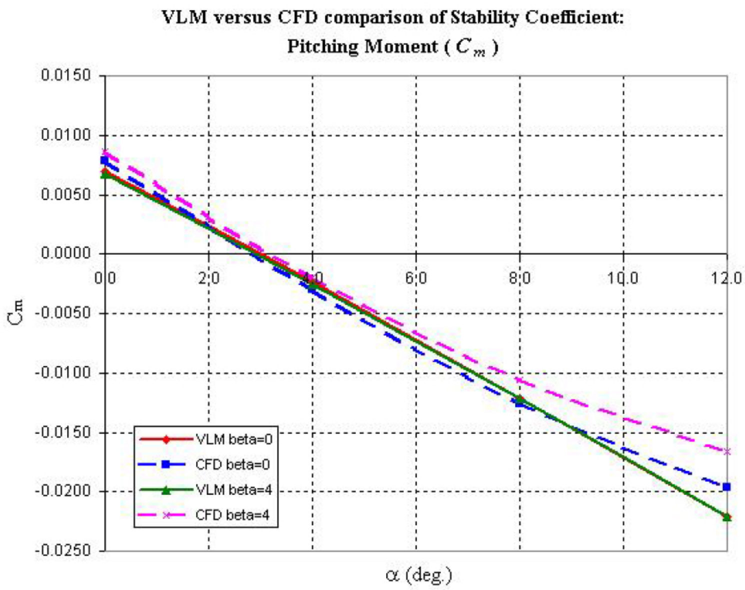

Figure 4.16: Pitching moment results for AVL vs. CFD from reference [59]

moment and elevator effectiveness. All that can be said is that the deflection of the elevator is too large to be feasible and should not be taken into account yet.

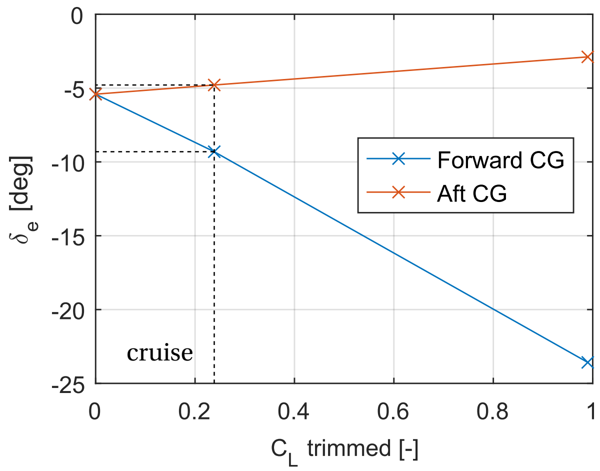

Figure 4.17: BWB150

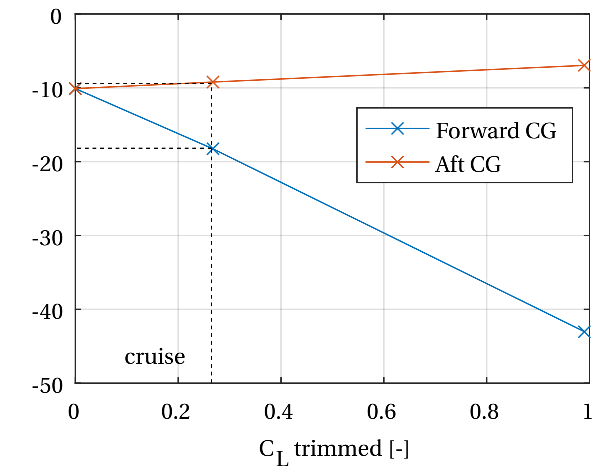

Figure 4.18: BWB250

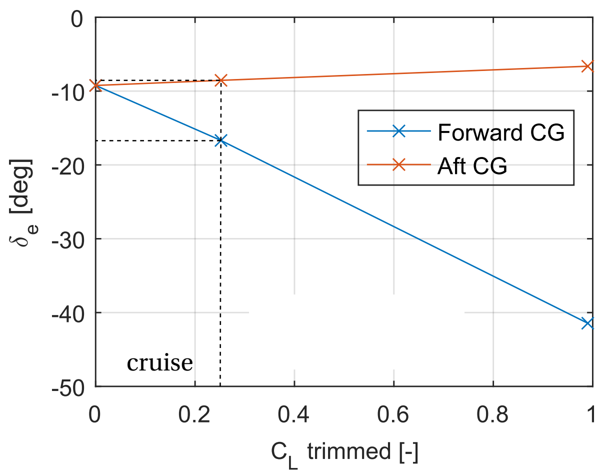

Figure 4.19: BWB400

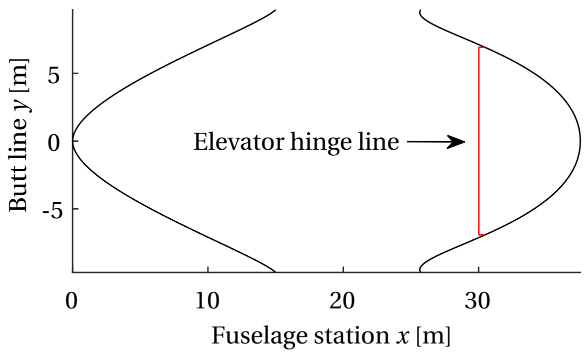

Figure 4.20: Elevator definition of the BWB250

Figure 4.21: Elevator deflection required to trim the test case BWB

5

Results and Discussion

In this chapter the results of the analyses of three different classes of BWB and TAW aircraft is given. Firstly these test cases are presented followed by their requirement analysis and design point results. The mass components of the two concepts are compared where after the drag breakdowns are given and behaviour of the drag polars are analysed for their trends.

5.1. Test Cases

Suitable BWB aircraft are chosen as test cases are chosen that represent a thorough investigation of the design space. Considering it is the goal of this work to compare blended wing body aircraft with their conventional tube and wing counterparts the BWB aircraft input TLRs were chosen to be the same as for the TAW aircraft. This can however sometimes be at a deficit to the BWB as the same requirements might not lead to an optimal design. The choice of test cases is thus based upon the TAW aircraft from each size class in the 150, 250 and 400 pax range. The aircraft chosen are the Airbus A320-300, Boeing 767-300ER and the Boeing 777-300 giving the BWB150, BWB250 and BWB400 respectively. Furthermore the aircraft selected are based upon market trends, leaning more towards dense short haul and medium sized long haul TAW aircraft which are currently in service and have been successful aircraft families. The method does however still work for larger aircraft up to about 800 passengers, as some early BWB studies used [11]. The input TLRs for each aircraft are summarised in Table 5.1.

Not all TLRs can be exactly the same however, due to the characteristics of the BWB design and its limitations need to be taken into account. This is evident in the $C_{L\,\max}$ values as BWB aircraft are not able to achieve values common for TAW aircraft due to the infeasibility of high lift devices due to longitudinal control constraints [1, 11, 13]. Actual $C_{L\,\max}$ values for BWB aircraft are scarce in literature due to a combination of the difficulty of analysing it adequately, research goals which have focused more on cruise performance or data being proprietary. Reference [13] has quoted a clean max lift of 0.7 and just over 1.0 with leading edge slats. Previous preliminary investigations on BWB aircraft at TU Delft by reference [8] have used a clean value of 1.2 and 1.4 in take-off and landing configuration. It was chosen to use a value between these reference values which still produce acceptable results with the Initiator. $C_{L\,\max}$ can however have significant effects on the design results as it usually sizes the wing loading through the landing distance constraint which in turn has a snowball effect on the mass and aerodynamic performance. Furthermore no method is currently implemented which is able to determine the actual $C_{L\,\max}$ of the BWB design at hand thus it is assumed that the input value can indeed be achieved. This forms on of the main assumptions of the current work and a weakness in the analyses which should be taken into account when considering the results. Aspect ratio is another TLR which is much lower than the TAW aircraft. This is a design philosophy result of the BWB [1] and is evident in many BWB design studies [8, 12, 17, 64]. The chosen aspect ratios are in line with those found in these studies and it has also been tweaked to achieve good results in terms of wing span gate limits, climb gradients and the resulting sizing of the fuselage and outer wing combination. The chosen TAW aircraft all use mainly aluminium structures so aluminium is also chosen for the BWB aircraft. Lastly it should be noted that due to the unusual payload-range characteristics of the Boeing 777-300, having a very short harmonic range but very long partial loading range, it was chosen to design a BWB with an intermediate range, representative of other aircraft in this class.

Table 5.1: Top level input requirements for TAW and BWB test cases

	A320-200	BWB150	B767-300ER	BWB250	B777-300	BWB400
Pax	156	156	248	248	368	368
Payload [t]	20.50	20.50	43.80	43.80	64.00	64.00
Range [km]	3917	3917	7264	7264	3142/12081	6700
Mach	0.78	0.78	0.80	0.80	0.84	0.84
Altitude [m]	11280	11280	10668	10668	10425	10425
Take-off length [m]	2180	2180	2505	2505	3232	3232
Landing length [m]	1840	1430	1660	1660	1838	1838
Airport class [FAR25]	III	III	IV	IV	V	V
A	9.50	4.00	8.00	4.70	8.67	4.80
$C_{L\text{ max, clean}}$	1.6	1.1	1.4	1.1	1.5	1.1
$C_{L\text{ max, TO}}$	2.2	1.3	2.4	1.3	2.1	1.3
$C_{L\text{ max, L}}$	2.8	1.3	2.6	1.3	2.9	1.3
SFC [lb/hr/lb]	0.60	0.60	0.58	0.58	0.58	0.58
BPR	5.70	5.70	5.06	5.06	5.80	5.80

Table 5.2: KPI for the test cases run through the Initiator

	A320	BWB150	B767	BWB250	B777	BWB400
MTOM [t]	72.94	71.35	209.05	166.47	292.53	258.24
OEM [t]	39.11	37.88	105.72	78.16	160.43	130.19
FM [t]	12.85	12.96	59.53	44.51	68.10	64.05
FF [-]	0.177	0.182	0.285	0.267	0.233	0.248
L/D_{cruise}	18.38	18.21	17.78	19.78	16.05	19.62
L/D_{max}	18.40	18.40	17.79	20.41	16.30	20.26
$C_{L\text{ cruise}}$	0.682	0.248	0.593	0.269	0.573	0.257
$C_{L\ L/D\text{max}}$	0.705	0.276	0.605	0.345	0.683	0.345
$\bar{C}_f$ [cts]	27	28	26	28	25	27
SFC [lb/hr/lb]	0.551	0.551	0.569	0.569	0.580	0.579
Fuel economy [kg/pax/km]	0.021	0.021	0.033	0.024	0.037	0.026

A short summary of the resulting key performance indicators (KPI) of the TAW and BWB test cases is given in Table 5.2. More information and analyses of these metrics will be given in subsequent sections.

5.2. Requirement Satisfaction and Design Space

The requirements listed in Section 3.2 have been satisfied for all aircraft tested. The design space for the A320 and BWB150 are given in Figures 5.1a and 5.1b respectively with the chosen design point in terms of wing and thrust loading. The design spaces for the rest of the aircraft follow the same trends. It can be seen that the design wing loading of the BWB is much lower than that of the TAW as expected. This is due to the much lower $C_{L\text{ max}}$ which limits the landing distance requirement. Landing distance is also limiting for TAW but the increased $C_{L\text{ max}}$ allows it to achieve the requirement with a higher wing loading, giving a smaller wing. Thrust loading is being constrained by the climb gradient with one engine inoperative given by §FAR25.121a but the take-off distance is almost sizing as for the TAW aircraft. Climb gradient requirements are harsher for the BWB since it has a lower aspect ratio than the TAW aircraft which negatively affects climb gradient performance [52]. The resulting thrust loading is however very close to the TAW aircraft and as such, the required engine performance, and thus size and mass, is similar. This is a positive result as lower thrust requirements benefit fuel efficiency and noise issues [41].

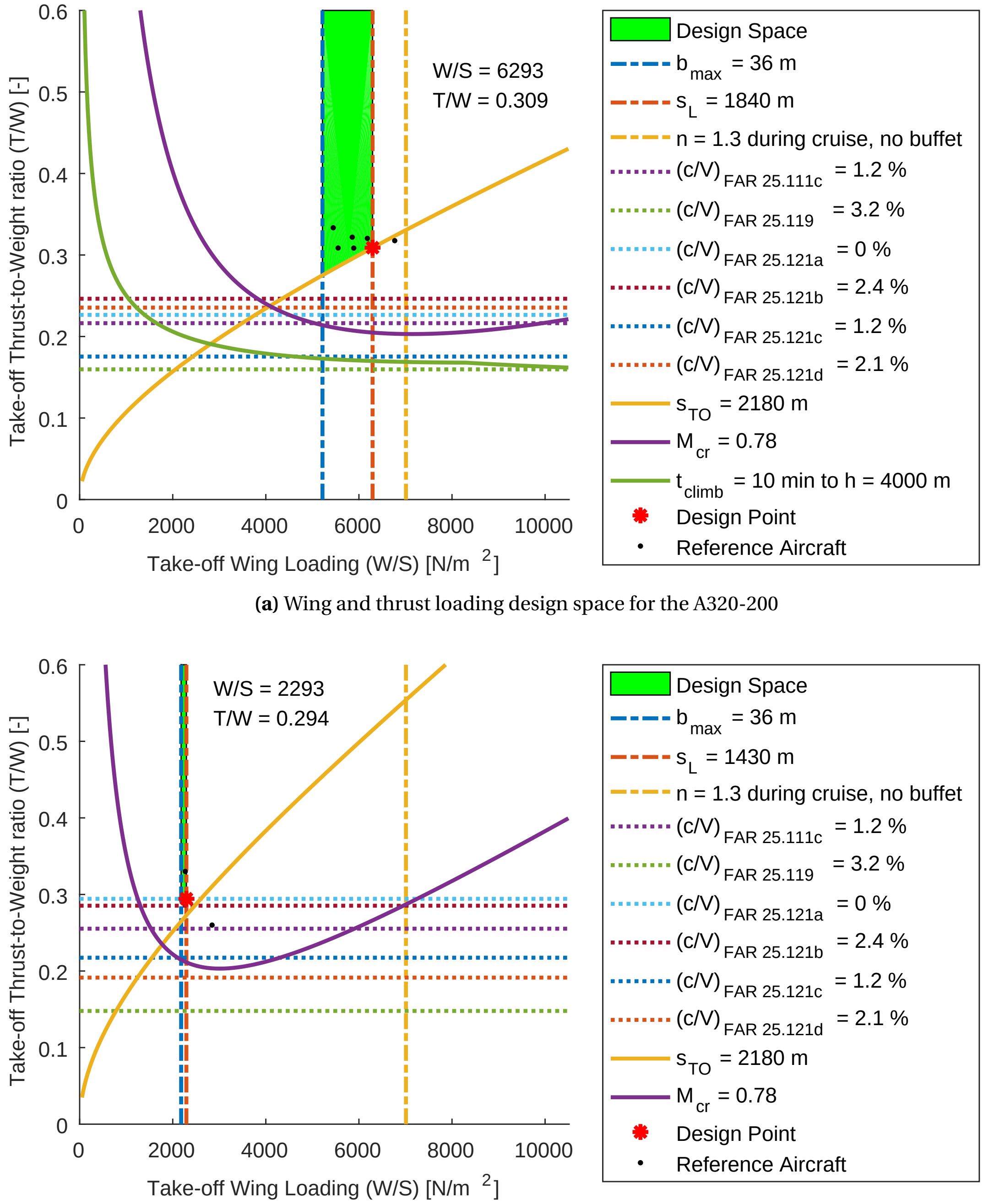

(a) Wing and thrust loading design space for the A320-200

(b) Wing and thrust loading design space for the BWB150

Figure 5.1: Design space resulting from the Initiator for the 150 pax test aircraft class

5.3. Aircraft Geometry and Layout

The geometry that results from the Initiator for the test case aircraft is shown in Figures 5.2,5.3 and 5.4 for the 150, 250 and 400 pax aircraft respectively. The TAW and BWB aircraft are plotted to the same scale so size comparisons can be made. The overall dimensions of each aircraft can be found in Table 5.3.

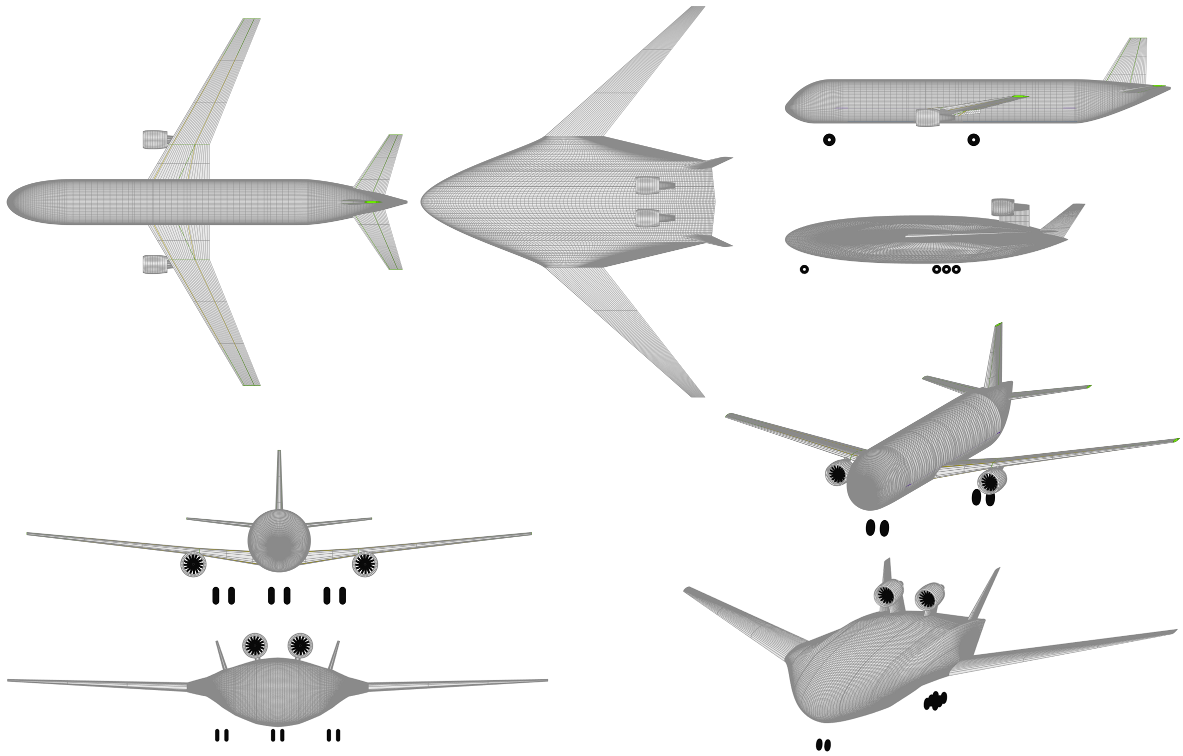

Figure 5.2: Aircraft geometry and layout of the A320-200 and BWB150 to the same scale

Firstly a discussion on the geometry resulting from the parametrisation is held. The verification and validation of the geometry parametrisation has already been done but now the results of different test cases can be seen and indeed the geometry for each case is feasible from a consistency and integrated design standpoint. It is seen that in all BWB cases the geometry parametrisation has been successful in modelling quite different planform shapes and these are by no means the limit of what is possible. One possible weakness with the parametrisation is that the location of the join between the fuselage and outer wing, or the kink, is at the same location for the LE and TE. This limits the layout possibilities slightly as some BWB designs have a more outboard location of the TE kink. This could in theory be updated in future if it is deemed necessary but it is inconvenient and tedious with the current definition of a wing in the Initiator programming structure.

Table 5.3: Overall dimensions and geometry parameters of the BWB and TAW test case results

	Unit	A320	BWB150	B767	BWB250	B777	BWB400
S_{ref}	[m^2]	113	307	323	568	418	806
Span	[m]	32.8	35.0	50.9	51.7	60.2	62.2
Length	[m]	35.8	26.4	54.0	32.1	67.7	37.5
MAC	[m]	4.0	17.2	7.3	17.7	9.1	21.8
$\Lambda_{\mathrm{LE\ outer}}$	[°]	30.6	48.5	35.3	34.5	37.8	48.4

Considering the fuselage, the BWB is much shorter, due of course to its increased cabin width. This is an expected result and agrees with general literature. Diameter or max thickness of the fuselages are quite similar, owing to the same cabin height requirements and the vertical alignment of cabin and cargo bays.

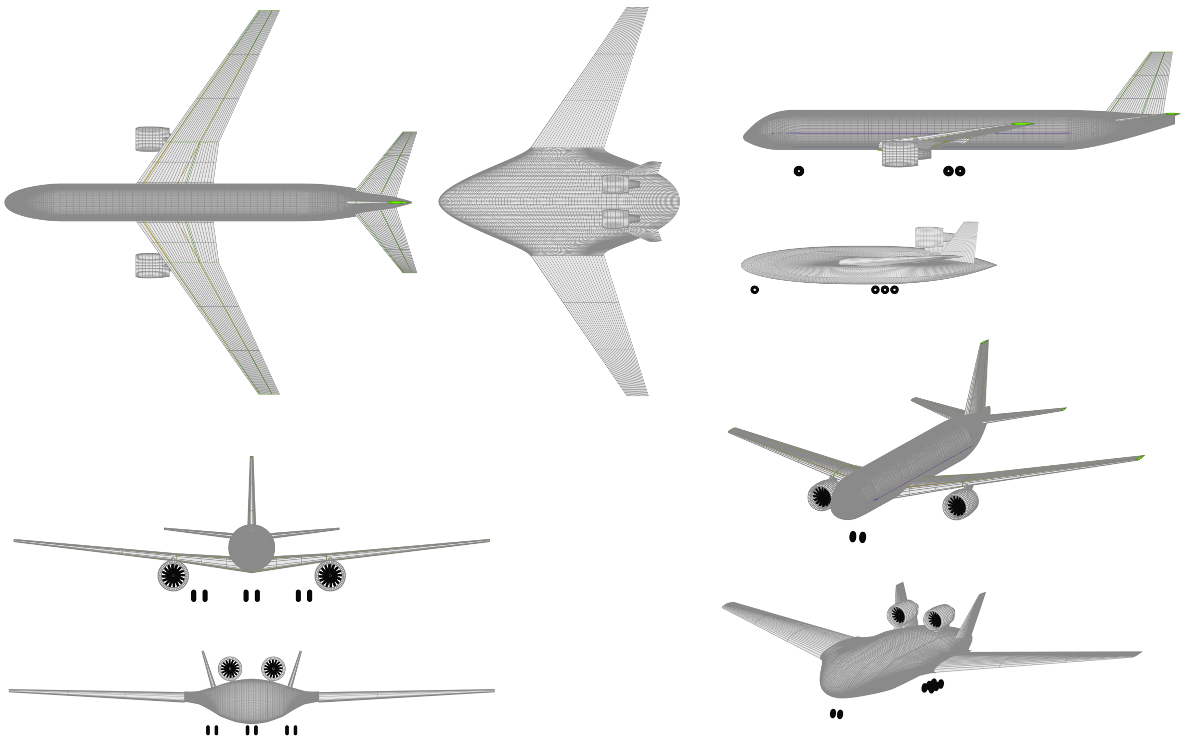

Figure 5.3: Aircraft geometry and layout of the B767-300ER and BWB250 to the same scale

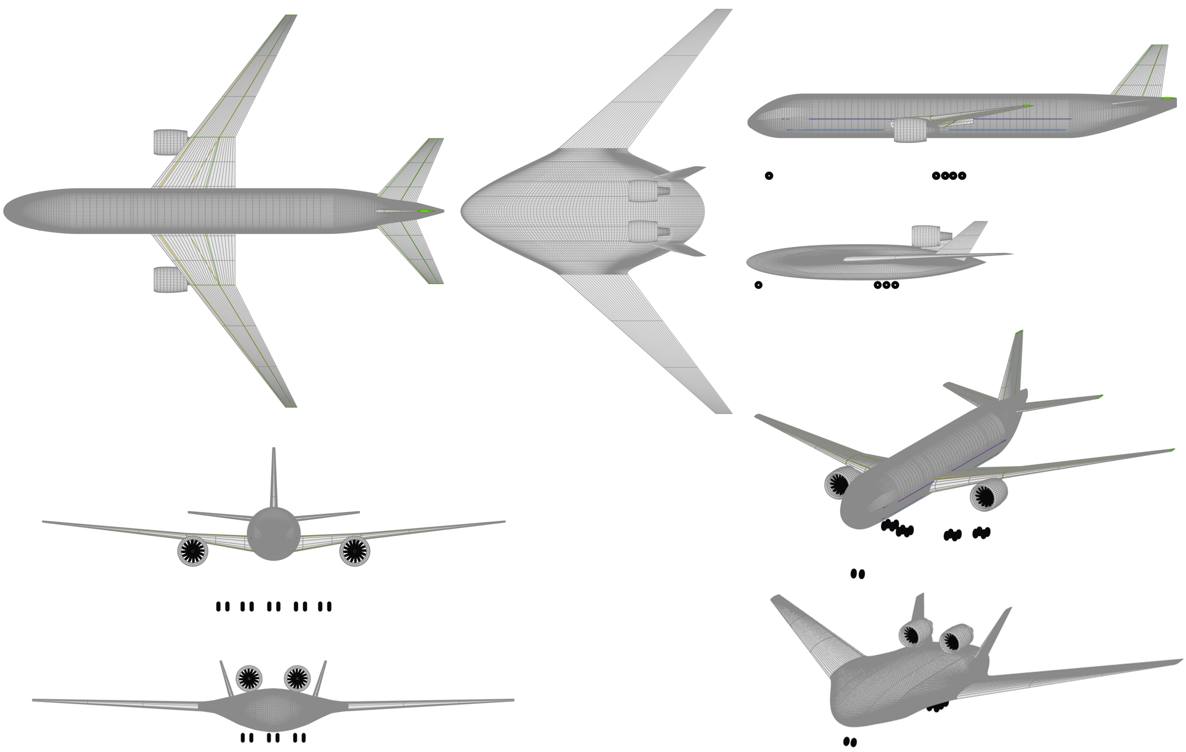

Figure 5.4: Aircraft geometry and layout of the B777-300 and BWB400 to the same scale

The sweep angle of the BWB outer wing is significantly higher than that of the TAW wing due to longitudinal stability limitations. This will give the BWB a wing mass penalty over the TAW. Wing span on the other hand is basically the same, due to using the same airport class in the TLRs as both the TAW and BWB are either span limited or very close as seen in the design point diagrams in the next section.

5.4. Mass Breakdown

The overall mass results of the TAW and BWB aircraft are given in Table 5.4. The actual mass of each TAW aircraft is also given as a reference and is the value used to calculate the differences in MTOM. These reference masses are sourced from references [44, 65, 66] and from the Aircraft Characteristics and Capability and Planning (ACAP) documents published by Airbus and Boeing for each aircraft. Results for the BWB and TAW show the masses to be similar but the BWB is marginally lighter than its TAW counterpart. Trends in the mass reductions favour larger aircraft where the best results are achieved in the 400 pax class. Payload efficiency is also marginally higher for the BWB there the improvements over TAW increase with aircraft size. The trend in reference data is for payload efficiency to decrease with aircraft size, and this is also reflected in the Initiator results. OEM fractions on the other hand do not show an obvious trend, neither in reference values nor in the Initiator results for either concept.

TAW masses are also similar to the reference values and within the accuracy bounds of the Initiator [10], bar the B767. The B767 has a significant error of 13% on MTOM which is mostly caused by an overestimation of the OEM by 17%. This also partly causes the additional fuel burn. The reason for this overestimation is unknown as all parameters (geometry) were checked and comply well with references and the mass estimation routine ran as expected. In order to further investigate this, the Airbus A330-200 has also been modelled since is an aircraft of similar class. Again an error of 8.7% was found, showing that this class seems to be a difficult point for the Initiator to analyse. However, if the BWB results of this class are studied they conform better to what is expected looking at the trends between BWB150 and BWB400, and other unmentioned results. If the cause of the TAW error is indeed the OEM, then it explains why the BWB is less or unaffected because it uses a different method to estimate airframe mass. Uncertainty of the source of this error demonstrates why novel methods need to be found which are capable of modelling different aircraft with the same analysis method to remove as many of these uncertainties as possible.

Table 5.4: Aircraft mass breakdown for the test cases and reference TAW aircraft

	A320 ref	A320	BWB150	B767 ref	B767	BWB250	B777 ref	B777	BWB400
PM [t]	20.5	20.5	20.5	43.8	43.8	43.8	64.0	64.0	64.0
OEM [t]	42.1	39.1	38.0	90.0	105.7	79.9	160.0	160.4	130.9
FM $_{\text{harmonic}}$ [t]	14.4	13.4	13.3	50.8	59.6	46.6	76.0	68.1	66.6
MTOM [t]	77.0	73.0	71.8	184.6	209.1	170.3	300.0	292.5	261.5
ΔMTOM [%]	-	-5.2	-6.8	-	13.3	-7.7	-	-2.5	-12.8
ΔOEM [%]	-	-7.1	-9.7	-	17.4	-11.2	-	0.3	-18.2
$\frac{\text{OEM}}{\text{MTOM}}$	0.55	0.54	0.53	0.49	0.51	0.47	0.53	0.55	0.50
$\frac{\text{PM}}{\text{MTOM}}$	0.27	0.28	0.29	0.24	0.21	0.26	0.21	0.22	0.24

5.5. Drag Breakdown

Moving to the next main comparison topic, the drag breakdowns of the TAW and BWB aircraft are given in Table 5.5. Available trustworthy reference drag data for the TAW aircraft is scarce so reference breakdowns are not shown. Figures 4.3 and 4.11 give indications as to the accuracy of the Initiator's drag estimations for TAW aircraft. The Initiator estimates $M(L/D)_{\text{max}}$ with an error of 7.5%, 10.9% and -10.7% for the A320, B767 and B777 respectively. These are acceptable results if one considers the remarkable scatter present in Figure 4.11 for both TAW and BWB, which stands testament to the difficulty in estimating drag and judging if drag values for a given aircraft are appropriate. Figure 4.3 shows that C_{D_0} is being slightly underestimated for the TAW according to the trend for conventional aircraft. It does however indicate that the B767 is an outlier and this could also play a role in the larger MTOM error for this aircraft. Overall it can be assumed that the Initiator drag results for TAW aircraft are accurate enough to form the base of the TAW and BWB comparisons.

Returning to Table 5.5 it can be seen that the large difference in reference planform area (S_{ref}) between the BWB and TAW results in very different drag coefficients. This makes one-to-one comparisons difficult. In

Table 5.5: Drag breakdown for test case aircraft, all drag values in [cts].

	A320	BWB150	B767	BWB250	B777	BWB400
C_{D_0}	169	67	139	68	150	68
C_{D_misc}	14	12	13	12	3	12
C_{D_w}	17	3	13	7	62	8
C_{D_i}	172	57	170	54	141	47
$C_{D\ \text{cruise}}$	371	138	334	141	356	134
$C_{L\ \text{cruise}}$	0.68	0.25	0.59	0.27	0.57	0.26
L/D_cruise	18.4	18.0	17.7	19.4	16.1	19.1
L/D_max	18.4	18.2	17.8	19.9	16.3	20.0
$M(L/D)_\text{max}$	14.4	14.2	14.2	15.9	13.7	16.8
S_ref [m^2]	113	308	323	575	431	818

Table 5.6: Scaled drag breakdown for test case aircraft, all drag values in [cts][a].

	A320	BWB150	B767	BWB250	B777	BWB400
C_{D_0}	64	69	150	131	215	185
C_{D_misc}	5	12	14	22	4	32
C_{D_w}	6	3	14	14	89	21
C_{D_i}	65	58	182	103	202	129
$C_{D\ \text{cruise}}$	140	142	360	270	510	367
$C_{L\ \text{cruise}}$	0.26	0.26	0.64	0.52	0.82	0.70
L/D_cruise	18.4	18.0	17.7	19.4	16.1	19.1
L/D_max	18.4	18.2	17.8	19.9	16.3	20.0
$M(L/D)_\text{max}$	14.4	14.2	14.2	15.9	13.7	16.8
S_ref [m^2]	113	308	323	575	431	818

[a] All drag and lift values in this table have been scaled to a reference area of 300 m^2.

order to lessen this effect, the drag values have been scaled to the same reference area in Table 5.6. This gives a notional comparison for aircraft size, type and the actual drag force produced which allows for an improved correlation between the TAW and BWB aircraft in each class. It is expected that the BWB should produce less drag than the TAW and attain a higher L/D_{max} [1]. This is indeed the case for the 250 and 400 pax class but the 150 pax aircraft have very similar drag performance. Studying the trend it is seen that the gains in L/D increase with aircraft size, showing that the BWB is more advantageous at larger aircraft sizes in terms of drag reduction. This result is confirmed by reference [64] which found similar results. It should not be forgotten that it is likely that the Initiator is overestimating the BWB drag (as discussed in Section 4.2) and, in general, underestimating the drag of the TAW. These factors both stand in favour of the BWB and further supports the evidence that a BWB is more aerodynamically efficient than a TAW.

Drag polars for the test case aircraft are given in Figure 5.5. It is clear that the BWB aircraft have very different drag behaviour than TAW. Induced drag rises more quickly with lift due to the lower aspect ratio. This is also confirmed in the L/D polars given in Figure 5.6. The BWB also has a steeper peak in L/D than TAW aircraft giving it a smaller high efficiency $C_{L\ \text{cruise}}$ range. This would have an impact on the cruise profile of the aircraft, requiring more increases in altitude (step climbs) to remain at an efficient C_L. This effect could be reduced by finding a more optimum initial cruise altitude [1, 64] but it was the goal of this study to compare the BWB and TAW for the same input TLRs.

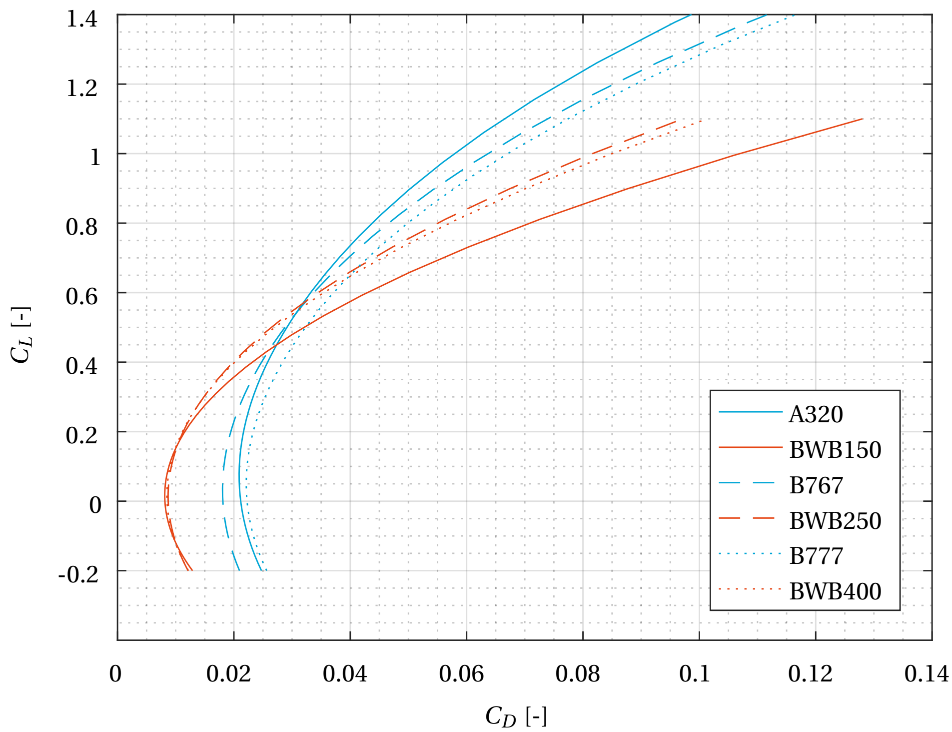

Figure 5.5: Drag polars for the test aircraft in the clean condition

As mentioned in Section 3.5.3 there are some preliminary attempts made within the current work to reduce induced drag. This occurs during the optimisation for stability, where sweep and twist of the outer wing are adjusted such that the aircraft is made stable but subject to the objective of minimum fuel burn and wing mass. As a result of this optimisation, an improvement is made to the lift distribution and thus induced drag. This change is shown in Figure 5.7 resulting in an induced drag reduction of 4 counts. However, the distribution over the fuselage is not smooth and varies from a theoretical optimum elliptical distribution. Since planform parameters of the fuselage such as sweep or chords are fixed around the cabin they can not be altered to improve lift distribution. The airfoil shaping parameters explained in Section 2.3 can be modified to vary the LE and TE shape of the fuselage airfoils, and influence their characteristics to increase or decrease the local lift produced. As explained before it is not known if AVL would result in suitable airfoil designs and the programming of such an optimiser fell outside the scope of this thesis. It is thus left for future attention.

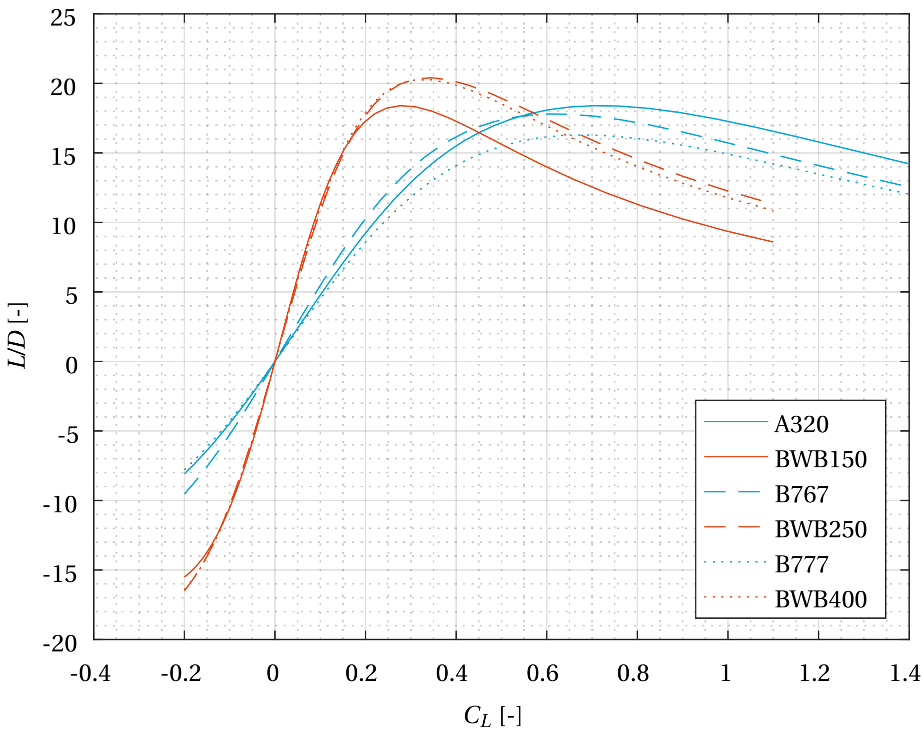

Figure 5.6: *L/D* polar for the test aircraft in the clean condition

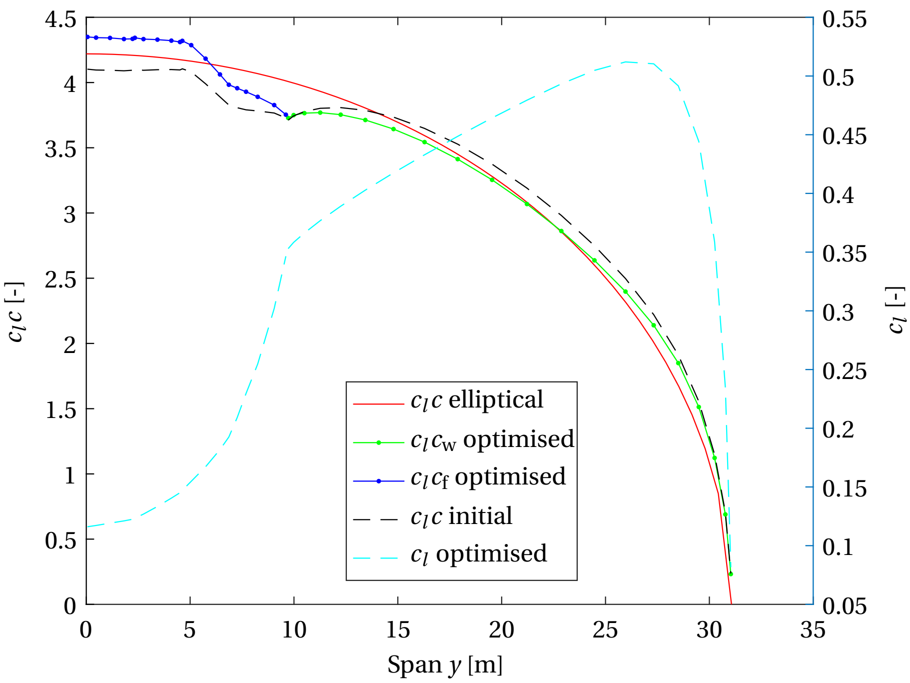

Figure 5.7: Example of initial and optimised lift distributions

6
Conclusions

A conceptual design methodology for the blended wing body within the semi-automatic design environment of the Initiator has been presented. The methodology allows for the rapid layout, sizing and analysis of a wide range of passenger BWB airliners. Resulting aircraft can be compared to conventional TAW aircraft that have been sized for the same top level requirements and the performance estimated to the same level of fidelity using similar analysis methods. The short execution time of the process (<20 min on a standard desktop PC) allows for investigations of the impacts of a multitude of design aspects such as the input requirements, shaping and configuration layout. This allows for qualitative and preliminary quantitative conclusions to be drawn as to the most optimum design choices in terms of the design target which could be fuel burn, MTOM, L/D and so forth. One of the main advantages of the Initiator, and the implemented BWB method, is that while performing these estimations, all of the aircraft design sub-disciplines are simultaneously taken into account resulting in an aircraft that is consistent and feasible in all aspects. This is often a weakness in literature as issues such as the cabin layout or landing gear integration are either not taken into account or remain fixed during the design process and subsequent optimisations. Due to the stronger coupling between disciplines with the BWB this point gains even more merit. It must be clearly noted that while the Initiator is able to consider almost all disciplines, the current implementation for the BWB is not complete and the resulting aircraft are likely to change once these topics are implemented. These include, but are not limited to, longitudinal control, lateral and directional stability and control, high lift estimation, detailed aircraft performance analysis, higher fidelity Class II.5 mass analysis and noise production. The current work however forms a flexible, robust and validated base onto which these future investigations can be made.

The novel geometry parametrisation that was developed for the BWB allows for almost any shape of BWB to be designed using basic input parameters. The implementation of the oval fuselage has allowed for a BWB design that has improved cabin layout options over other BWB fuselages and the concept has proven to increase the shaping flexibility of the pressure shell while strongly limiting the required number of input parameters. Furthermore the innovative fuselage shaping procedure around this oval cabin results in BWB aircraft that have very little unused volume which increased packing and payload carrying efficiency over those found in literature, on the order of 6% higher payload mass fraction. Seating configuration and cabin layout could still be improved upon, in terms of galley and lavatory placement and emergency exit integration issues, but the resulting cabin is still feasible as far as required floor area for seating passengers and cabin items. The dependency of the outer wing sizing on the fuselage shape necessitated a design convergence loop between the fuselage and outer wing sizing routines which results in a total planform shape which is consistent with the chosen design point. A weakness with the BWB concept was found in this respect. As the mass of the aircraft decreases so too does its required wing area for a chosen design wing loading. Since the fuselage planform area remains relatively constant around the cabin, the change in wing area is applied mostly to the outer wing. In cases where the aircraft becomes very light, these area reductions lead to infeasibly small outer wings for a fixed input overall aspect ratio. Reducing the aspect ratio does help ease this effect but a lower limit is also reached where performance requirements become limiting such as the climb gradient after take-off.

Mass and drag estimation methods have been formulated which are able to adequately determine the mass and drag components of the BWB to an accuracy that is suitable for conceptual design. Mass estimations have been validated to fall within 10% of reference values with 5% difference being common. The applicability of Howe's fuselage mass estimation method to the oval fuselage can be brought into question but the mass results mentioned stand in favour of the assumption that it can be successfully applied. Drag analyses are likely overestimating the drag of the BWB. Higher induced drag and penalties to correct for unaccounted drag sources are leading to somewhat lower *L*/*D* ratios. Reduction of the unaccounted and miscellaneous drag values could improve *L*/*D* by as much as 10%, bringing the values much closer to those of reference studies. The accuracy of the method is still within bounds which could be considered suitable for conceptual design and the level of integration of the BWB in the Initiator. It does produce the correct trends between BWB of different size and can be used to make estimations of the impact of design choices as intended with the Initiator. Longitudinal stability is provided for the BWB by a combination of the user defined location of the outer wing and automatically varying the outer wing sweep angle. Longitudinal control routines were implemented but the results were disappointing and the feedback of results on the aircraft design was disabled. The longitudinal control of the BWB can therefore not always be guaranteed.

Results of the preliminary comparisons between BWB and TAW aircraft tested reveal that the same trends are achieved as could be expected from literature. The BWB is more aerodynamically efficient than the TAW especially at larger aircraft sizes. The mass estimations predict the OEM to be lower for a BWB than for a TAW and together with the higher aerodynamic efficiency, results in lower fuel burn per passenger kilometre with values as high as 30%. Considering the current level of implementation of the BWB and the coupling between design disciplines that exists, it can be expected that the quantitative results of this study between BWB and TAW will change with further BWB implementation. However the qualitative results and trends should remain valid. The stated improvements of the BWB over the TAW are thus provisional.

7
Recommendations

Recommendations for future work regarding the Initiator and the blended wing body are summarised in the following list:

- Reduction of the miscellaneous and unaccounted drag inputs as the zero-lift drag predictions for the BWB seem to be conservative enough to include at least a portion of these secondary penalties.
- Implementation of the Class II.V methods of references [25, 27] in order to perform a higher fidelity analysis of the oval fuselage structural mass, improving the trustworthiness of the mass estimations and providing further verification and validation sources for the Class II methods implemented in this work.
- Implementation of centrally located galleys and lavatories following the work of [38]. This will add cabin layout flexibility and improve the feasibility of the cabins produced. Aisles should also be aligned and provision should be made for diagonal aisles, as also performed in [38]. Lastly filling of the last row of a seating class and adding this to the passenger requirement should either be improved or disabled for the BWB as a large number of pax can be added due to the increased seats per row.
- The impact of the assumption of a linear interpolation between airfoils while in actuality the surface follows the oval arcs should be investigated. Aerodynamic drag and pitching moment results could change somewhat as the intermediate airfoil shapes will be different. Thus the aerodynamic results given should be compared with those from panel methods or CFD that are able analyse the actual oval surface geometry. This will simultaneously allow for a higher fidelity validation of the AC and pitching moment estimated by AVL as this was found to be an area of high uncertainty.
- Estimation of the actual maximum attainable lift coefficient of the BWB design at hand should be implemented. The current analyses methods do not cover this topic and it is a critical parameter for the requirement satisfaction of the aircraft. The results of the analysis should be used to update the design point chosen such that input TLRs are still achieved with the actual $C_{L\,\mathrm{max}}$ of the BWB.
- The sweep of the vertical tail of the BWB is linked to the sweep angle of the outer wing as for conventional TAW aircraft. However, the sweep angle assigned to the wing during the design for longitudinal stability is usually higher than what is required for acceptable wave drag as predicted by the simple sweep and Korn adjustment method. Thus the sweep angle of the vertical tail is also higher than it needs to be to prevent separation at or above the dive Mach number. It is therefore recommended that the sweep of the vertical tail be set using the value resulting from the simple sweep theory and Korn adjustment method for the wing and then multiplied by the vertical sweep correction for separation prevention as usual. Alternately the sweep of the vertical tail can be set during the design for directional stability once it is implemented in future.

Bibliography

[1] P. Okonkwo and H. Smith, “Review of evolving trends in blended wing body aircraft design”, *Progress in Aerospace Sciences*, vol. 82, pp. 1–23, 2016.

[2] G. Larkin and G. Coates, “A design analysis of vertical stabilisers for blended wing body aircraft”, *Aerospace Science and Technology*, vol. 64, pp. 237–252, 2017. DOI: 10.1016/j.ast.2017.02.001.

[3] R. Martínez-Val, C. Cuerno, and E. Pérez, “Potential effects of blended wing bodies on the air transportation system”, *Journal of Aircraft*, vol. 47, pp. 1599–1604, 2010.

[4] J. J. Lee, S. P. Lukachko, I. A.Waitz, and A. Schafer, “Historical and future trends in aircraft performance, cost, and emissions”, *Annual Review of Energy and the Environment*, vol. 26, pp. 167–200, 2001. DOI: 10.1146/annurev.energy.26.1.167.

[5] J. R. Quinlan and F. H. Gern, “Conceptual design and structural optimization of nasa environmentally responsible aviation (era) hybrid wing body aircraft”, *57th AIAA/ASCE/AHS/ASC Structures, Structural Dynamics, and Materials Conference*, AIAA, San Diego, California, Jan. 2016.

[6] J. R. Hooker and A. Wick, “Design of the hybrid wing body for fuel efficient air mobility operations”, *52nd Aerospace Sciences Meeting*, AIAA, National Harbor, Maryland, Jan. 2014.

[7] P. Okonkwo, “Conceptual design methodology for blended wing body aircraft”, PhD thesis, Cranfield University, 2016.

[8] J. van Dommelen and R. Vos, “Conceptual design and analysis of blended-wing-body aircraft”, *Proceedings of the Institution of Mechanical Engineers, Part G: Journal of Aerospace Engineering*, vol. 228, 2014. DOI: 10.1177/0954410013518696.

[9] N. Cavus, “Aircraft design optimization with artificial intelligence”, *54th AIAA Aerospace Sciences Meeting*, AIAA, San Diego, California, Jan. 2016.

[10] R. Elmendorp, R. Vos, and G. L. Rocca, “A conceptual design and analysis method for conventional and unconventional airplanes”, *ICAS 2014: Proceedings of the 29th Congress of the International Council of the Aeronautical Sciences*, AIAA, St. Petersburg, Russia, Sep. 2014.

[11] J. Frota, K. Nicholls, J. Whurr, *et al.*, “Nacre - new aircraft concepts research: Final activity report 2005 – 2010”, Airbus SAS, Tech. Rep., 2011.

[12] D. M. Pitera, M. DeHaan, D. Brown, *et al.*, “Blended wing body concept development with open rotor engine integration”, Boeing and NASA, Tech. Rep. NASA/CR–2011-217303, 2011.

[13] R. T. Kawai, “Acoustic prediction methodology and test validation for an efficient low-noise hybrid wing body subsonic transport”, NASA, Tech. Rep. NF1676L-14465, 2011.

[14] R. Maier, “Acfa 2020 an fp7 project on active control of flexible fuel efficient aircraft configurations”, *Progress in Flight Dynamics, GNC, and Avionics*, EUCASS, vol. 6, Dec. 2013, pp. 585–600. DOI: 10.1051/eucass/201306585.

[15] T. A. Reist and D. W. Zingg, “Aerodynamic shape optimization of a blended-wing-body regional transport for a short range mission”, *31st AIAA Applied Aerodynamics Conference*, AIAA, San Diego, California, Jun. 2013.

[16] R. H. Liebeck, “Design of the blendedwing body subsonic transport”, *Journal of Aircraft*, vol. 41, pp. 10–25, 2004.

[17] C. L. Nickol and W. J. Haller, “Assessment of the performance potential of advanced subsonic transport concepts for nasa’s environmentally responsible aviation project”, *54th AIAA Aerospace Sciences Meeting*, AIAA, San Diego, California, Jan. 2016. DOI: 10.2514/6.2016-1030.

[18] A. Filippone, “Cruise altitude flexibility of jet transport aircraft”, *Aerospace Science and Technology*, vol. 14, pp. 283–294, 2010.

[19] R. Vos, F. Geuskens, and M. Hoogreef, “A new structural design concept for blended wing body cabins”, *53rd AIAA/ASME/ASCE/AHS/ASC Structures, Structural Dynamics and Materials Conference*, AIAA, Honolulu, Hawaii, Apr. 2012.

[20] A. Wortmann, M. Hoogreef, and R. Vos, “Effect of wing loading and fuel type on optimal cruise altitude for civil aircraft”, *15th AIAA Aviation Technology, Integration, and Operations Conference*, AIAA, Dallas,TX, Jun. 2015.

[21] N. Qin, A. Vavalle, A. L. Moigne, M. Laban, K. Hackett, and P. Weinerfelt, “Aerodynamic considerations of blended wing body aircraft”, *Progress in Aerospace Sciences*, vol. 40, pp. 321–343, 2004.

[22] D. Roman, R. Gilmore, and S. Wakayama, “Aerodynamics of high-subsonic blended-wing-body configurations”, *41st Aerospace Sciences Meeting and Exhibit*, AIAA, Reno, Nevada, Jan. 2003.

[23] V. Mukhopadhyay, “Blended-wing-body (bwb) fuselage structural design for weight reduction”, *57th AIAA/ASME/ASCE/AHS/ASC Structures, Structural Dynamics, and Materials Conference*, AIAA, Austin, TX, Apr. 2005.

[24] Z. van der Voet, F. J. J. M. M. Geuskens, T. J. Ahmed, B. N. van Eyben, and A. Beukers, “Configuration of the multibubble pressure cabin in blended wing body aircraft”, *Journal of Aircraft*, vol. 49, pp. 991–1007, 2012.

[25] K. Schmidt and R. Vos, “A semi-analytical weight estimation method for oval fuselages in conventional and novel aircraft”, *52nd Aerospace Sciences Meeting*, AIAA, National Harbor, Maryland, Jan. 2014.

[26] D. Howe, “Blended wing body airframe mass prediction”, *Proceedings of the Institution of Mechanical Engineers, Part G: Journal of Aerospace Engineering*, vol. 215, pp. 319–331, 2001. DOI: 10.1243/0954410011533329.

[27] M. Roelofs and R. Vos, “Semi-analytical composite oval fuselage mass estimation”, *55th AIAA Aerospace Sciences Meeting*, AIAA, Grapevine, Texas, Jan. 2017.

[28] M. Sargeant, T. Hynes, W. Graham, J. Hileman, M. Drela, and Z. Spakovszky, “Stability of hybrid-wing–body-type aircraft with centerbody leading-edge carving”, *Journal of Aircraft*, vol. 47, pp. 970–974, 2010.

[29] C. Huijts and M. Voskuijl, “The impact of control allocation on trim drag of blended wing body aircraft”, *Aerospace Science and Technology*, vol. 46, pp. 72–81, 2015. DOI: 10.1016/j.ast.2015.07.001.

[30] A. J. Slingerland, “Development of a preliminary sizing module for conventional and unconventional aircraft”, Master’s thesis, TU Delft, 2014.

[31] D. Decloedt, “Investigation into the effect of relaxed static stability on a business jet’s preliminary design”, Master’s thesis, TU Delft, 2016.

[32] J. Vargas, “Development of a wave drag prediction tool for the conceptual design phase”, Master’s thesis, TU Delft, 2015.

[33] Q. Jansen and R. Vos, “Assessing the effect of decreased longitudinal stability on aircraft size and performance”, *54th AIAA Aerospace Sciences Meeting*, AIAA, San Diego, California, Jan. 2016.

[34] A. Hettema, “Vertical tail design: Development of a rapid aerodynamic analysis method”, Master’s thesis, TU Delft, 2015.

[35] A. Elham, “Weight indexing for multidisciplinary design optimization of lifting surfaces”, PhD thesis, Delft University of Technology, 2013.

[36] C. L. Nickol and L. A. McCullers, “Hybrid wing body configuration system studies”, *47th AIAA Aerospace Sciences Meeting Including The New Horizons Forum and Aerospace Exposition*, AIAA, Orlando, Florida, Jan. 2009.

[37] C. L. Nickol, “Hybrid wing body configuration scaling study”, *50th AIAA Aerospace Sciences Meeting including the New Horizons Forum and Aerospace Exposition*, AIAA, Nashville, Tennessee, Jan. 2012.

[38] Y. M. Baan, “A hybrid method for the interior and exterior design of blended-wing-body cabins”, Master’s thesis, TU Delft, 2015.

[39] M. Kanazaki, R. Hanida, T. Nara, *et al.*, “Challenge of design exploration for small blended wing body using unstructured flow solver”, *Computers & Fluids*, vol. 85, pp. 71–77, 2013.

[40] Z. Lyu and J. R. R. A. Martins, “Aerodynamic design optimization studies of a blended-wing-body aircraft”, *Journal of Aircraft*, vol. 51, pp. 1604–1617, 2014.

[41] J. I. Hileman, Z. S. Spakovszky, M. Drela, M. A. Sargeant, and A. Jones, "Airframe design for silent fuel-efficient aircraft", *Journal of Aircraft*, vol. 47, pp. 956–969, 2010.

[42] W. Mason, "Analytic models for technology integration in aircraft design", *Aircraft Design, Systems and Operations Conference*, AIAA, Dayton, OH, Sep. 1990.

[43] E. Torenbeek, *Synthesis of Subsonic Airplane Design*. Kluwer Academic Publishers, 1982.

[44] E. Obert, *Aerodynamic Design of Transport Aircraft*. IOS Press BV, 2009.

[45] N. Qin, A. Vavalle, and A. L. Moigne, "Spanwise lift distribution for blended wing body aircraft", *Journal of Aircraft*, vol. 42, pp. 356–365, 2005.

[46] R. Hageman, "Rudder incorporated winglet design for blended wing body aircraft", Master's thesis, TU Delft, 2016.

[47] D. P. Raymer, *Aircraft Design: A Conceptual Approach*. American Institute of Aeronautics and Astronautics, 1992.

[48] M. T. Tong, S. M. Jones, W. J. Haller, and R. F. Handschuh, "Engine conceptual design studies for a hybrid wing body aircraft", NASA, Tech. Rep. NASA/TM—2009-215680, 2009.

[49] A. Urang, M. Drela, E. M. Greitzer, *et al.*, "Preliminary experimental assessment of the boundary layer ingestion benefit for the d8 aircraft", *52nd Aerospace Sciences Meeting*, AIAA, National Harbor, Maryland, Jan. 2014.

[50] M.-S. Liou, H. Kim, and M.-F. Liou, "Challenges and progress in aerodynamic design of hybrid wing-body aircraft with embedded engines", NASA, Tech. Rep. NASA/TM—2016-218309, 2016.

[51] R. Elmendorp, "Synthesis of novel aircraft concepts for future air travel", Master's thesis, TU Delft, 2014.

[52] J. Roskam, *Airplane Design: Part I-VII*. Design, Analysis and Research Corporation, 2008.

[53] P. C. Mody, S. Sato, D. K. Hall, E. de la Rosa Blanco, J. I. Hileman, and E. Wen, "Conceptual design of an n+3 hybrid wing body subsonic transport", *28th AIAA Applied Aerodynamics Conference*, AIAA, Chicago, Illinois, Jun. 2010.

[54] A. Velicki, P. Thrash, and D. Jegley, "Airframe development for the hybrid wing body aircraft", *47th AIAA Aerospace Sciences Meeting Including The New Horizons Forum and Aerospace Exposition*, AIAA, Orlando, Florida, Jan. 2009.

[55] J. Y. Boersma, "Business jet design using laminar flow", Master's thesis, TU Delft, 2016.

[56] R. C. Feagin and W. D. Morrison, "Delta method, an empirical drag buildup technique", NASA, Tech. Rep. NASA-CR-151971, 1978.

[57] J. A. Vargas and R. Vos, "Development of a wave drag prediction tool for the conceptual design phase", *54th AIAA Aerospace Sciences Meeting*, AIAA, San Diego, California, USA, Jan. 2016.

[58] A. A. Cusher and A. Gopalarathnam, "Drag reduction methodology for adaptive tailless aircraft", *Journal of Aircraft*, vol. 49, pp. 161–172, 2012.

[59] P. Roysdon, "Blended wing body lateral-directional stability investigation using 6dof simulation", *Proceedings of the Institution of Mechanical Engineers, Part G: Journal of Aerospace Engineering*, vol. 228, pp. 7–19, 2013. DOI: 10.1177/0954410013483633.

[60] Q. Jansen, "Relaxed static stability performance assessment on conventional and unconventional aircraft configurations", Master's thesis, TU Delft, 2015.

[61] M. Brown, "Improving the performance of longitudinal stability estimation within the initiator", Internal unpublished TU Delft report, 2016.

[62] J. E. Williams and S. R. Vukelich, "The usaf stability and control digital datcom volume hi. implementation of datcom methods", AIR FORCE FLIGHT DYNAMICS LABORATORY, Tech. Rep. AFFDL-TR-79-3032, 1979.

[63] M. N. Roelofs, "Semi-analytical composite oval fuselage mass estimation", Master's thesis, TU Delft, 2016.

[64] T. A. Reist and D. W. Zingg, "Aerodynamic design of blended wing-body and lifting-fuselage aircraft", *34th AIAA Applied Aerodynamics Conference, AIAA AVIATION Forum*, AIAA, Washington, D.C., Jun. 2016.

[65] E. Roux, *Avions civils à réaction*. Elodie ROUX, 2007.

[66] B. G. D. Willis, K. Munson, P. Jackson, and S. Bushell, *Jane's All the World's Aircraft 2015-2016: Development and Production*. IHS, 2005.